Article:
Ghatak, H, Gardner, RL, Daczko, NR et al. (2022) Oxide enrichment by syntectonic melt-rock interaction. Lithos, 414-415. 106617. ISSN: 0024-4937

https://doi.org/10.1016/j.lithos.2022.106617

LITHOS

Oxide enrichment by syntectonic melt-rock interaction

--Manuscript Draft--

Manuscript Number:	LITHOS10170R1
Article Type:	Regular Article
Keywords:	Scientific ocean drilling; oceanic core complex; intracontinental orogeny; melt microstructures; melt-present deformation; oxide enrichment
Corresponding Author:	Robyn L Gardner Macquarie University Faculty of Science and Engineering North Ryde, AUSTRALIA
First Author:	Hindol Ghatak
Order of Authors:	Hindol Ghatak
	Robyn L Gardner
	Nathan R. Daczko
	Sandra Piazolo
	Luke Milan
Abstract:	Processes that enrich rocks in oxides, such as ilmenite, are controversial. Current models include magmatic accumulation, crystallisation of veins from immiscible liquids and syntectonic differentiation. In this contribution, we investigate examples of oxide enrichment in both the oceanic and continental crust. The oceanic samples are of oxide gabbros (with up to 45 vol.% oxides) from the Atlantis Bank oceanic core complex, Southwest Indian Ridge. The continental sample is from the Cattle Water Pass shear zone (with up to 20 vol.% oxides) associated with the intracontinental Alice Springs Orogeny, central Australia. We argue for the occurrence of an open chemical system, with melt rock reactions as a key process involved in oxide enrichment in melt-fluxed shear zones. Our detailed microstructural characterisation reveals that oxides replace silicates and form interstitial grains, grain boundary films and low dihedral angles between silicates often making up an interconnected skeletal texture. Quantitative orientation data reveals that the oxides: 1) have limited internal deformation, 2) form clusters of grains that are connected in 3D, 3) have crystal faces matching the orientation of the grain boundary of nearby newly crystallised diopside (oceanic sample) and 4) form part of the foliation defining assemblage with biotite (continental sample). This evidence suggests the oxides crystallised in the presence of melt and formed during melt-rock interaction. Syntectonic melt migration is known to result in low strain microstructures in shear zones, as the strain is accommodated by the melt that existed in the deforming rock. This produces a high strain rock with silicate and oxide minerals that show limited internal deformation. Microchemical data shows major element variability in silicates and ilmenite at the thin section scale, supporting an open chemical system with local variability in both oceanic and continental settings. It further argues that syntectonic melt migration is important in oxide enrichment. Mineral chemistry data implies that the oceanic tectonic setting involved melt-rock interaction with fractionated gabbroic melt while the continental setting involved peraluminous granite melt driving mineral replacement and enrichment of oxides. We propose that deformation assisted reactive porous flow of near liquidus melt through rocks in any tectonic setting may result in melt-rock interaction induced crystallisation of oxides in preference to silicates and that with high time-integrated melt flux, the accumulation of oxides can be significant.
Suggested Reviewers:	Barbara John UW: University of Wyoming bjohn@uwyo.edu Barbara has worked extensively in this area.
	Thomas Mueller Georg-August-Universität Göttingen: Georg-August-Universitat Gottingen thomas.mueller@geo.uni-goettingen.de

	Christian Teyssier University of Minnesota College of Science and Engineering teyssier@umn.edu
Opposed Reviewers:	

Oxide enrichment by syntectonic melt-rock interaction

Hindol Ghatak[1], Robyn L. Gardner[1], Nathan R. Daczko[1], Sandra Piazolo[2], Luke Milan[3]

[1]Australian Research Council Centre of Excellence for Core to Crust Fluid Systems/GEMOC, Department of Earth and Environmental Sciences, Macquarie University, NSW 2109, Australia

[2] School of Earth and Environment, University of Leeds, Leeds LS2 9JT, United Kingdom

[3] Earth Sciences, School of Environmental and Rural Science, The University of New England, Armidale, NSW, 2351, Australia

*corresponding author: robyn.gardner@mq.edu.au Phone: 61-2-9850 8371

Cover letter

Robyn Gardner
DEPARTMENT OF EARTH & ENVIRONMENTAL SCIENCE
Faculty of Science

Macquarie University
NSW 2109 Australia
T : +61 (0)2 9850 4728
F : +61 (0)2 9850 8943

Email: robyn.gardner@mq.edu.au

25th January, 2022

Dear Professor Shellnutt,

Please find attached the revised version of our manuscript “Oxide enrichment by syntectonic melt-rock interaction” (manuscript # LITHOS10170). We thank the reviewers for the time and effort they’ve given to the critical, constructive and overall positive assessment of our manuscript.

Many of the comments from both reviewers indicate that even though the reviewers could follow our arguments for the proposed evolutionary model, the manuscript lacked consideration of alternative models for the oxide accumulation. Specifically, the reviewers were not convinced of our proposal of high rates of flux of a typical near-liquidus melt in an open system suggesting instead (1) the breakdown of olivine/garnet, (2) high temperature hydrothermal activity or (3) a Fe-Ti-rich melt. We now address all of these possibilities. To summarise here (1) calculations show that the whole rock (specifically, olivine, pyroxene and garnet minerals) lacks sufficient titanium to form the amount of oxides observed, (2) there is no evidence geochemically or microstructurally of hydrothermal activity in the studied samples and (3) the source of a melt significantly enriched in Fe and Ti remains enigmatic. In addition, the reviews brought out that in the original manuscript the distinction between metamorphic reactions and growth versus igneous crystallisation of minerals was not made clear. Based on the reviewer’s comments we have undertaken thorough revisions, reworking the relevant sections and further justifying our arguments. We have added additional supplementary data to prove the need for an external melt. We believe this allows greater understanding of the important impact melt flux has on the development of oxide enrichment at core complexes in both oceanic and continental situations.

Please find details on how we have addressed the general comments and specific questions/suggestions raised by the reviewers. The constructive comments and suggestions have helped improve and clarify this contribution. We are confident that this manuscript has markedly improved and hope you agree that the manuscript in its revised form is now acceptable for publication in Lithos.

Thank you for considering our manuscript.

With kind regards,

Robyn Gardner, Hindol Ghatak, Nathan Daczko, Sandra Piazolo and Luke Milan

Editor's Comments:

Thank you for submitting your manuscript entitled "Oxide enrichment by syntectonic melt-rock interaction" to Lithos. Below and attached are the comments of two reviewers. The reviewers are supportive of publication after moderate revisions.

Reviewer #1 (below and attached) highlights a few conceptual issues regarding the nature of origin of the melt flux.

RG: Yes, Reviewer 1 was not convinced of our proposal of high rates of flux of a typical near-liquidus melt in an open system suggesting instead the source of oxides could be due to (1) the breakdown of olivine/garnet, (2) high temperature hydrothermal activity or (3) a Fe-Ti-rich melt. In the revised manuscript we have now explicitly evaluated all of these alternative possibilities. To summarise here (1) calculations show that the whole rock (olivine, pyroxene and garnet) lacks sufficient titanium to form the amount of oxides observed, (2) there is no evidence geochemically or microstructurally of hydrothermal activity in the studied samples and (3) the source of a melt significantly enriched in Fe and-Ti remains enigmatic. See full explanations below for our detailed replies to Reviewer #1's comments.

Reviewer #2 points out a few minor issues, but is seeking clarification for:

A) the distinction between metamorphic and igneous processes in the system,

RG: This comment and Reviewer 1's similar comment both highlight the complexity of the rocks we've investigated. Igneous processes crystallise minerals directly from a melt without interaction with any host rock, whereas metamorphic processes modify these igneous minerals by reactions with a fluid, at changing temperature or pressure conditions. We've clarified this in the introduction indicating how the microstructures would differ between the two different sets of processes. See full explanation below for further details (R1_1 and R2_Line 329).

B) explanation for homogeneous mineral compositions,

RG: In the circumstances in the samples we've investigated we believe the grains in contact with the melt were continuously recrystallising causing the chemistry of the grains to be continuously reset and homogenised by each melt flux event. See full explanation below for further details. (R2 Line 414-419 and R1_4).

C) effects on the early crystallization of oxide minerals, and

RG: The melt we propose is not a large volume MORB creating pillow basalts at the surface of the oceanic ridge. Rather, it is a melt highly localised interstitially in the oxide-rich sections of the oceanic crust. We have included some information on experimentally determined conditions that increase oxide crystallisation and decrease silicate crystallisation. See full explanation below for further details (R2 Line 468).

D) if alterative compositions to S-type granite melt can infiltrate the system.

RG: Previous researchers have speculated on a Fe-Ti--rich melt crystallising the oxides. However, the source of this Fe-Ti-rich melt is elusive, particularly in the continental environment. Our proposal of near-liquidus continuous precipitation of oxides as the melt passes through the rock is simple and avoids the need for specialised Fe-Ti-rich melt source. Our proposal for an S-type granitic melt is based on other references that suggest granitic melts in the nearby Cattle Water Pass shear zones. In

central Australia the source rocks are sedimentary rift fill so when these partially melt an S-type granitic melt is formed. See full explanation below for further details. (R2_527, 560, 569 and R1_4).

In the revised version of the manuscript please provide point-to-point responses to the reviewers' comments and make sure the text, tables, figures (no more than 15), highlights (no more than 85 characters + spaces), and references (no more than 80) are properly formatted. The guidelines will be strictly enforced.

RG: Please find our detailed point-to-point responses to the reviewer's comment below.

All the best.

Greg Shellnutt
Co-Editor-in-Chief

Reviewer #1:

Major comments

This manuscript is a great piece of research and I enjoyed very much reviewing it. I would like to apologize to the authors that it took a little longer though!

RG: No apology needed – constructive criticism is always welcome.

The manuscript describes two samples representing oceanic and continental crust for which melt rock interactions have previously been established. This new contribution is aimed at studying the role of melt/rock interaction in the formation of oxide minerals which are commonly found in these kind of rocks.

The paper is very well written and the figures are of high quality. I have attached an annotated pdf marking some minor edits and highlighting specific questions and comments.

I very much like the deformational description of the paper, which is very solid. If there is a substantial point of criticism to make then I would say that the authors are, in my view, a little bit too focussed on their interpretation. The paper would benefit from a bit more petrological details regarding the possible reaction pathways and the addition of some quantitative data.

RG: We have taken heed of this comment and have addressed the concerns. Please see the individual responses as detailed below in particular R1_1, R1_2, R1_3 and R1_4

R1_1. One of the first things to think about is the fact that the metamorphic origin needs to be stated clearer in the abstract and introduction. At present the distinction between igneous origin accompanied by deformation vs. syntectonic high grade metamorphism including melt fluxes becomes only clear at the beginning of the discussion. Thus, the origin of the melt fluxes need to be stated clearer at the beginning. There is a perfect sentence at the beginning of the discussion that would have been much better placed at an early stage in the introduction.

RG: To make our proposal for a metamorphic origin clearer we have added to the abstract: "We argue for the occurrence of an open chemical system, with melt rock reactions as a key process involved in oxide enrichment in melt-fluxed shear zones."

The issue of igneous versus metamorphic origin was also commented on by Reviewer 2 (line 329). In general, igneous processes crystallise minerals directly from a melt whereas metamorphic processes modify these igneous minerals by reactions with a fluid, and/or response to temperature or pressure changes. The analysed rock preserves evidence of the metamorphic reactions triggered by the porous flow of a fractionated gabbroic melt. Minerals inferred to pseudomorph melt (interstitial LDA, films etc.) may be considered igneous as they crystallise directly from the local melt.

As the distinction between igneous and metamorphic origin was not clearly stated, we have modified the introduction to say:

"For the gabbroic rocks in oceanic settings, two key petrogenetic models relative to the timing of oxide crystallisation, deformation and strain localisation have been proposed: (1) oxides were concentrated by igneous processes of magmatic accumulation or immiscibility processes prior to strain localisation and the formation of shear zones (Cannat et al., 1991), or (2) strain localisation formed a shear zone in oxide-poor gabbro and was followed by metamorphic processes including melt-rock reactions and oxide crystallisation during deformation-assisted diffuse porous melt flow through the shear zone, called syntectonic differentiation (Bloomer et al., 1991; Dick et al., 1991; Hopkinson and Roberts, 1995).

"These two petrogenetic models result in the formation of rocks with distinct igneous versus metamorphic microstructures. In the first model indicative microstructures would be largely of igneous origin and include euhedral to subhedral crystals with interlocking and interstitial microstructures with possibly a magmatic foliation. In this scenario, we would expect a typical igneous crystallisation sequence, where both ilmenite and magnetite crystallise from the fractionating melt. In the second model, indicative microstructures would be largely metamorphic in origin and include, interstitial microstructures, fewer crystal faces, melt-rock reaction textures and possibly the absence of typical mylonitic shear zone characteristics (Lee et al., 2018; Meek et al., 2019; Prakash et al., 2018; Stuart et al., 2018)."

This reply applies to Reviewer 1's comment on Line 345 too.

R1_2. My main criticism is about the carte blanche that the authors introduce with the open system behaviour in which a melt of variable composition comes in, triggers some reaction and changes in melt composition before propagating further. I would like to encourage the authors to consider the melt more as a mediating phase and considering the formation of oxides to be controlled by the local chemistry induced by the breakdown reactions of garnet and olivine. In other words: What about Fe and Ti exsolution during metamorphic reactions? Currently there is too much focus on melt as the only viable mechanism apart from primary crystallization. In particular Atlantis Massif is known for its high hydrothermal activity. Thus, high T fluids could equally do the trick.

RG: We show in the next comment reply (R1_3) (and have added to Fig. 1 and the text) that an open system is required to add enough Ti to form the ilmenite in both oceanic and continental scenarios. The precursor (olivine gabbro or gabbro) whole rock Fe-Ti concentrations are too low to form the ilmenite from garnet and olivine as suggested. The point is taken, however, that in some cases a flux of high temperature hydrous fluids with high concentrations of Fe-Ti could cause the ilmenite and magnetite to crystallise. We believe this not to be the case as the samples have clear melt present signatures. We have added to the discussion:

"The flux of a high temperature hydrous fluid is not considered likely as the samples examined lack evidence of hydrous minerals such as chlorite, epidote, sericite replacing feldspar, or veins of these minerals and preservation of reaction textures where igneous minerals are partially consumed. However, these microstructures are documented elsewhere in the core, suggesting that hydrous fluids are important agents of metamorphism in other sections of the core. Further support for the presence of melt instead of a hot hydrous fluid is the lack of amphibole in our samples. This lack of amphibole suggests either the presence of melt with low activity of water during melt-rock interaction or that the temperature of fluid-rock interaction was higher than the stability field of amphibole".

Also, this manuscript is on Atlantis Bank (South West Indian Ridge) rather than Atlantis Massif which is on the Mid Atlantic Ridge – this is probably a typo.

This reply applies to Reviewer 1's comment on Line 58 too.

R1_3. The authors base the open chemical system among other indicators on the bimodal variations of plg composition. Fair enough, the evidence of melt in these samples has been well established by the same group. The question is now what is the role of plag and a change in Na/Ca with regard to the oxide formation? To make this a valid point one would need a mass balance to evaluate the Fe and Ti mobility when placing the oxide formation into an open chemical system context. The authors compare the mineralogy of their samples with evidence of melt/rock-interaction to those further down in the core still containing (fresh?) ol-gabbro. Similar they report the granulite samples with garnet. Would it be possible to take the modal abundance and composition of olivine and garnet in these precursor rocks to evaluate how much additional Fe & Ti would be needed?

RG: Olivine, diopside and enstatite in the oceanic core rocks have very little titanium and TiO_2 concentrations do not vary throughout the core (refer to Fig. 1c(iii) and Supplementary Figure 2). We have now included whole rock TiO_2 concentration variability to Figure 1c and added an extra supplementary figure highlighting the lack of variability of TiO_2 in pyroxenes which suggests that a closed system with limited titanium is not a viable option for the formation of the oxides in these rocks. We have included the following in a paragraph at the beginning of the discussion:

"In the gabbros the TiO_2 whole rock data (Fig. 1c(iii) shows a distinct increase in titanium in the oxide-rich rocks (Fig. 1c(iii)) relative to the oxide-poor gabbros. From the shipboard mineral analysis data (Dick et al., 2002), olivine has very little titanium (TiO_2 was below detection limit in half of the samples, and most values are <0.013%). Clinopyroxene (0.5 to 1.0 TiO_2 wt%) and orthopyroxene (to 0.5% TiO_2 wt%) both show no variation between the oxide-rich and oxide-poor samples (Supplementary Figure 2). In a closed system, all titanium to form ilmenite must come from local minerals, hence the whole rock chemistry should not change between oxide rich and oxide poor gabbros. This is not the case in the 735B core data, hence an open system with in-fluxing fluids is required for the increase in TiO_2 and formation of ilmenite. In supplementary Data 2 we provide the average amount of additional TiO_2 required to form the oxide gabbros from olivine gabbro."

In addition, as suggested, we have added two tables to Supplementary Data 2 to calculate the additional TiO_2 required. For our continental sample, there is not the same legacy data available as for the oceanic core complex for analysis. However, we infer the same process based on the biotite and garnet concentrations. This issue is now explicitly discussed in the Sections 5.1.3 and 5.2.3 of the discussion. We believe a further calculation of specific modal abundances in the manuscript is unnecessary. The new Supplementary Data 2 is included here:

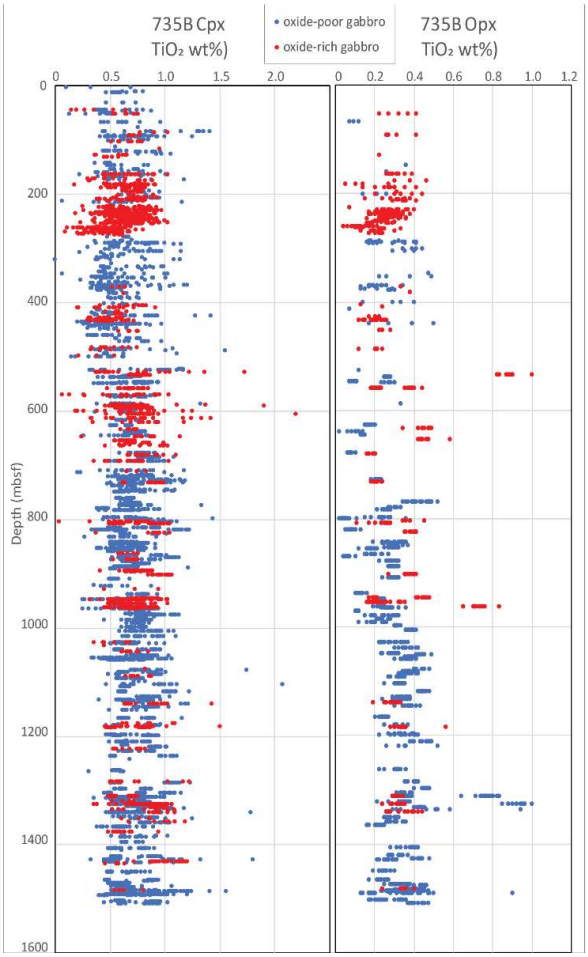

Supplementary Figure 2. Clinopyroxene and orthopyroxene TiO_2 concentrations across the 735B core, highlighting the lack of variability between oxide-rich and oxide-poor samples

	Olivine gabbro	Oxide gabbro	Average mineral TiO_2
Plagioclase	59%	60%	0
Clinopyroxene	30%	30%	1%
Olivine	10%	3%	0.001%
Other	1%	7%	
Total	100%	100%	
Whole rock % TiO_2	0.44	4.1	

Table 1. Average mineral modes and TiO_2 concentration (Dick et al 2002, table 3)

Supplementary figure 2 shows that the TiO_2 concentration in olivine is negligible and does not vary in clinopyroxene. An additional 3.66% (4.1-0.44) of TiO_2 is required to form the oxide gabbro.

	Quartz-plagioclase-rich band	Garnet-biotite-ilmenite-rich band	Average mineral TiO_2
Quartz	49%		0
Plagioclase	30%		0
Biotite	14%	50%	2.05%

Garnet	5%	30%	0 (below detection limit)
Ilmenite		18%	50%
Other	2%	2%	
Total	100%		
Whole rock % TiO_2	0.3	10%	

Table 2. CP1604C average mineral modes and TiO_2 concentration.

Supplementary Table 2 shows clearly that an additional 9.7% (10-0.3%) of TiO_2 is required to form the garnet-biotite-ilmenite-rich band.

This reply also applies to Reviewer 1's comments for Lines 495 and 570 below.

R1_4. At present, the sequence of reactions is rather complex and not very well constrained. NOTE: grt and bt CANNOT be on both sides of the reaction!!

RG: We believe there is constant re-equilibration between the melt and the garnet and biotite minerals at the time of each melt flux event. The chemistry of the final garnets and biotite in the thin section reflect only the last melt flux. As the chemistry of the melt is likely to be similar for each flux, there is possibly little variation in the garnet and biotite chemistry over time. However, we do take the point, and have added numerical subscripts in the reaction equations to highlight the different Bt and Grt minerals and have added the following text in Section 5.2.3:

"We interpret melts 1, 2 and 3 (Fig. 8b, Eq. 4, 5 and 6) are likely to be very similar in composition and suggest that they are externally derived S-type granitic melts formed when sedimentary rocks equivalent to the Harts Range Group (Fig. 1a) partially melted. We suggest that garnet and biotite chemistry re-equilibrated continuously with the melt and was aided by syn-melt flux deformation. Previous studies have also shown similar granitic melts fluxed through the nearby Gough Dam shear zone (Fig. 1b, Ghatak, 2021; Piazolo et al., 2020; Silva et al., 2021)."

This reply also applies to Reviewer 1's comments for Lines 516 & 519 below.

R1_5. I could envision a much simpler reaction path in the presence of melt in which olivine becomes unstable and breaks down to form diopside and an Fe(Ti)-oxide. Same could be true for a garnet breakdown reaction to form biotite, putting excess Fe and Ti into the oxide in agreement with the textural observations.

RG: This issue has been addressed in the reply for comment 3 from this reviewer (R1_3 above). The olivine and diopside do not have sufficient concentrations of titanium to allow the formation of ilmenite on the scale required for these samples in the oceanic environment. The same can be said for garnet in the continental sample. Details for this are now included in a new Supplementary Data 2 file and highlighted in the discussion in Sections 5.1.3 and 5.2.3.

R1 6. To avoid any misunderstanding, I do think that the proposed explanation by the authors is plausible and viable, but it would be good to at least discuss the alternative reaction mechanisms.

RG: Yes, in light of the comments here, we have now added in some discussion of the alternative scenarios suggested by the reviewer and why we believe these not to be the case in the samples we've analysed (Sections 5.1.5). See the other comments and replies for how we have undertaken this.

R1 7. Finally, as for all fluid/melt-rock-interaction papers, the question of where does the melt/fluid come from? In the case of the oceanic sample one could argue for the high T hydrothermal setting. I am very happy with the evidence for melt structures in both rocks, but I wonder whether this could equally be explained by localized melt production in at high T in the presence of fluid with subsequent melt extraction? This would equally produce a bimodal distribution of plg and melt flilms along the grain boundaries. In other words, without mass balance, trace elements or isotopes, where is the evidence for externally derived melt?

RG: Yes, we agree this could be a suitable scenario if the chemistry of the whole rock and minerals supported it. However, in light of the reply to comment 3 above (on the lack of Ti available in the local system) we cannot see how hydrous in situ melting could produce the amount of oxides present in the samples investigated. However, we do understand the issue and have modified the discussion in Section 5.1.5 to say:

"Previous researchers have suggested Fe-Ti-rich melts (c.f. Zhang et al., 2020) as the source of iron and titanium for ilmenite and magnetite. However, the source of these Fe-Ti-enriched melts remains an issue. Koepke et al. (2005) found in one of 25 hydrous partial melting experiments using 735B core gabbros that two immiscible melts were formed, one rich in REE, P, Zr, Ti and Fe from late crystallising submicron grains of apatite, zircon and oxides on the grain boundaries, forming small inclusions in albite-rich plagioclase, and the other, a larger volume melt with typical plagiogranitic features. However, in agreement with our proposed model for an open system melt influx, Koepke et al. (2005) also found that an external source of titanium was required to form the minerals found in the local system."

This reply also for comments by Reviewer 1 on Line 431 and Reviewer 2 on Lines 527, 560, 569 below.

That said, I do not think that any of my comments are critical but rather some food for thought to improve the manuscript. I am very much looking forward to see this published and encourage the authors to expand a bit on the petrological aspects.

RG: We have taken into consideration all of the comments made and believe that by adding the alternative options for the oxide formation as suggested by the reviewer that this has made the manuscript more readable and our arguments for near liquidus crystallisation from a fluxing melt more convincing.

Minor comments (from the pdf supplied)

RG: A number of missing spaces, full stops etc. highlighted by Reviewer 1 have been fixed.

Line 50: Please check with formatting guidelines, but typically you cite from old to young.

RG: The author guidelines indicate references should be alphabetical then chronological. In the highlighted example Charlier et al., 2012 has a second author of Grove, while Charlier et al., 2010 has a second author of Namur, hence the order is alphabetical per the guidelines.

Line 51: Well, if you use economic interest as a hook, then you need to state the degree of enrichment necessary to become an economic resource.

RG: Yes, this is a good idea, so we have expanded the introduction to say:

"For titanium to become an economic resource, it needs to be enriched as the average crustal abundance is < 1% TiO_2 but concentrations > 2 % are needed for viable mining (Woodruff et al., 2017)."

Line 58: What about low T processes such as serpentinization? Ol breakdown to antigorite also produces large amounts of Fe.oxide. You should at least mention the possibility of alteration for full disclosure.

RG: See major comment 2 above

Line 191: Why did you use low vac mode here? You uses a carbon coated polished sample, so no charging and no topography and no organics. Should that say 'high' vac? If not, please explain why you used low vac mode and give the pressure you used.

RG: Yes, we're very sorry, on checking, this was a mistake. It should be high. We've updated the methods with the correct information.

Line 199: You need to state which reference materials you have used. Also, is there a reason for the different analytical conditions? Depending on which silicates you measured, the focussed beam might cause some loss of light elements compared to the defocussed 10 micron beam and lower current.

RG: Yes, the reference standards were omitted by mistake. These have now been included in Supplementary Table 4. The different analytical conditions are due to the collection of data on different machines at different sites (Central Science Laboratory, University of Tasmania and Macquarie GeoAnalytical, Macquarie University. We were guided by the technical experts at each site as to the analytical conditions for their machine which would best suit our samples and our purpose.

Line 320: While technically correct, the term pyrope-rich almandine sounds somewhat harmful to the petrologic soul... please change to almandine (Xfalm = ...) with substantial pyrope component (Xpyr = ...)

RG: Modified as requested.

Section 5.1.1

Line 345: The second model should be clarified in the introduction. This sentences makes it much clearer compared to what you use in the intro!

RG: See major comment R1_1 above

Line 389: Progressive reaction of what?

RG: Yes, this is unclear. It has been altered to say:

"These observations of disequilibrium microstructures are consistent with progressive reaction from the original igneous olivine gabbro to melt-reaction modified oxide-rich gabbros."

Line 395: Why? You still have not defined an oxide forming reaction! What is the role of plg in that case?

RG: Yes, this was confusing. We had incorporated it into the first section as it highlighted the open nature of the system. But in light of this comment we have moved this to Section 5.1.3 where the melt composition is discussed. The oxide forming reactions are in Section 5.1.2. Section 5.1.3 now says:

"This bimodal variation of plagioclase composition between the oxide-rich and oxide-poor gabbros (Fig. 1d(iv)) reinforces that open rather than closed system processes were operating during the oxide formation. This is further supported by the abundant evidence for replacement microstructures. In fluid-rock interaction systems, relationships between fluid induced reactions and mineral equilibration are very complex and therefore a spectrum of rock buffered to melt-buffered mineral compositions may be observed (Rampone et al., 2020). Nevertheless, it can be inferred from the anorthite content of plagioclase that the migrating fluid is most likely a fractionated melt (Dick et al., 2019; Zhang et al., 2020) richer in sodium than the melt forming the original igneous oxide-poor gabbros."

Section 5.1.2

Line 410: I think this should come earlier.

RG: In light of the previous comment and reply, we have modified the order of the Discussion section. We start with a review of the microstructures indicating metamorphic reactions in our samples (Section 5.1.1) and then discuss the specific melt-rock reactions and formation of the oxides (Section 5.1.2). This is followed by an analysis of the likely melt composition (Section 5.1.3), the prevailing deformation conditions (Section 5.1.4) and finally our proposal for the crystallisation of the oxides (Section 5.1.5). This logical progression has been undertaken for both the oceanic and continental environments.

Section 5.1.3

Line 431: Could be olivine breakdown in the presence of a high T fluid as well....

RG: See major comment R1_7 above

Section 5.2.1

Line 495: I would argue that in the absence of a free Ti phase such as rutile, your Ti uptake in ilmenite will depend on the reaction kinetics of the breakdown reaction (grt?) controlling the local availability. Mass balance would be needed to check for Ti mobility otherwise.

RG: See major comment R1_3 above

Section 5.2.2

Line 516 & 519: you can't have the same mineral phase being reactant and product! BTW, given the association of oxides wth grt, I would strongly suspect them to be a leftover of the breakdown reaction....

RG: See major comment R1_4 above.

Section 5.3

Line 570: To make this argument you need some quantitative data here. Playing devil's advocate you need to show that you cannot form the modal abundance of oxides by the grt breakdown and at least calculate how much Fe and Ti would need to be externally derived.

RG: See major comment R1_3 above

Line 573: Based on what? Explain your calculation! Where do you get the melt concentrations from?

RG: Sorry for this confusion. This was a simple ball park calculation using the percentages in the previous sentence. To clarify, we have rephrased this:

"Typical silicate melts precipitate only 1-3 vol.% oxides. Therefore, significant enrichment of oxides requires precipitation from multiple batches of fluxing melt, progressively increasing the mode of oxides. Using the upper value of 3% oxides for the precipitation from a typical silicate melt, oxide modes of ~20 vol.% in the continental setting and ~45 vol.% in the oceanic setting require precipitation of oxides from a minimum volume of melt that is in the order of 6 to 15 times the volume of the rock, for continental and oceanic crusts, respectively."

Reviewer #2:

Major comments

Review of the manuscript "Oxide enrichment by syntectonic melt-rock interaction" by Ghatak et al.

The manuscript presents EBSD and mineral chemical data of oxide-rich oceanic (Atlantis Bank oceanic core complex, Southwest Indian Ridge) and continental (Cattle Water Pass shear zone, central Australia) crustal rocks. The authors utilize these microstructure and chemical data to understand the formation process of oxide phases (ilmenite, magnetite) in the rocks, which suggests their formation (along with some surrounding silicate phases) during syntectonic melt-rock reaction.

While I am not an expert in the field, I found the microstructural evidences for syntectonic melt-rock reaction to be quite convincing (e.g., limited internal deformation of oxides, clusters of oxide grains connected in 3D, microstructures of silicate grains such as diopside and enstatite). The manuscript is well written data is well presented. I do have some minor issues with and/or difficulty understanding some of the detailed geochemical processes of the oxide forming melt-rock reactions that the authors infer from their data. I recommend publication of this manuscript in Lithos after minor revision. Please see below for my specific comments.

Graphical abstract: In step 1, "melt" missing after "gabbroic".

RG: Updated

Line 23 and other parts: I am not sure if all reactions in this study can be described as being disequilibrium reactions, since it appears that at least some of the reactions are complete such as reaction (1), given that olivine is no longer observed.

RG: Thanks for this comment. However, we believe our use of "disequilibrium reactions" is valid as the reactions we describe are very complex and occur in an open chemical system where equilibrium between a particular melt and the host rock is only very locally achieved, even though as the reviewer rightly points out some phases, such as the olivine may have been completely consumed.

Line 38: If the highlights format allows, it may be useful to say "… within shear zones in crustal rocks" since it is unclear what material the shear zones are in.

RG: Unfortunately, this is too long (85 char limit with spaces), so I've changed this highlight to:

- Microstructures indicate former presence of melt within crustal shear zones

Line 88: 100-300 m

RG: Updated

Figure 1b: The axes should have tick marks.

RG: Updated. Please note we have also updated (c) Rock type as we had Gabbronorite red (as an oxide-rich gabbro, per Dick et al., 2019, Fig 40), but it is in fact oxide poor (per Dick et al., 1999 where the original figure is found). The oxide-rich gabbronorite continues to be red in our graph. The reference for this graph has been updated to reflect the original source.

Figure 4e: The blue lines were a bit hard to see since it's hard (at least for me) to differentiate it from the green line. Perhaps a magenta line might make it pop more.

RG: Yes, good idea. Updated.

Figure 7b, c, d: There should be tick marks on the axes.

RG: Updated

Line 329: Perhaps I am not aware of how the distinction is made between metamorphic and igneous processes in different fields, but I found it a bit strange for the porous flow of fractionated gabbroic melt through the oceanic crust to be considered a metamorphic process. Given that the melt that is infiltrating the oceanic crust is of igneous origin, can this process really be considered a metamorphic process? Again, perhaps I am not aware of how igneous vs. metamorphic processes are distinguished in different fields.

RG: This comment and Reviewer 1's comment above both highlight the complexity of the rocks we've investigated and the fact that such rocks are unusual as they are at the borderline between igneous and metamorphic rocks sensu stricto. We now make clear in the introduction, how we use the terms in this manuscript. In particular, we are clear that Igneous processes crystallise minerals directly from a melt without interaction with any host rock/solid, whereas metamorphic processes modify pre-existing mineral phases by reactions with a fluid, at temperatures or pressure where chemical composition of a pre-existing phase may change, or the pre-existing phase reacts with the melt to form a new phase or phases. In our case, the melt-rock interactions we document indicate metamorphic processes if this definition is used.

See also the reply to Reviewer 1 major comment R1_1.

Line 361 and 385: As a non-expert, I wasn't sure what is the significance of the straight boundaries. Perhaps a brief explanation such as "straight boundaries with the diopside rims, which suggests …" in the case of line 385 would be helpful.

RG: Straight boundaries are formed when the crystal face is formed with no impingement from other growing crystals, usually when the phase grows into "free space" – ie. a liquid (in this case, a melt). We've added "... indicating the original ilmenite crystal face grew into a melt (Vernon, 2000)".

Line 402: a period is missing after the closing parenthesis

RG Added

Line 414-419: Is there an explanation for the homogeneous mineral compositions considering the

different possible ways in which the composition of melt could have varied? This is especially the case if there was a high time-integrated melt flux (line 457) during which the melt composition may have had time to vary.

RG: This is a good point and is linked to R1_4, as zoning is often cited as indicative of changing fluid compositions. In the circumstances in the samples we've investigated we believe that the high flux rate allowed continuous recharge of the melt causing the localised melt to vary little in composition during the individual flux event. In addition, the grains in contact with the melt were continuously recrystallising causing the chemistry of the grains to be continuously reset and homogenised by each melt flux even though these melts may have had slightly differing compositions. We have added to the discussion:

"The titanium content in individual ilmenite grains is uniform (Supplementary Fig. 1a, b), ruling out solid-state diffusional processes, and is consistent with fluid-mediated replacement reactions (e.g. Putnis, 2009). However, even though the manganese and magnesium content show minor variation between grains within a sample, a geochemical trend between the two samples is seen (Fig. 7c, d, red arrows). This suggests while the fluxing melts may have been heterogeneous in composition, the grains in contact with the localised melt are chemically re-equilibrating continuously with the deforming rock; thus, their chemistry and microstructures are continuously reset. The chemistry and microstructure of any given mineral records a snapshot of the last interaction with migrating melt."

Line 464: Considering the absence of amphibole (line 439), could this be ruled out in the case of the oceanic samples in the study?

RG: The reviewer is correct as there is no amphibole in the samples we've examined, though amphibole is seen in other sections of the core including much lower in the core, i.e. not seawater infiltration. We believe the temperatures proposed for the ilmenite precipitation are too high for amphibole to be stable. We infer that amphibole would crystallise structurally higher in the core where temperatures were cooler. This is now made clear explicitly in Section 5.1.2. See R1_2 above for details.

Line 468: Early crystallization of oxides from a melt would cause Fe depletion early on in the liquid line of descent of basalts (e.g., MgO of 9 wt%). This is not observed in MORB that are reduced, and it is only observed in arc magmas that are oxidized. In the case of MORB, initial Fe- and Ti-enrichments due to magmatic differentiation (i.e., fractional crystallization of olivine, plagioclase, cpx) are required until the melt saturates in Fe-Ti oxides, so I am not sure how Fe-Ti-rich melts are not required in the scenario that the authors are envisioning, given absence of evidence for oxidized MORB.

RG: Thanks very much for this comment as it indicates the arguments for our proposed evolutionary model were not sufficiently clear. We believe there is some oxidation of the rocks seen in the core as magnetite has twice as much Fe3+ (the oxidating ion) as Fe2+ (the reducing ion). The melt we propose is not a large volume MORB creating pillow basalts at the surface of the oceanic ridge. Rather, it is a fractionated melt which is ascending in a highly localised manner by porous melt flow, i.e. following a grain boundary network in the oxide-rich sections of the oceanic crust. To clarify this, we have modified the discussion, Section 5.1.5 to include the current research on formation of an Fe-Ti-rich melt:

"Previous researchers have suggested Fe-Ti-rich melts (c.f. Zhang et al., 2020) as the source of iron and titanium for ilmenite and magnetite. However, the source of these Fe-Ti-enriched melts remains an issue. Koepke et al. (2005) found in one of 25 hydrous partial melting experiments using 735B

core gabbros that two immiscible melts formed, including a minor melt rich in REE, P, Zr, Ti and Fe with a larger volume of plagiogranitic melt. However, in agreement with our proposed model for an open system melt influx, Koepke et al. (2005) also found that an external source of titanium was required to form the oxides.

"Experiments have shown the onset of Fe-Ti oxide crystallisation in mafic magmas is marked on melt differentiation paths by strong depletion of FeO and TiO_2 in the melt, and early crystallisation of oxides. Crystallisation onset also has variable timing depending on the composition and conditions of the magma, including fugacity of oxygen (Toplis and Carroll, 1995) and concentration of volatiles (e.g., Botcharnikov et al., 2008). For example, water content of ~2% lowers the crystallisation temperature of clinopyroxene and olivine and promotes the early crystallisation of Fe-Ti oxides (Botcharnikov et al., 2008; Howarth et al., 2013) and 1% phosphorus can increase ilmenite precipitation (Toplis et al., 1994).

Natural examples of Fe-Ti-rich melts are rare. Clague et al. (2018) document an example of extreme fractionation of mid-ocean ridge basalt at Alarcon Rise where TiO_2 and FeO decrease, and titanomagnetite and ilmenite crystallise as the melts fractionate from andesite, through dacite to rhyolite. In addition, Charlier et al. (2010) hypothesise that ilmenite was the only mineral to crystallise at times during the evolution of the Allard Lake anorthositic system. However, from our study we suggest melt-rock interaction is the key mechanism to locally produce a near-liquidus oxide-saturated melt which drives oxide-forming reactions in the oceanic crust.

"We combine this concept of early crystallisation of Fe-Ti oxides at high temperature with a scenario of melt-buffered melt-rock interaction (Fig. 8a) and infer that a melt migrating with enhanced near liquidus oxide crystallisation conditions will destabilise silicates in favour of Fe-Ti oxides (reactions (2) and (3) above). In our model of melt-rock interaction (Fig. 8a), the stability of oxides over silicates drives reactions that consume silicate minerals and precipitate oxide minerals in an open system. The degree of oxide enrichment is proportional to the time integrated melt flux through the rocks (see Section 5.3). Our proposed migrating melt could form rare fractionated volcanic rocks as observed at Allarcon Rise (Clague et al., 2018)."

Line 504: I am not able to find a green arrow in fig. 4i

RG: No there were none – sorry. We've added some to 4h as they are easier to see in the image, and modified the reference to the figure appropriately.

Line 527, 560, 569: The inference of incremental crystallization of ilmenite and the migration of large volume of melt seems to hinge on the assumption that the infiltrating melt is an S-type granite that does not crystallize a significant amount of Fe-Ti oxides. If the infiltrating melt (e.g., melt 3) is an Fe-Ti rich melt, it may crystallize enough Fe-Ti oxides that such incremental crystallization may not be necessary.

RG: The assumption of S-type granitic melt was based on the other refs that suggested granitic melts in the Cattle Water Pass shear zones. Yes, the reviewer is correct, these could be Fe-Ti-rich melts, but the issue remains that the source of this Fe-Ti-rich melt is elusive. Our proposal of near-liquidus continuous precipitation of oxides as the melt passes through the rock is conceptually simple and avoids the need for this specialised melt source. To make this clearer we've added to section 5.2.3:

"We interpret melts 1, 2 and 3 (Fig. 8b, Eq. 4, 5 and 6) are likely to be very similar in composition and suggest that they are externally derived S-type granitic melts formed when sedimentary rocks equivalent to the Harts Range Group (Fig. 1a) partially melted. Previous studies have also shown

similar granitic melts fluxed through the nearby Gough Dam shear zone (Fig. 1b, Ghatak, 2021; Piazolo et al., 2020; Silva et al., 2021)."

See the reply to Reviewer 1 major comment 7.

References:

Bloomer, S.H., Meyer, P.S., Dick, H.J.B., Ozawa, K., Natland, J.H., 1991. 2. Textural and mineralogic variations in gabbroic rocks from hole 735B, in: Von Herzon, R.P., Fox, J., Palmer-Julson, A., Robinson, P.T. (Eds.), Proceedings of the International Ocean Drilling Program volume 118. International Drilling Program, Texas, pp. 21-39.

Botcharnikov, R., Almeev, R., Koepke, J., Holtz, F., 2008. Phase relations and liquid lines of descent in hydrous ferrobasalt—implications for the Skaergaard intrusion and Columbia River flood basalts. Journal of Petrology 49, 1687-1727.

Cannat, M., Mével, C., Stakes, D., 1991. 24. Normal ductile shear zones at an oceanic spreading ridge: tectonic evolution of site 735 gabbros (Southwest Indian Ocean), in: Von Herzon, R.P., Fox, J., Palmer-Julson, A., Robinson, P.T. (Eds.), Proceedings fo the Ocean Drilling Program, scientific results volume 118. Ocean Drilling Program, Texas, pp. 415-429.

Charlier, B., Namur, O., Malpas, S., de Marneffe, C., Duchesne, J.-C., Auwera, J.V., Bolle, O., 2010. Origin of the giant Allard Lake ilmenite ore deposit (Canada) by fractional crystallization, multiple magma pulses and mixing. Lithos 117, 119-134.

Clague, D.A., Caress, D.W., Dreyer, B.M., Lundsten, L., Paduan, J.B., Portner, R.A., Spelz-Madero, R., Bowles, J.A., Castillo, P.R., Guardado-France, R., 2018. Geology of the Alarcon Rise, Southern Gulf of California. Geochemistry, Geophysics, Geosystems 19, 807-837.

Dick, H.J.B., Kvassnes, A.J.S., Robinson, P.T., MacLeod, C.J., Kinoshita, H., 2019. The Atlantis Bank Gabbro Massif, Southwest Indian Ridge. Progress in Earth and Planetary Science 6, 64.

Dick, H.J.B., Meyer, P.S., Bloomer, S.H., Kirby, S.H., Stakes, D., Mawer, C., 1991. 26. Lithostratigraphic evolution of an in-situ section of oceanic layer 3, in: Von Herzon, R.P., Fox, J., Palmer-Julson, A., Robinson, P.T. (Eds.), Proceeding of the Ocean Drilling Program, Scientific Results Volume 118. Ocean Drilling Program, Texas, pp. 439-538.

Dick, H.J.B., Ozawa, K., Meyer, P.S., Niu, Y., Robinson, P.T., Constantin, M., Hebert, R., Maeda, J., Natland, J.H., Hirth, J.G., Mackie, S.M., 2002. 10. Primary silicate mineral chemistry of a 1.5-km section of very slow spreading lower ocean crust: ODP hole 735B, Southwest Indian Ridge, in: Natland, J.H., Dick, H.J.B., Miller, D.J., Von Herzon, R.P. (Eds.), Proceedings of the Ocean Drilling Program, scientific results volume 176. Ocean Drilling Program, Texas, pp. 1-61.

Ghatak, H., 2021. Deformation-assisted melt migration and melt-rock interaction during the intraconinental Alice Springs orogeny, central Australia, Faculty of Science and Engineering, Department of Earth and Environmental Sciences. Macquarie University,, Sydney, Australia, p. 218.

Hopkinson, L., Roberts, S., 1995. Ridge axis deformation and coeval melt migration within layer 3 gabbros: evidence from the Lizard Complex, U.K. Contrib Mineral Petrol 121, 126.

Howarth, G.H., Prevec, S.A., Zhou, M.-F., 2013. Timing of Ti-magnetite crystallisation and silicate disequilibrium in the Panzhihua mafic layered intrusion: Implications for ore-forming processes. Lithos 170-171, 73-89.

Koepke, J., Feig, S.T., Snow, J., 2005. Hydrous partial melting within the lower oceanic crust. Terra Nova 17, 286-291.

Lee, A.L., Torvela, T., Lloyd, G.E., Walker, A.M., 2018. Melt organisation and strain partitioning in the lower crust. Journal of Structural Geology 113, 188-199.

Meek, U., Piazolo, S., Daczko, N.R., 2019. The field and microstructural signatures of deformation-assisted melt transfer: Insights from magmatic arc lower crust, New Zealand. Journal of Metamorphic Geology 37, 795-821.

Piazolo, S., Daczko, N.R., Silva, D., Raimondo, T., 2020. Melt-present shear zones enable intracontinental orogenesis. Geology 48, 643-648.

Prakash, A., Piazolo, S., Saha, L., Bhattacharya, A., Pal, D.K., Sarkar, S., 2018. Deformation behavior of migmatites: insights from microstructural analysis of a garnet–sillimanite–mullite–quartz–feldspar-bearing anatectic migmatite at Rampura–Agucha, Aravalli–Delhi Fold Belt, NW India. Int J Earth Sci (Geol Rundsch).
Putnis, A., 2009. Mineral replacement reactions. Reviews in mineralogy and geochemistry 70, 87-124.
Rampone, E., Borghini, G., Basch, V., 2020. Melt migration and melt-rock reaction in the Alpine-Apennine peridotites: Insights on mantle dynamics in extending lithosphere. Geoscience Frontiers 11, 151-166.
Silva, D., Daczko, N.R., Piazolo, S., Raimondo, T., 2021. Glimmerite: a product of melt-rock interaction within a crustal-scale high-strain zone. Gondwana Research.
Stuart, C.A., Piazolo, S., Daczko, N.R., 2018. The recognition of former melt flux through high-strain zones. Journal of Metamorphic Geology 36, 1049-1069.
Toplis, M.J., Carroll, M.R., 1995. An Experimental Study of the Influence of Oxygen Fugacity on Fe-Ti Oxide Stability, Phase Relations, and Mineral—Melt Equilibria in Ferro-Basaltic Systems. Journal of Petrology 36, 1137-1170.
Toplis, M.J., Libourel, G., Carroll, M.R., 1994. The role of phosphorus in crystallisation processes of basalt: An experimental study. Geochimica et Cosmochimica Acta 58, 797-810.
Vernon, R.H., 2000. Review of Microstructural Evidence of Magmatic and Solid-State Flow. Vis Geosci 5, 1-23.
Zhang, W.-Q., Liu, C.-Z., Dick, H.J.B., 2020. Evidence for Multi-stage Melt Transport in the Lower Ocean Crust: the Atlantis Bank Gabbroic Massif (IODP Hole U1473A, SW Indian Ridge). Journal of Petrology 61.

Abstract

Processes that enrich rocks in oxides, such as ilmenite, are controversial. Current models include magmatic accumulation, crystallisation of veins from immiscible liquids and syntectonic differentiation. In this contribution, we investigate examples of oxide enrichment in both the oceanic and continental crust. The oceanic samples are of oxide gabbros (with up to 45 vol.% oxides) from the Atlantis Bank oceanic core complex, Southwest Indian Ridge. The continental sample is from the Cattle Water Pass shear zone (with up to 20 vol.% oxides) associated with the intracontinental Alice Springs Orogeny, central Australia. We argue for the occurrence of an open chemical system, with melt rock reactions as a key process involved in oxide enrichment in melt-fluxed shear zones. Our detailed microstructural characterisation reveals that oxides replace silicates and form interstitial grains, grain boundary films and low dihedral angles between silicates often making up an interconnected skeletal texture. Quantitative orientation data reveals that the oxides: 1) have limited internal deformation, 2) form clusters of grains that are connected in 3D, 3) have crystal faces matching the orientation of the grain boundary of nearby newly crystallised diopside (oceanic sample) and 4) form part of the foliation defining assemblage with biotite (continental sample). This evidence suggests the oxides crystallised in the presence of melt and formed during melt-rock interaction. Syntectonic melt migration is known to result in low strain microstructures in shear zones, as the strain is accommodated by the melt that existed in the deforming rock. This produces a high strain rock with silicate and oxide minerals that show limited internal deformation. Microchemical data shows major element variability in silicates and ilmenite at the thin section scale, supporting an open chemical system with local variability in both oceanic and continental settings. It further argues that syntectonic melt migration is important in oxide enrichment. Mineral chemistry data implies that the oceanic tectonic setting involved melt-rock interaction with fractionated gabbroic melt while the continental setting involved peraluminous granite melt driving mineral replacement and enrichment of oxides. We propose that deformation assisted

reactive porous flow of near liquidus melt through rocks in any tectonic setting may result in melt-rock interaction induced crystallisation of oxides in preference to silicates and that with high time-integrated melt flux, the accumulation of oxides can be significant.

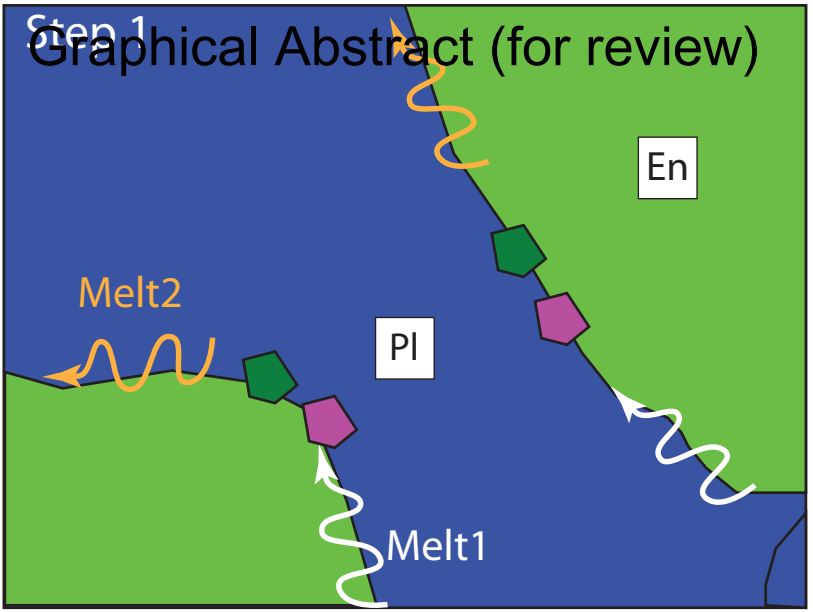

Infiltration of a fractionated gabbroic into an En-Pl-rich gabbro initiates melt-rock interaction → enriching rock in ilmenite

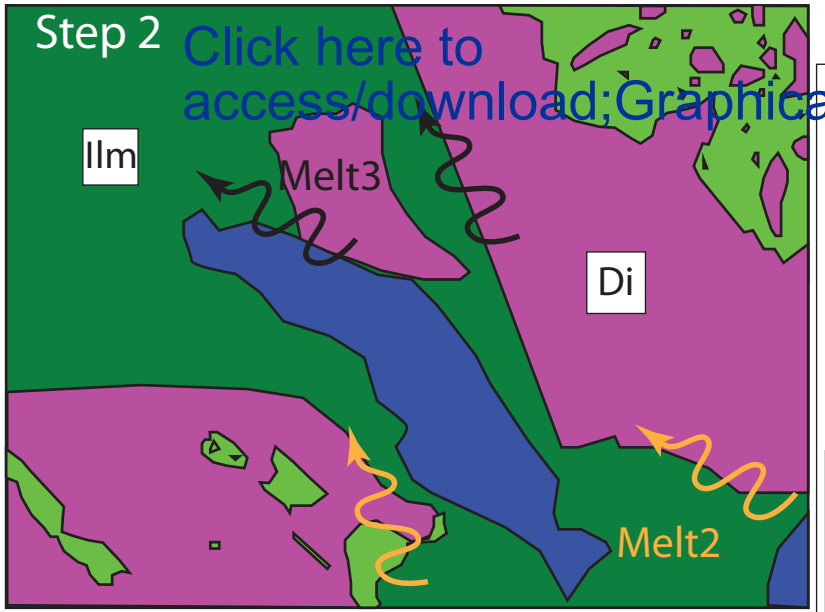

Modified melt causes further melt-rock interaction and further enriches the rock in ilmenite

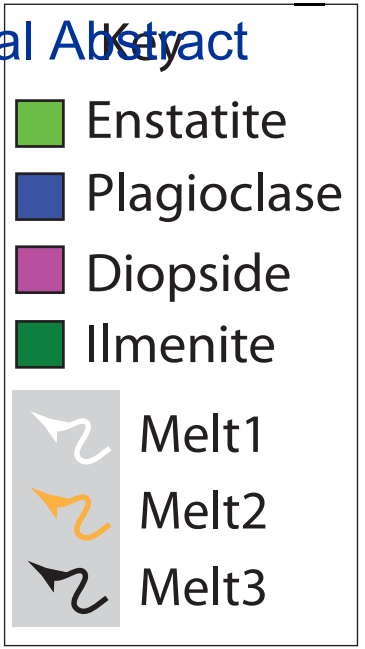

Highlights:

- Microstructures indicate former presence of melt within crustal shear zones
- Fractionated gabbroic melt interacts with oceanic crust to enrich oxides
- Peraluminous granite melt interacts with continental crust to enrich oxides
- High volumes of fluxing and reacting melt enrich host rock in oxides
- Multiple fluxes of external melt are associated with strain localisation

Oxide enrichment by syntectonic melt-rock interaction

Hindol Ghatak[1], Robyn L. Gardner[1], Nathan R. Daczko[1], Sandra Piazolo[2], Luke Milan[3]

[1]Australian Research Council Centre of Excellence for Core to Crust Fluid Systems/GEMOC, Department of Earth and Environmental Sciences, Macquarie University, NSW 2109, Australia

[2] School of Earth and Environment, University of Leeds, Leeds LS2 9JT, United Kingdom

[3] Earth Sciences, School of Environmental and Rural Science, The University of New England, Armidale, NSW, 2351, Australia

*corresponding author: robyn.gardner@mq.edu.au Phone: 61-2-9850 8371

Abstract

Processes that enrich rocks in oxides, such as ilmenite, are controversial. Current models include magmatic accumulation, crystallisation of veins from immiscible liquids and syntectonic differentiation. In this contribution, we investigate examples of oxide enrichment in both the oceanic and continental crust. The oceanic samples are of oxide gabbros (with up to 45 vol.% oxides) from the Atlantis Bank oceanic core complex, Southwest Indian Ridge. The continental sample is from the Cattle Water Pass shear zone (with up to 20 vol.% oxides) associated with the intracontinental Alice Springs Orogeny, central Australia. We argue for the occurrence of an open chemical system, with melt rock reactions as a key process involved in oxide enrichment in melt-fluxed shear zones. Our detailed microstructural

characterisation reveals that oxides replace silicates and form interstitial grains, grain boundary films and low dihedral angles between silicates often making up an interconnected skeletal texture. Quantitative orientation data reveals that the oxides: 1) have limited internal deformation, 2) form clusters of grains that are connected in 3D, 3) have crystal faces matching the orientation of the grain boundary of nearby newly crystallised diopside (oceanic sample) and 4) form part of the foliation defining assemblage with biotite (continental sample). This evidence suggests the oxides crystallised in the presence of melt and formed during melt-rock interaction. Syntectonic melt migration is known to result in low strain microstructures in shear zones, as the strain is accommodated by the melt that existed in the deforming rock. This produces a high strain rock with silicate and oxide minerals that show limited internal deformation. Microchemical data shows major element variability in silicates and ilmenite at the thin section scale, supporting an open chemical system with local variability in both oceanic and continental settings. It further argues that syntectonic melt migration is important in oxide enrichment. Mineral chemistry data implies that the oceanic tectonic setting involved melt-rock interaction with fractionated gabbroic melt while the continental setting involved peraluminous granite melt driving mineral replacement and enrichment of oxides. We propose that deformation assisted reactive porous flow of near liquidus melt through rocks in any tectonic setting may result in melt-rock interaction induced crystallisation of oxides in preference to silicates and that with high time-integrated melt flux, the accumulation of oxides can be significant.

Highlights:

- Microstructures indicate former presence of melt within crustal shear zones
- Fractionated gabbroic melt interacts with oceanic crust to enrich oxides
- Peraluminous granite melt interacts with continental crust to enrich oxides
- High volumes of fluxing and reacting melt enrich host rock in oxides

- Multiple fluxes of external melt are associated with strain localisation

Keywords:

Scientific ocean drilling; oceanic core complex; intracontinental orogeny; melt microstructures; melt-present deformation; oxide enrichment.

1. Introduction

Titanium, a critical industrial metal, is predominantly sourced from rutile and ilmenite in mineral sands (Roy et al., 2000), which have weathered from igneous or metamorphic rocks. Besides mineral sands, hard rock Fe-Ti oxide-rich deposits of magmatic origin like Allard Lake, Canada and Tellnes, Norway have been mined for years (Charlier et al., 2010). For titanium to become an economic resource, it needs to be enriched as the average crustal abundance is < 1% TiO_2 but concentrations > 2 % are needed for viable mining (Woodruff et al., 2017). Thus, it is crucial to understand the primary mechanism of Fe-Ti oxide deposit formation. However, the processes responsible for Fe-Ti oxide enrichment remain controversial. Proposed processes include: (i) formation of oxide cumulate layers (Duchesne and Charlier, 2005) through density-driven mineral settling, (ii) crystallisation from immiscible liquids forming ore-rich veins (e.g. Dixon and Rutherford, 1979; Holness et al., 2011), and (iii) crystallisation during syntectonic differentiation (Agar and Lloyd, 1997; Dick et al., 1991; Hopkinson and Roberts, 1995), where fractionated intercumulus melt is mobilised into shear zones by deformation and compaction (Bloomer et al., 1991).

In this study, we focus on the syntectonic differentiation model which is based on observations from shear zones in oceanic gabbros that are enriched in oxides (Robinson et al., 2000). However, oxide enrichment associated with shear zones is not restricted to the oceanic crust alone. Geologists have documented several locations within the continental crust where similar oxide enrichment is associated

with high strain zones (Emslie et al., 1994; Gross et al., 1995; Scoates and Chamberlain, 1997). The latter may be an important source for the Fe-Ti sands mined worldwide.

Despite the potential importance of Fe-Ti oxide enrichment in shear zones, there is relatively little work on the processes associated with this mineralisation. For the gabbroic rocks in oceanic settings, two key petrogenetic models relative to the timing of oxide crystallisation, deformation and strain localisation have been proposed: (1) oxides were concentrated by igneous processes of magmatic accumulation or immiscibility processes prior to strain localisation and the formation of shear zones (Cannat et al., 1991), or (2) strain localisation formed a shear zone in oxide-poor gabbro and was followed by metamorphic processes including melt-rock reactions and oxide crystallisation during deformation-assisted diffuse porous melt flow through the shear zone, called syntectonic differentiation (Bloomer et al., 1991; Dick et al., 1991; Hopkinson and Roberts, 1995).

These two petrogenetic models result in the formation of rocks with distinct igneous versus metamorphic microstructures. Igneous processes crystallise minerals directly from a melt whereas metamorphic processes modify these igneous minerals by reactions with a fluid, and/or in response to temperature or pressure changes. In the first model indicative microstructures would be predominantly of igneous origin and include euhedral to subhedral crystals with interlocking and interstitial microstructures with possibly a magmatic foliation. In this scenario, we would expect a typical igneous crystallisation sequence, where both ilmenite and magnetite crystallise from the fractionating melt. In the second model, indicative microstructures would be predominantly metamorphic in origin and include, interstitial microstructures, fewer crystal faces, melt-rock reaction textures and possibly the absence of typical mylonitic shear zone characteristics (Lee et al., 2018; Meek et al., 2019; Prakash et al., 2018; Stuart et al., 2018b).

Consequently, the microstructural characteristics of the minerals in oxide-rich rocks are key to distinguish between these two scenarios. In addition, in model (1), deformation microstructures will be evident in both the silicate and oxide minerals. In contrast, melt accommodates stress during melt-present deformation in model (2); consequently, the solid framework will remain generally undeformed.

To elucidate the processes associated with oxide enrichment in high strain zones, we investigate oxide enrichment in two contrasting environments: oxide-rich gabbros associated with shear zones within an oceanic core complex, and oxide-biotite-rich schist belts from central Australia. Our research is at the interface between igneous and metamorphic systems and involves reactive flow of melt through crustal rocks driving metamorphic reactions.

We use detailed microstructural and microchemical analyses to recognise microstructures indicative of the former presence of melt. We determine that flux of externally derived melts caused melt-rock interactions to form new minerals, including oxides, in reaction textures in both oceanic and continental crust. Melt present shear zone activity is supported by the fact that minerals identified as solid during syntectonic melt migration remain largely undeformed, as the viscous melt accommodates much of the strain (Stuart et al., 2018b). Consequently, our data supports the syntectonic differentiation model facilitated by reactive porous melt flow as outlined above, in both the oceanic and continental settings.

2. General geological background

2.1. Oceanic environment: Atlantis Bank

The Atlantis Bank oceanic core complex is a ridge 720 m below the sea surface approximately 9 km long and 4 km wide situated south-east of Madagascar (Fig. 1a and inset) on the ultra-slow spreading Southwest Indian Ridge (SWIR). It is adjacent to the Atlantis II transform valley and ~19 km south of the SWIR axis. Pillow basalts and sheeted dykes typically found at the top of oceanic crust are missing

suggesting an estimated 1.5–2.0 km of the crust has been unroofed during core complex uplift on the detachment fault (Dick et al., 2000; Dick et al., 1999a; John et al., 2004), thereby exposing massive gabbro at the seafloor. The 735B (32°43.392'S, 57°15.960'E) core was initially drilled to 500 mbsf on IODP expedition 118, then subsequently drilled to 1508 mbsf on IODP expedition 176 (Dick et al., 1999a).

The following core summary is based on information in Dick et al. (1999a), unless otherwise specified. The core is divided into 12 rock units (I – XII) based on mineral assemblage and rock type. The major rock types in the core are olivine gabbro (69.9%) and gabbro (14.9%), with lower proportions of oxide-rich gabbro (7%) and gabbronorite/oxide-rich gabbronorite (8%). Rock units can be further simplified (Dick et al., 2002; Hertogen et al., 2002) into (1) oxide-poor gabbro cut by hundreds of bodies of (2) oxide-rich gabbro (including both disseminated oxide gabbro and oxide gabbro) (Fig. 1ci). The oxides in the oxide-rich rocks have oxide modes to 45% and are predominantly magnetite and ilmenite with minor presence of sulphides. High titanium concentrations (Fig. 1c(iii)), generally in the form of ilmenite are typical of the oxide-rich gabbros. The core is variably deformed with the extent of crystal-plastic deformation being classed based on observed foliation, recrystallisation and preservation of relict igneous texture (Fig.1c(ii), Dick et al., 2019). Overall, three-quarters of the core lacks a foliation, 18% has a very weak foliation, 6% is strongly foliated and only 1% has mylonitic or ultra-mylonitic characteristics. The upper half of the core has many minor faults with major brittle faults of unknown displacement occurring at 560 and 690–700 mbsf (Fig. 1c(i), yellow dashed lines). A 20 m wide shear zone occurs lower in the core at 944–964 mbsf (Fig. 1c(i), white dashed lines). High strain zones, particularly those in the top half of the core, are often associated with high oxide abundance (Fig. 1c (i) and (ii)), though this is not always the case. Plagioclase compositions are bimodal with oxide-rich gabbros having generally lower X_{An} values (Fig. 1c(iv)). Evidence of melt-rock interaction within shear zones at Atlantis Bank has been previously reported by Gardner et al. (2020) and Zhang et al. (2020). Higher temperature deformation and melt-

rock interaction are variably overprinted in the top half of the core by seawater infiltration, brittle deformation and hydrothermal alteration as the rocks were exhumed and cooled. The whole-rock TiO_2 vs Fe_2O_3 plot (Fig. 1b) of oceanic gabbros shows extensive variation of iron and titanium, though a general positive correlation is formed (Fig. 1b, grey arrow). Core 735B samples follow the same general trend.

For this study, we examined two adjacent oxide gabbro samples from unit IV at ~228 mbsf of the 735B core (Fig. 1d). This unit is within the upper half of the core (units I to IX) which is distinguished from the lower half (units X to XII) by higher proportions of oxide-rich gabbros (Fig. 1c(i)) and a weak foliation. However, the boundary between units III and IV (at 224 mbsf) is a <1 m thick mylonitic shear zone. The two oxide-rich gabbro samples are taken within 4 m of this mylonitic shear zone.

2.2. Continental environment: The Alice Springs Orogeny – Cattle Water Pass Shear Zone

The study area lies in the central Australian Arunta region (Fig. 2a, top) where the last regional tectono-metamorphic event was the Upper Palaeozoic (450–300 Ma) Alice Springs Orogeny (ASO) (Hand and Sandiford, 1999; Raimondo et al., 2014). The intraplate nature of the ASO involved N-S contraction (Piazolo et al., 2020; Silva et al., 2018; Teyssier, 1985) which resulted in the exhumation of mid to deep crustal rocks and the formation of anastomosing shear zones (Cartwright et al., 1999; Raimondo et al., 2011). The orogen (Fig. 2a, bottom) comprises, from W to E, amphibolite facies mid-crustal rocks, the mid to deep crustal Strangways Metamorphic Complex (SMC) and the deep crustal inverted rift-fill Harts Range Group.

The SMC is a broad belt, up to ~ 125 km wide, metamorphosed during the Strangways Event (c. 1735-1690 Ma) cut by schist belts with general S-directed thrusting (Bendall, 2000; Collins and Teyssier, 1989) in the southern side of the orogen (Fig. 2a). The shear zone examined here is the Cattle Water Pass

shear zone (Fig. 2b) which was melt-present at the time of deformation (Silva et al., 2021). The high strain zones within the Cattle Water Pass shear zone are 100–300 m wide, steeply west-dipping, with reverse shear sense and characterised by sillimanite-garnet-muscovite-biotite schist. The schists cut Proterozoic mafic, felsic, and pelitic granulites resulting in lenses of variably deformed and modified granulite within high strain zones dominated by schist. Deformed and hydrated granulite contains anastomosing layers rich in biotite ± muscovite where sub-layers rich in ilmenite are also common.

3. Method of analysis

3.1. Petrography and quantitative orientation analysis

Sample mineral observations were made on polished thin sections cut in the structural XZ plane using a petrographic microscope. Microstructural/crystallographic characterisation of thin sections was performed both in the Leeds Electron Microscopy and Spectroscopy Centre, University of Leeds and at Macquarie GeoAnalytical, Macquarie University. The data was acquired using an FEI Quanta 650 FEG-Environmental Scanning Electron Microscope and a Zeiss IVO Scanning Electron Microscope, respectively. Both instruments were equipped with an HKL NordlysNano Electron backscatter diffraction (EBSD) detector and supported by Aztec analysis software (Oxford Instruments). EBSD mapping was performed covering a large area of the thin section in addition to small individual maps in specific regions, recording Energy Dispersive Spectroscopy (EDS) spectra along with the EBSD data. Working conditions were: 20 kV accelerating voltage, 20–26 mm working distance, 70° specimen tilt and step size between 4 and 10 µm depending on the area covered and grain size. Data were processed using HKL Channel5 v5.11 and AztecCrystal with noise reduction performed on the raw data following the procedure of Piazolo et al. (2006). Wherever necessary, pole figure representations use one point per grain to eliminate the issue of large grains distorting the interpretation by causing single-crystal maxima.

178 Where there is no dominance of individual grains, all data points have been plotted. We also show maps
179 depicting the relative change in crystal orientation within grains as a graded colour scale overlay on the
180 phase maps and pole figures. Misorientation angles between adjacent analysed points of 2–10° and ≥
181 10° define subgrain and grain boundaries, respectively. We use mineral abbreviations following Whitney
182 and Evans (2010).

183 A high resolution image of the thin sections and other associated data can be examined at
184 https://imagematrix.science.mq.edu.au/viewer/?mode=view&id=487 for 47R2-1, id=488 for 47R2-3 and
185 id=443 for CP1604C.

186 *3.2. Imaging and geochemical analysis*

187 *3.2.1. Micro X-ray fluorescence (µ-XRF)*

188 Analyses of the polished thin sections were used for mineral identification, to show the spatial
189 distribution of oxide minerals and to calculate modal percentages of oxide minerals. µ-XRF analyses
190 were performed using a Bruker M4 Tornado spectrometer at Macquarie GeoAnalytical, Macquarie
191 University. The µ-XRF analyses were run with tube voltage of 50 kV, beam current of 200 µA, chamber
192 pressure of 20 mbar, acquisition time of 15 ms/pixel and step size of 25 µm. Bruker AMICS (Advanced
193 Mineral Identification and Characterisation System) was used to convert the X-ray fluorescence spectra
194 to produce detailed mineral maps.

195 *3.2.2. Backscatter electron imaging (BSE)*

196 Scanned BSE images were used to identify and show the association of different minerals across the
197 samples. Polished thin sections were carbon coated and imaged in an FEI Teneo Field Emission Scanning
198 Electron Microscope (SEM) with Nanomin software at Macquarie GeoAnalytical, Macquarie University.
199 The operating conditions of the SEM were high vacuum at 10kV with a dwell time of 2 µs.

3.2.3. Electron microprobe (EMP)

Additional compositional data of both the silicates and oxides was obtained for the sample from central Australia (CP1604C) using a JEOL JXA 8530F Plus field emission electron microprobe at the Central Science Laboratory, University of Tasmania. The instrument has a field emission source, running at an accelerating voltage of 15 kV, a beam current of 15 nA and a spot size of 10 µm. The ODP samples (47R2-1 and 47R2-3) were analysed using a Cameca SX-100 electron microprobe at Macquarie GeoAnalytical, Macquarie University. The operating conditions were a voltage of 15 kV, a beam current of 20 nA and a spot size of 1 µm. Standards used for calibration are included in Supplementary Table 4. Electron microprobe maps of the minerals were acquired using the Cameca SX-100 electron microprobe at Macquarie GeoAnalytical, Macquarie University. The element maps show the chemical variation within specific grains of interest and were collected with a focused beam of 15 kV, beam current of 100 nA, spot size of 1 µm, step size of 4 µm and dwell time of 100 ms.

3.3. Micro-computed tomography (micro-CT)

Micro-CT analysis of the high-oxide gabbro was undertaken in a GE Phoenix V|tome|xs CT scanner at The University of New England, Australia. The block was rotated about its vertical axis and scans were taken in 3 perpendicular directions. Scanning was performed at voltage of 220 kV and current of 70 µA for 200 ms for each scan. Individual sections were extracted and processed in '3D slicer' software (https://www.slicer.org/, Fedorov et al., 2012). Oxide 3D models were made using the density data and Meshlab (Cignoni et al., 2008) was used to highlight the microstructures and oxide 3D connectivity.

4. Results

4.1. General sample description and petrography

4.1.1. Oceanic environment

The investigated samples exhibit moderate (15 vol.%; 47R2-3) to very high (44 vol.%; 47R2-1) modes of ilmenite and magnetite. Both samples are coarse-grained and comprise plagioclase (~18–21 vol.%), diopside (~27–52 vol.%), enstatite (~5–8 vol.%), ilmenite (~13–38 vol.%) and magnetite (~1–6 vol.%) with minor amphibole, sulphides, apatite, and spinel (Fig. 3a–h). Silicates generally lack evidence of crystal-plastic deformation such as bimodal grain size distribution (a signature of dynamic recrystallisation), undulose extinction or deformation twins (Fig. 3b, f). The oxide grains form a network of interconnected grains (Fig. 3c, g, 4l-n). Sample 47R2-3 exhibits 15 vol.% oxides dominated by ilmenite, while 47R2-1 has 44 vol.% oxides with a mix of ilmenite and magnetite (Fig. 3d, h).

Oxide grains show highly irregular shapes with elongate finger-like protrusions that cut into grains of plagioclase (Fig. 4a, d; yellow arrow) and diopside (Fig. 4e; blue lines, yellow arrow), as well as along like and unlike mineral boundaries (Fig. 4b, d, e, f, l, m, red arrows). The oxide-rich domains form skeletal-like textures around silicate grains (Fig. 4e), and the domains are connected in three-dimensions by oxide bridges (Fig. 4l-n, red arrows). These domains preserve low dihedral angles against two adjoining diopside grains (Fig. 4e, f, n, green arrow). Some ilmenite grains appear as inclusions in diopside (Fig. 4f; white arrow), while other ilmenite-magnetite domains show straight faces against diopside (Fig. 4b; yellow line). Ilmenite grain boundaries with plagioclase tend to be more irregular (Fig. 4f; yellow lines). Ilmenite is commonly associated with magnetite in the high oxide content sample (47R2-1), where magnetite is mostly observed at the boundary of ilmenite with other minerals (Fig. 4e–g; green dashed line shows ilmenite-magnetite boundaries). The magnetite has a dusty appearance in BSE images (Fig.

4e–g) due to very fine inclusions of spinel and ilmenite and forms some lobate and finger-like shapes within the ilmenite. The inclusions in magnetite show three preferred orientations (Fig. 4g, inset (i), red lines). Ilmenite commonly lacks inclusions except at the boundaries between ilmenite and magnetite, where fine spinel grains are included in the ilmenite (Fig. 4g, inset (ii)). Diopside appears in two textural settings: (i) as large single grains (Fig. 4c, e, f) and (ii) as rims of diopside around two-pyroxene domains where the proportions of enstatite and diopside are variable (labelled En-Di symplectite on Fig. 4b–d). Neighbouring fine and coarse enstatite grains share similar interference colour under crossed polarised light (orange arrows, Fig. 4c), indicating similar orientation. Fingers of diopside project into enstatite with low dihedral angles (green arrow, Fig. 4c). The finger shown in Figure 4c shares extinction positions with a diopside inclusion within the enstatite (inset Fig. 4c, purple arrow). Plagioclase forms large single grains (Fig. 3f, 4a, d) which rarely show deformation microstructures (e.g., undulose extinction, deformation twins, dynamic recrystallisation). Rare grains of plagioclase are cut by veins of very fine grained green hornblende (Fig. 4a).

4.1.2. Continental environment

The high-strain continental CWP shear zone sample is a fine- to medium-grained rock with a well-developed foliation defined by bands of variable ilmenite content and alignment of biotite and ilmenite minerals. It exhibits two distinct bands based on minerals present: (i) quartz-plagioclase-rich, and (ii) garnet-biotite-ilmenite-rich bands (Fig. 3i). The quartz-plagioclase-rich, low-oxide domain comprises quartz (~45–50 vol.%), plagioclase (~25–30 vol.%), biotite (~10–15 vol.%), garnet (~3–5 vol.%), and minor ilmenite (~2 vol.%) (Fig. 3i–l, bottom). The high-oxide (ilmenite) domain comprises garnet (~25–30 vol.%), biotite (~45–50 vol.%), ilmenite (~16-18 vol.%), and minor apatite (<2 vol.%) (Fig. 3i–l, top). The silicates generally lack evidence of crystal-plastic deformation such as recrystallisation, undulose extinction or deformation twins (Fig. 3j).

Oxide grains form interstitial textures with elongate grain shapes along grain boundaries (Fig. 4h, i; red arrows). The oxide grains show both straight (Fig. 4h, j; yellow lines) and irregular (Fig. 4h–k; yellow arrows) boundaries with garnet and biotite. Some ilmenite grains form lobes (Fig. 4i; yellow arrows) or inclusions (Fig. 4k; white arrow) in garnet, while others have shapes and sizes similar to garnet (Fig. 4j; blue arrow).

4.2. Quantitative orientation data (EBSD analysis)

EBSD analysis is used mainly to identify (i) interconnectivity of interstitial phases in three dimensions, (ii) relationships between grain shape and crystal orientation (e.g., identification of faceting) and (iii) presence of internal deformation features (e.g., sub-grains and crystallographic orientation variations) which are signatures of dynamic recrystallisation and crystal plasticity. The assessment of interconnectivity of interstitial phases assumes that in the two-dimensional section of a thin section, grains that are spatially close to each other but not connected to each other, are interconnected in three dimensions if they exhibit the same or very similar crystallographic orientation (Meek et al., 2019).

4.2.1. Oceanic environment

A single area of EBSD phase map with orientation overlays is presented as representative for oxide-rich sample 47R2-1 from the oceanic gabbros (Fig. 5). The map shows two two-pyroxene (enstatite-diopside) domains (Fig. 5a, upper right, lower left) with a distinct diopside rim on the upper right domain. Between the two domains there are grains of plagioclase, ilmenite and magnetite. Most ilmenite grains show only minor internal deformation based on few 2–10° subgrain boundaries (Fig. 5a, b, white lines) and minor changes in internal orientations across a grain (grain I3, Fig. 5b, green overlay, 0–10°, and misorientation profile). The diopside rim shares a straight grain boundary with an oxide rich domain (Fig. 5c). The orientation of the diopside boundary (red line, Fig. 5c) corresponds to the crystal face of the adjacent relict ilmenite, I1, (Fig. 5c, red line, ilmenite {10-10} pole figure). Rare grains of ilmenite and

most grains of diopside and enstatite show no internal deformation (i.e., have few white lines on Fig. 5a, c, d).

Small diopside grains within enstatite in the two-pyroxene domain (Fig. 5a, top right) share the same crystallographic orientation with the wide diopside rim (Fig. 5c, grain D1, Euler map and pole figure). The coarse grained diopside rim shows very little crystallographic orientation change across the grain (Fig. 5c, grain D1, misorientation profile). A cluster of enstatite grains, E1, is present at the boundary between two diopside grains forming the diopside rim (Fig. 5c, grains D1 and D2). These enstatite grains show similar orientations to each other (green in Fig. 5d;) and a c axis orientation similar to the two diopside rim grains (compare pole figures; Fig. 5c, d, grains E1, D1 and D2). The cluster of diopside grains (Fig. 5c, grain D2) share the same crystallographic orientation with each other, so are likely to be interconnected in 3D. In the area dominated by oxides (upper left of Fig. 5a), a cluster of ilmenite grains included within magnetite show similar orientation (Fig. 5b, grains marked I3), so are also likely connected in 3D, but the adjacent ilmenite and surrounding magnetite do not share a similar orientation.

4.2.2. Continental environment

A single large area EBSD phase map with orientation overlays is presented for the high-oxide domain of sample CP1604C from the Cattle Water Pass shear zone (Fig. 6). The map shows most oxide grains lack significant internal orientation changes, exhibit a limited number of subgrain boundaries (Fig. 6a, b) and have little variation in the orientation across individual grains (Fig. $6b_1$, misorientation profile). Two clusters of ilmenite grains (Fig. 6b, I1 and I2) show similar orientation based on Euler orientation maps and a c-axis pole figure. Garnet grains also show very little orientation change within individual grains (Fig. $6c_1$) while clusters of adjoining grains have very similar orientation (Fig. 6c, Euler map and pole figure). Clustered c-axis orientations with a maximum of 10 for all ilmenite grains (Fig. 6d) indicate a

strong crystallographic preferred orientation (CPO) that matches the strong c-axis alignment of biotite grains (Fig. 6f). In contrast, garnet presents no pronounced CPO (Fig. 6e).

4.3. Mineral chemistry data

All silicate minerals in all samples show limited chemical variation (Fig. 7; Supplementary Table 1). This is also apparent in microprobe chemical maps (Supplementary Figure 1) which show remarkably uniform compositions for each grain. Below we present the detailed mineral chemistry.

4.3.1. Oceanic environment

Plagioclase in ODP high oxide sample 47R2-1 is andesine of restricted composition (X_{An} = Ca/(Ca+Na+K) = 0.37–0.40) (Fig. 7a), typical of plagioclase compositions in most oxide-rich gabbro in the core (Fig. 1c(iv)). Diopside has the most variability from predominantly diopside to minor augite (X_{Mg} = Mg/(Mg+Fe) = 0.61–0.71) (Fig. 7a). Enstatite composition has little variability (X_{Mg} = 0.60–0.61) (Fig. 7a). Ilmenite grains in the two ODP samples show minor variation in TiO_2 content but increasing FeO and MgO (Fig. 7b, c) and decreasing MnO (Fig. 7d) as the proportion of oxides increased between sample 47R2-3 (low-oxide sample) to 47R2-1 (high-oxide sample).

4.3.2. Continental environment

Plagioclase in sample CP1604C is andesine of restricted composition (X_{An} = 0.43–0.47) with two analyses of lower anorthite content (X_{An} = 0.23 and 0.33) (Fig. 7a). Garnet is almandine (X_{Alm} = Fe/(Fe+Mg+Ca+Mn) = 0.78–0.82) with substantial pyrope (X_{Pyr} = Mg/(Fe+Mg+Ca+Mn) = 0.14–0.18) and minor grossular (X_{Grs} = Ca/(Fe+Mg+Ca+Mn) = 0.01–0.06) and spessartine (X_{Sps} = Mn/(Fe+Mg+Ca+Mn) = 0.03;) components (Fig. 7a). Biotite is Fe-Mn-rich and plots at the boundary between 'primary magmatic' and 're-equilibrated' biotite on the classification scheme of Nachit et al. (2005) (X_{Mg} = 0.46–0.51). In contrast to the ODP samples, ilmenite grains from Cattle Water Pass vary from 42–47 wt.% TiO_2 but show very limited variation in MgO, FeO and MnO content (Fig. 7b–d).

5. Discussion

We argue for the occurrence of an open chemical system maintained by syntectonic porous melt flow, with melt rock reactions as a key process involved in oxide enrichment in melt-fluxed shear zones. In the following discussion we provide evidence for a metamorphic rather than igneous origin of the oxides and show, using microstructures, that the oxide-rich rocks investigated formed in the presence of a reactive melt. Based on mineral chemistry and the regional tectonic setting of the rocks investigated we infer a fractionated gabbroic melt as the main reactant in the oceanic setting and a high temperature peraluminous granitic melt in the continental setting. We conclude the discussion by assessing the signatures and consequences of syntectonic reactive porous melt flow in crustal environments.

5.1. The origin of oxide-rich rocks in oceanic tectonic settings

The two key petrogenetic models, described in the introduction, result in the formation of rocks with distinct igneous versus metamorphic microstructures. In the second model described, oxide enrichment occurs via melt-rock metamorphic reactions during deformation-assisted melt flow through a shear zone (Bloomer et al., 1991; Dick et al., 1991; Hopkinson and Roberts, 1995). Indicative microstructures include some internal deformation within grains, interstitial microstructures, replacement reaction microstructures and fewer crystal faces.

5.1.1. Microstructures showing metamorphic replacement reactions

Although ilmenite and magnetite are spatially associated (e.g. Fig. 4e to g) we interpret earlier ilmenite is partially replaced by magnetite based on the following observations: (1) the proportion of ilmenite to magnetite increases from the low oxide sample 47R2-3 (ilmenite to magnetite proportions 9:1), to the high oxide sample 47R2-1(ilmenite to magnetite proportions of 7:1) (Fig. 3h); (2) presence of irregular boundaries between ilmenite and magnetite including finger-like protrusions of magnetite into ilmenite (Fig. 4g); (3) presence of magnetite as rims on ilmenite and as elongate grains at boundaries between

ilmenite and silicate minerals (Fig. 4e, f, 5a; e.g., plagioclase and diopside); (4) presence of a cluster of irregular ilmenite grains within magnetite that share identical orientation which represent relicts of a partially replaced single coarse crystal of ilmenite (Fig. 5b, I3); (5) presence of reaction front microstructures where spinel grains are included in ilmenite near the boundaries with magnetite (Fig. 4g(ii), Supplementary Fig. 1f; Bowles et al., 2011); and (6) straight boundaries between new diopside (red line, Fig. 5c) and magnetite that mimic crystal facets of relict ilmenite (Fig. 4c, ilmenite pole figure, grain I1), indicating the original ilmenite crystal face grew into a melt (Vernon, 2000). In addition, fine grained spinel and ilmenite included within magnetite show three different crystallographic orientations and are interpreted as exsolution microstructures which formed during cooling (Fig. 4g(i)). Adjacent to the magnetite replacement texture shown in Figure 5a, the diopside (Fig. 5c, grain D1) is partially replaced by a new diopside (Fig. 5c, grain D2) with enstatite (Fig. 5d, grain E1) that is epitaxial on the old diopside (Fig. 5c, d). We interpret these to have formed coevally with the partial replacement of ilmenite by magnetite (Fig. 8a).

In addition to the reaction microstructures associated with magnetite as outlined above, we observe other evidence of metamorphic reactions that involve pyroxenes. A cluster of enstatite grains (orange arrows, Fig. 4c) shares very similar interference colours and extinction angles, suggesting that they formed a single relict enstatite grain partially replaced by the diopside. This is further supported by the finger of diopside projecting into and replacing the coarse enstatite (green arrow, Fig. 4c). The proportion of enstatite is higher in the lower left and lower in the upper right of Figure 4c, consistent with the progressive replacement of enstatite by diopside (Fig. 8a). This reaction replacement microstructure is confirmed by diopside in both the rims around two-pyroxene domains and all the diopside within the two-pyroxene domain sharing a single crystallographic orientation (Fig. 4b, 5c, grain D1), and mineral chemistry (Supplementary Fig. 1e). However, the two-pyroxene domains have previously been interpreted as inverted pigeonite that has rims of later diopside (Dick et al., 1991;

Ozawa et al., 1991). We argue against this as the diopside rim is crystallographically continuous with the diopside in the two-pyroxene domain. Additionally, the elongation of the diopside grains within the two-pyroxene domains is not oriented parallel to either enstatite (001) or (100) as would be expected for inverted pigeonite (Philpotts and Ague, 2009).

The diopside rims around two-pyroxene domains are spatially associated with high proportions of oxides (e.g., Fig. 4b, d, Supplementary Fig. 1e). The oxide grains share some straight boundaries with the diopside rims (e.g., yellow line on Fig. 4b corresponds with an ilmenite {10-10} crystal face, Fig. 5c), suggesting the original ilmenite crystal face grew into a free melt and the diopside rim crystallised later. The oxide grains commonly form films along grain boundaries (Fig. 4, red arrows) and protrusions into plagioclase grains (Fig. 4, yellow arrows). These observations of disequilibrium microstructures are consistent with progressive reaction from the original igneous olivine gabbro to melt-reaction-modified oxide-rich gabbros.

5.1.2. Former presence of melt and inferred melt-rock reactions

Early research on the oceanic crust drilled at hole 735B inferred melt migration as an important process in the development of the microstructures observed in gabbroic samples (Dick et al., 1991). Recent works have further established multiple fluxes of external melt through shear zones (Casini et al., 2021; Gardner et al., 2020; Zhang et al., 2021; Zhang et al., 2020). The flux of a high temperature hydrous fluid is not considered likely as the samples examined lack evidence of hydrous minerals such as chlorite, epidote, sericite replacing feldspar, or veins of these minerals and preservation of reaction textures where igneous minerals are partially consumed. However, these microstructures are documented elsewhere in the core, suggesting that hydrous fluids are important agents of metamorphism in other sections of the core. Further support for the presence of melt instead of a hot hydrous fluid is the lack of amphibole in our samples. This lack of amphibole suggests either the presence of melt with low activity

of water during melt-rock interaction or that the temperature of fluid-rock interaction was higher than the stability field of amphibole.

Microstructures indicative of the former presence of melt (Holness et al., 2011; Lee et al., 2018; Stuart et al., 2018b; Vernon, 2000) in the oceanic rocks confirm previous research; they include: (1) films along grain boundaries forming skeletal-like microstructures (Fig. 3g, 4e), with or without crystal faces (Fig. 4b, yellow line, Fig. 5a), (2) grains with low dihedral angles (Fig. 4e, f, green arrows), and (3) 3D connectivity of a cluster of grains (Fig. 5b, c, d). A lack of local partial melting textures (e.g., peritectic minerals surrounded by leucosome) suggests the melt was externally derived, resulting in sequential rock transformation from precursor olivine gabbro under the influence of a chemically dynamic and reactive fluxing melt (forming the En-Pl-rich gabbro shown in Fig. 8a):

Precursor olivine gabbro + melt ➔ En-Pl-rich gabbro + melt1 (1)

The replacement of olivine by enstatite during melt-rock interaction is consistent with the findings in Gardner et al. (2020). The lack of olivine in the studied samples, which is nearly ubiquitous in the core at hole 735B (Dick et al., 2019), suggests melt-rock reactions have completely replaced the precursor olivine-bearing gabbroic rocks. The compositions of melt on either side of reaction (1) were likely highly variable depending on the (i) composition of the melt source (i.e., gabbroic versus fractionated gabbroic melts; Dick et al., 2019; Zhang et al., 2020), (ii) extent of geochemical modification of the melt during reactive flow (Daczko et al., 2016; Stuart et al., 2018a), (iii) variation in rock types interacted with along melt migration pathways, and (iv) possible trapping of early crystallised minerals (i.e. phenocrysts in the migrating melts) during the collapse of pathways (Bons et al., 2004; Silva et al., 2021; Žák et al., 2008) as melt supply is reduced. These variable controls on the compositions of melt in reaction (1) are also true for all melt in all reactions discussed below.

425 Concurrent and subsequent melt migration of highly variable melts caused local reactions (Fig 8a, steps1
426 and 2):

427 En-Pl-rich gabbro + melt1 or 2 ➔ rock + Di + Ilm + melt2 or 3 (2)

428 The final melt-rock reaction in the sample (Fig 8a, step3) is:

429 Ilm + Di + melt3 ➔ Mag + Sp + (new) Di + melt4 (3)

430 Reactions (2) and (3) (Fig. 8a, step 1 to 3) have been discussed earlier (section 5.1.1) wherein diopside
431 replaces enstatite and magnetite replaces ilmenite (Fig. 4 and 5).

432 *5.1.3. Mineral compositions: inferences for composition of the fluxing melt(s)*

433 In the gabbros, the TiO_2 whole rock data (Fig. 1c(iii) shows a distinct increase in titanium in the oxide-
434 rich rocks (Fig. 1c(iii)) relative to the oxide-poor gabbros. From the shipboard mineral analysis data (Dick
435 et al., 2002), olivine has very little titanium (TiO_2 was below detection limit in half of the samples, and
436 most values are <0.013%). Clinopyroxene (0.5 to 1.0 TiO_2 wt%) and orthopyroxene (to 0.5% TiO_2 wt%)
437 both show no variation between the oxide-rich and oxide-poor samples (Supplementary Figure 2). In a
438 closed system, all titanium to form ilmenite must come from local minerals, hence the whole rock
439 chemistry should not change between oxide rich and oxide poor gabbros. This is not the case in the
440 735B core data, hence an open system with in-fluxing fluids is required for the increase in TiO_2 and
441 formation of ilmenite. In Supplementary Data 2 we provide the average amount of additional TiO_2
442 required to form the oxide gabbros from olivine gabbro.

443 The titanium content in individual ilmenite grains is uniform (Supplementary Fig. 1a, b), ruling out solid-
444 state diffusional processes and is consistent with fluid-mediated replacement reactions (e.g. Putnis,
445 2009). However, even though manganese and magnesium content show minor variation between grains
446 within a sample, a geochemical trend between the two samples is seen (Fig. 7c, d, red arrows). This

447 suggests while the fluxing melt may have been heterogeneous in composition, the grains in contact with
448 the localised melt are chemically re-equilibrating continuously within the deforming rock; thus, their
449 chemistry and microstructures are continuously reset. The chemistry and microstructure of any given
450 mineral records a snapshot of the last interaction with migrating melt.

451 The X_{An} composition of plagioclase in the studied samples ranges from 0.37–0.40 (Fig. 7a) which is at the
452 lower end of plagioclase in the oxide-rich gabbro throughout the core at hole 735B (Fig. 1c(iv), Dick et
453 al., 2019). This is consistent with the decreasing anorthite content shown in the later melt-rock reaction
454 events in Gardner et al. (2020) and Zhang et al. (2021) which showed X_{An}=0.40–0.45. This bimodal
455 variation of plagioclase composition between the oxide-rich and oxide-poor gabbros (Fig. 1d(iv))
456 reinforces that open rather than closed system processes were operating during the oxide formation.
457 This is further supported by the abundant evidence for replacement microstructures. In fluid-rock
458 interaction systems, relationships between fluid-induced reactions and mineral equilibration are very
459 complex and therefore a spectrum of rock-buffered to melt-buffered mineral compositions may be
460 observed (Rampone et al., 2020). Nevertheless, it can be inferred from the anorthite content of
461 plagioclase that the migrating fluid is most likely a fractionated melt (Dick et al., 2019; Zhang et al.,
462 2020) richer in sodium than the melt forming the original igneous oxide-poor gabbros.

463 *5.1.4. Evidence of deformation in melt-fluxed rocks.*

464 Previous research at Atlantis Bank has shown that the oxide-rich gabbroic rocks are associated along or
465 near zones described in the core descriptions as having strong foliation and inferred crystal-plastic
466 deformation (Fig. 1b; Dick et al., 2019; Dick et al., 1991; Dick et al., 2000; Dick et al., 2002; Zhang et al.,
467 2020). In contrast, the high oxide samples examined here display low degrees of crystal-plastic
468 deformation when analysed in thin section, particularly in diopside and ilmenite (Figs. 5b, c), which lack
469 a well-defined foliation and show low degrees of CPO (Fig. 3c, g). The core images (Fig. 1d) do show the

oxides form a foliation though this is not evident at the thin section scale. Deformation microstructures can be cryptic in scenarios of melt present deformation (Daczko et al., 2016; Lee et al., 2018; Meek et al., 2019; Stuart et al., 2018b). Rocks deformed in the presence of melt exhibit several features unusual to solid-state high strain zones, such as thin elongate grain boundary films of plagioclase and low degrees of CPO at least for some minerals (Stuart et al., 2018b). We infer that as melt cannot support shear stresses, deformation of the rock system was accommodated by melt movement rather than the deformation of the solid framework (Rutter and Neumann, 1995; van der Molen and Paterson, 1979). This interpretation suggests units III and IV in hole 735B may represent a shear zone system that experienced a very high time-integrated melt flux while being rheologically exceptionally weak. This can explain those parts of the core where high oxide mode is decoupled from features of solid-state, crystal-plastic deformation (Fig. 1c(i) and (ii)).

5.1.5. Near liquidus oxide crystallisation: the role of high-T melt-rock interaction in oxide enrichment

Previous researchers have suggested Fe-Ti-rich melts (c.f. Zhang et al., 2020) as the source of iron and titanium for ilmenite and magnetite. However, the source of these Fe-Ti-enriched melts remains an issue. Koepke et al. (2005) found in only one of 25 hydrous partial melting experiments using 735B core gabbros, that two immiscible melts formed: a minor melt rich in REE, P, Zr, Ti and Fe and a larger volume of plagiogranitic melt. However, in agreement with our proposed model for an open system melt influx, Koepke et al. (2005) also found that an external source of titanium was required to form the oxides.

Experiments have shown the onset of Fe-Ti oxide crystallisation in mafic magmas is marked on melt differentiation paths by strong depletion of FeO and TiO_2 in the melt, and early crystallisation of oxides. Crystallisation onset also has variable timing depending on the composition and conditions of the magma, including fugacity of oxygen (Toplis and Carroll, 1995) and concentration of volatiles (e.g., Botcharnikov et al., 2008). For example, water content of ~2% lowers the crystallisation temperature of

493 clinopyroxene and olivine and promotes the early crystallisation of Fe-Ti oxides (Botcharnikov et al.,
494 2008; Howarth et al., 2013) and 1% phosphorus can increase ilmenite precipitation (Toplis et al., 1994).

495 Natural examples of Fe-Ti-rich melts are rare. Clague et al. (2018) document an example of extreme
496 fractionation of mid-ocean ridge basalt at Alarcon Rise where TiO_2 and FeO decrease, and
497 titanomagnetite and ilmenite crystallise as the melts fractionate from andesite, through dacite to
498 rhyolite. In addition, Charlier et al. (2010) hypothesise that ilmenite was the only mineral to crystallise at
499 times during the evolution of the Allard Lake anorthositic system. However, from our study, we suggest
500 melt-rock interaction is the key mechanism to locally produce a near-liquidus oxide-saturated melt
501 which drives oxide-forming reactions in the oceanic crust.

502 We combine this concept of early crystallisation of Fe-Ti oxides at high temperature with a scenario of
503 melt-buffered melt-rock interaction (Fig. 8a) and infer that a melt migrating with enhanced near liquidus
504 oxide crystallisation conditions will destabilise silicates in favour of Fe-Ti oxides (reactions (2) and (3)
505 above). In our model of melt-rock interaction (Fig. 8a), the stability of oxides over silicates drives
506 reactions that consume silicate minerals and precipitate oxide minerals in an open system. The degree
507 of oxide enrichment is proportional to the time integrated melt flux through the rocks (see Section 5.3).
508 Our proposed migrating melt could form rare fractionated volcanic rocks as observed at Alarcon Rise
509 (Clague et al., 2018). Our model of deformation-assisted migration of fractionated melts through
510 gabbroic shear zones is also consistent with the interpretation of (Agar and Lloyd, 1997) who linked
511 fractionated melts with oxide enrichment at the Mid-Atlantic Ridge Kane fracture zone area. Currently
512 our understanding of the timing of the crystallisation of oxides relies on equilibrium experiments. In the
513 future we need disequilibrium melt-rock interaction experiments to replicate our inferred melt-mineral
514 reactions (section 5.1.2). Additionally, new melt-rock interaction experiments involving melt flux
515 through the rock are required to best reproduce our samples and to confirm our model.

5.2. The origin of high-oxide rocks in continental tectonic settings

5.2.1. Microstructures showing metamorphic replacement reactions

Similar reaction microstructures as those observed in the oceanic setting are observed in the continental case study of sample CP1604C from Cattle Water Pass, central Australia. The field relationships show that the precursor rock type, a granulite facies felsic gneiss, is replaced in a high strain zone by the garnet-biotite schist of this study. The interpretation that ilmenite partially replaces garnet is supported by the following observations: (1) the presence of irregular boundaries between garnet and ilmenite including finger-like protrusions into garnet (Fig. 4h, k); (2) presence of ilmenite as rims on garnet and as elongate grains at boundaries between garnet and biotite (Fig. 4h-k); (3) multiple groups of neighbouring ilmenite grains, some of which are inclusions within garnet, that share identical orientation which represent relicts of a partially replaced single coarse garnet grain (e.g., Fig. 6b, grain I2) and (4) straight boundaries on ilmenite that mimic the crystal facets of relict garnet (Fig. 4j). In addition, ilmenite and biotite share a strong CPO (Fig. d and f) without strong internal crystal bending suggesting the grains grew syntectonically i.e. grew in a stressed regime.

5.2.2. Former presence of melt and inferred melt-rock reactions

Melt-present deformation was interpreted for biotite-rich shear zones in central Australia by (Piazolo et al., 2020). In the sample investigated here, microstructures indicative of the former presence of melt (Holness et al., 2011; Lee et al., 2018; Stuart et al., 2018b; Vernon, 2000) confirm this previous research as they include: (1) interstitial ilmenite grains between garnet grains that may have low dihedral angles (Fig. 4h, i, red and green arrows), (2) films along grain boundaries (Fig. 4h, i, red arrows), (3) embayment microstructures (Fig. 4i, yellow arrows), (4) 3D connectivity of apparently isolated grains (Fig. 6b), and (5) limited internal deformation of grains (Fig. 6b). A lack of local partial melting microstructures and

538 significant hydration of precursor rocks at the site suggest the melt was hydrous and externally derived,
539 resulting in three stages (Fig. 8b) of mineral and melt transformation.

540 Initially, a granitic melt (melt1) infiltrates into a shear zone cutting the granulite (Fig. 8b, step 1). Melt-
541 rock interactions form biotite and small garnet grains and modifies the melt composition to melt2:

542 Precursor felsic granulite + melt1 ➔ modified granulite + Bt_1 + Grt_1 + melt2 (4)

543 Concurrent and subsequent melt2 migration caused the following local reaction (Fig. 8b, step 2),
544 completely replacing the precursor granulite minerals, further increasing the mode of biotite and garnet,
545 and continuing to modify the melt (melt3):

546 Modified granulite + Bt_1 + Grt_1 + melt2 ➔ Pl + Qz + Bt_2 + Grt_2 + melt3 (5)

547 Melt3 chemically evolves with continued melt-rock interaction during its flux and promotes ilmenite
548 crystallisation and destabilisation of quartz and plagioclase (Fig., 8b, step 3).

549 Pl + Qz + Bt_2 + Grt_2 + melt3 ➔ Bt_3 + Grt_3 + Ilm + melt4 (6)

550 Reaction (6) is evident from the replacement microstructures of ilmenite against garnet and biotite
551 grains (Fig. 4h, k, yellow arrows) and the reduced mode of plagioclase and quartz in the domains with
552 high ilmenite mode.

553 *5.2.3. Mineral composition: Composition of the fluxing melt(s)*

554 An open system is also inferred for the continental setting investigated here. Supplementary Data 2 has
555 a discussion of the average amounts of additional TiO_2 required to form the garnet-biotite-ilmenite-rich
556 band from the quartz-plagioclase-rich band.

557 Although MgO and MnO do not vary much within ilmenite grains in the sample, ilmenite shows a strong
558 variation in TiO_2 content (42–48 wt.%), consistent with open system processes (Fig. 7b), as ilmenites

559 from the adjoining high-grade terrain have higher values for TiO_2 with limited range (51-52 wt%, Cassidy
560 et al., 1988). Moreover, the variability of plagioclase chemistry (Fig. 7a, blue crosses) within the sample
561 also supports an open chemical system with the possibility of multiple melt flux events (Streck, 2008).

562 We interpret melts 1, 2 and 3 (Fig. 8b, Eq. 4, 5 and 6) are likely to be very similar in composition and
563 suggest that they are externally derived S-type granitic melts formed when sedimentary rocks
564 equivalent to the Harts Range Group (Fig. 1a) partially melted. We suggest that garnet and biotite
565 chemistry re-equilibrated continuously with the melt and was aided by syn-melt flux deformation.
566 Previous studies have also shown similar granitic melts fluxed through the nearby Gough Dam shear
567 zone (Fig. 1b, Piazolo et al., 2020; Silva et al., 2021). The relationships outlined in section 5.2.2 are
568 consistent with melt migration at temperatures below (Fig. 8b, melt1 and 2, Eq. 5), then above (Fig. 8b,
569 melt3, Eq. 6) the stability of plagioclase and quartz (~ 870 ºC; Clemens and Wall, 1981). As ilmenite is a
570 liquidus phase in S-type granites (Clemens and Wall, 1981), any scenario of high temperature (near
571 liquidus) melt flux increases the mode of oxides over silicates (Charlier et al., 2010).

572 In addition, the phase diagram of Clemens and Wall (1981) is consistent with the shear zones in central
573 Australia having been hydrated in the presence of an S-type granitic melt at variable melt flux
574 temperature conditions .

575 *5.2.4. Evidence of deformation in melt fluxed rocks*

576 The continental sample formed within the Cattle Water Pass shear zone as demonstrated by field
577 relationships and a well-developed foliation and lineation. The microstructural analysis demonstrates
578 the former presence of melt. However, EBSD analysis shows only minor internal deformation of grains
579 and microstructures contradictory to typical mid to deep crustal shear zones. Only rare ilmenite grains
580 preserve a high degree of internal deformation (Fig. $6b_1$). Similarly, some garnet grains display subgrain
581 boundaries (Fig. 6c) though any consistent CPO is lacking (Fig. 6e). Additionally, biotite lacks evidence of

internal deformation when examined under crossed polarised light microscopy. These observations do not support an interpretation of solid-state deformation and instead point to melt-present deformation, suggesting melt flow accommodated most of the strain.

We suggest that a high nucleation rate of garnet grains and random orientation of nuclei, (Fig. 6e, pole figure) and the formation of crystal facets (Fig. 4h, j) was facilitated by the presence of melt. Despite having no significant internal deformation, the ilmenite grains are aligned and show a CPO (Fig. 5d) which matches that of biotite (Fig. 6f). Since the formation of CPO by solid-state deformation in these rocks is highly unlikely, it is inferred that rigid body rotation (e.g., March, 1932) as well as growth in the presence of external stress (Wenk et al., 2019, and references therein) results in the strong alignment of platy and elastically highly anisotropic biotite.

5.2.5. Near liquidus oxide crystallisation: the role of high-T melt-rock interaction in oxide enrichment

Ilmenite is the first mineral to crystallise from the S-type granite studied by Clemens and Wall (1981), followed by, in crystallisation order, garnet, biotite, quartz, plagioclase and K-feldspar. Although the modal proportion of the oxides in such experiments (1-3%) is not significantly high compared to that seen in our CWP shear zone samples (18%, Fig. 3l), it is important to note the oxides are stable prior to the silicates. Thus, given a melt-rock interaction scenario where the temperature of a fluxing S-type granitic melt is near its liquidus, oxide minerals may be stable while silicate minerals are destabilised during melt-rock interaction with the hot melt. At slightly lower temperatures of melt-rock interaction, garnet and ilmenite are stable and then as the temperature decreases further biotite is added to the stable assemblage. The mineral assemblage and mineral proportions observed in the garnet-biotite schist sample examined here are consistent with having formed by the interaction between the precursor felsic granulite and a migrating S-type granitic melt broadly similar to that studied by Clemens and Wall (1981). Iterative melt-rock reaction and migration of reacted melt out of the local system is

needed to significantly enrich the rock in biotite, garnet, and ilmenite and deplete the rock of quartz and feldspar. This suggests a high time-integrated melt flux is required (see Section 5.3; Silva et al., 2021; Stuart et al., 2018b).

5.3. The signatures and consequences of deformation assisted reactive porous melt flow in crustal environments

A near liquidus temperature of the melt during melt-rock interaction can stabilise oxides relative to silicate minerals and is necessary to explain the enrichment of ilmenite in both the oceanic and continental case studies. A fractional crystallisation model alone for either a gabbroic melt or an S-type granitic melt cannot explain the high modal proportions of ilmenite in these rocks. Typical silicate melts precipitate only 1-3 vol.% oxides. Therefore, significant enrichment of oxides requires precipitation from multiple batches of fluxing melt, progressively increasing the mode of oxides. Using the upper value of 3% oxides for the precipitation from a typical silicate melt, oxide modes of ~20 vol.% in the continental setting and ~45 vol.% in the oceanic setting require precipitation of oxides from a minimum volume of melt that is in the order of 6 to 15 times the volume of the rock, for continental and oceanic crusts, respectively. In other words, a large volume of melt must migrate through our samples to progressively enrich the oxides to the observed degree.

One concept of reactive melt flow involves a crystal mush where a framework of solid crystals reacts as the residual melt is expelled and migrates during compaction. This forms core to rim elemental profiles of reactant minerals (Solano et al., 2014). A similar process occurs during syn-deformational melt migration of an externally derived melt through shear zones cutting formerly solid rocks. Enhanced porosity and permeability in zones of ductile deformation (e.g. Edmond and Paterson, 1972; Fischer and Paterson, 1989) result in lower fluid pressure sinks that draw melt towards zones of maximum deformation rate (Etheridge et al., 2021). Fusseis et al. (2009) describe a granular fluid pump model

628 involving the dynamic opening and closing of pores in deforming rocks that facilitates melt migration
629 through shear zones. These concepts of deformation assisted fluid flow through shear zones provide a
630 mechanism to transport large volumes of melt through small volumes of rock.

631 One of the outcomes of this study is to highlight the complexity of melt-rock reaction systems, beyond
632 the magma chamber setting, where fractional crystallisation and melt–crystal mush reactions occur.
633 Within magma chambers, the stability of minerals can be determined using experimental petrology and
634 thermodynamic modelling to produce phase diagrams. However, the complexity of modelling increases
635 in an open system melt migration scenario where the composition of both the reactant melts and the
636 rocks they pass through are possibly highly variable and dynamically evolving.

637 Studies have shown that reactive melt migration can significantly change the composition of melt by
638 fractionation and/or enrichment of specific elements. This in turn produces an evolved melt which is
639 hard to distinguish from the fractionation of parent melt (Lissenberg et al., 2013). Thus, the derivative
640 melt produced during melt-rock interaction and reactive crystallisation will form different liquid lines of
641 descent (Collier and Kelemen, 2010). Studies have further shown that reactive melt flow is not limited to
642 the grain scale, rather at a macro scale it can lead to complete transformation of one rock type to
643 another (Lissenberg and MacLeod, 2016). These studies reported the preferential growth of a specific
644 mineral over any other (e.g., clinopyroxene over olivine), in turn leading to a modal enrichment in that
645 mineral (Lissenberg and MacLeod, 2016). Similarly, we propose that oxide minerals in our oceanic case
646 study grew by replacing mostly plagioclase and diopside in the oceanic samples. These relationships
647 require an evolved melt infiltrating the precursor gabbro, forming derivative reactant melt, and leading
648 to further reactions and the development of the oxide gabbros. Similarly, in our case study of a
649 continental setting, variably fractionated S-type melt can readily react and enrich rocks in ilmenite.

In the oceanic case study (Fig. 8a), the parent melt forming ilmenite was likely gabbroic in composition and may have fractionated in a magma chamber setting or during melt-rock interaction resulting in the formation of the modified gabbroic melt (melt1) envisaged in our model. Step 1 shows enstatite and plagioclase reacting with melt1 (Equation 2), causing crystallisation of ilmenite and diopside and the formation of melt2. The derivative melt2 has a composition where oxides are also early crystallising minerals, ahead of silicates (Equation 2). Diopside replaces enstatite grains to form the two pyroxene domains and diopside rims. In subsequent melt-rock reactions, a later melt3 stabilises magnetite over ilmenite and locally recrystallises diopside.

Similarly, in the case of the continental case study (Fig. 8b), a primary or fractionated S-type melt1 drives hydration of a granulite facies felsic gneiss in step 1 due to deformation assisted melt migration through the shear zone. This leads to an increased mode of biotite and garnet in a band in step 2 (Fig. 3k), and progressive reaction leads to the formation of derivative melts (melt2 and melt3). The latter melt3 is evolved and has a composition enhancing near liquidus ilmenite growth. In step 3, the reactant melt3 forms interstitial ilmenite grains, thus increasing the mode of ilmenite along with consumption of some garnet grains (Fig. 4h, i, k; yellow arrow).

6. Conclusion

The microstructural characterisation of oxide-rich rocks from both oceanic and continental tectonic settings shows that oxide grains are common in metamorphic replacement microstructures, where the oxide grains replace silicate minerals during melt-rock interaction. The former presence of melt is implied by interstitial microstructures involving grain boundary films and grains that subtend to low dihedral angles. Grains show straight crystal faces and form an interconnected skeletal texture, including clusters of apparently isolated grains that are connected in three dimensions. Limited internal

deformation of grains is consistent with strain accommodation in shear zones by melt movement between grains in a solid framework, rather than deformation of the solid minerals by, for example, dislocation creep. Microchemical variation in silicates and ilmenite argues for open system behaviour in both oceanic and continental settings. We propose that deformation assisted reactive porous flow of melt through rocks in any tectonic setting, given near liquidus conditions, may significantly modify melts to enhance their ability to enrich oxide minerals in preference to silicates.

Acknowledgements

Logistical and analytical funding was provided by the Australian IODP Office (ANZIC Legacy Analytical funding), ARC Discovery grant DP160103449 and the Department of Earth and Environmental Sciences, Macquarie University. The authors would like to thank Karsten Gorman of University of Tasmania for his assistance collecting the EMP data and Malcolm Lambert from University of New England for his assistance collecting the micro-CT data. We would also like to thank Thomas Müller and an anonymous reviewer for their careful and constructive reviews, and Greg Shellnutt for editorial handling. This is contribution xxx from the ARC Centre of Excellence for Core to Crust Fluid Systems (http://www.ccfs.mq.edu.au) and xxx in the GEMOC Key Centre (http://www.gemoc.mq.edu.au).

References

Agar, S.M., Lloyd, G.E., 1997. Deformation of Fe-Ti oxides in gabbroic shear zones from the MARK area, Proceedings-Ocean Drilling Program Scientific Results. National Science Foundation, pp. 123-142.

Bendall, B., 2000. Mid-Palaeozoic shear zones in the Strangways Range : a record of intracratonic tectonism in the Arunta Inlier, Central Australia, Dept. of Geology. University of Adelaide, Adelaide, Australia, p. 210.

694 Bloomer, S.H., Meyer, P.S., Dick, H.J.B., Ozawa, K., Natland, J.H., 1991. 2. Textural
695 and mineralogic variations in gabbroic rocks from hole 735B, in: Von Herzon, R.P., Fox,
696 J., Palmer-Julson, A., Robinson, P.T. (Eds.), Proceedings of the International Ocean
697 Drilling Program volume 118. International Drilling Program, Texas, pp. 21-39.
698 Bons, P.D., Druguet, E., Hamann, I., Carreras, J., Passchier, C.W., 2004. Apparent
699 boudinage in dykes. Journal of Structural Geology 26, 625-636.
700 Botcharnikov, R., Almeev, R., Koepke, J., Holtz, F., 2008. Phase relations and liquid
701 lines of descent in hydrous ferrobasalt—implications for the Skaergaard intrusion and
702 Columbia River flood basalts. Journal of Petrology 49, 1687-1727.
703 Bowles, J., Howie, R., Vaughan, D., Zussman, J., 2011. Rock-forming minerals, 2nd ed.
704 The Geological Society, London, UK.
705 Cannat, M., Mével, C., Stakes, D., 1991. 24. Normal ductile shear zones at an oceanic
706 spreading ridge: tectonic evolution of site 735 gabbros (Southwest Indian Ocean), in:
707 Von Herzon, R.P., Fox, J., Palmer-Julson, A., Robinson, P.T. (Eds.), Proceedings fo the
708 Ocean Drilling Program, scientific results volume 118. Ocean Drilling Program, Texas,
709 pp. 415-429.
710 Cartwright, I., Buick, I.S., Foster, D.A., Lambert, D.D., 1999. Alice Springs age shear
711 zones from the southeastern Reynolds Range, central Australia. Australian Journal of
712 Earth Sciences 46, 355-363.
713 Casini, L., Maino, M., Sanfilippo, A., Ildefonse, B., Dick, H.J.B., 2021. High-Temperature
714 Strain Localization and the Nucleation of Oceanic Core Complexes (16.5°N, Mid-
715 Atlantic Ridge). Journal of Geophysical Research: Solid Earth 126, e2021JB022215.

716 Cassidy, K.F., Groves, D.I., Binns, R.A., 1988. Manganoan ilmenite formed during
717 regional metamorphism of Archean mafic and ultramafic rocks from Western Australia.
718 The Canadian Mineralogist 26, 999-1012.
719 Charlier, B., Namur, O., Malpas, S., de Marneffe, C., Duchesne, J.-C., Auwera, J.V.,
720 Bolle, O., 2010. Origin of the giant Allard Lake ilmenite ore deposit (Canada) by
721 fractional crystallization, multiple magma pulses and mixing. Lithos 117, 119-134.
722 Cignoni, P., Callieri, M., Corsini, M., Dellepiane, M., Ganovelli, F., Ranzuglia, G., 2008.
723 MeshLab: an Open-Source Mesh Processing Tool, Sixth Eurographics Italian Chapter
724 Conference. The Eurographics Association, pp. 129-136.
725 Clague, D.A., Caress, D.W., Dreyer, B.M., Lundsten, L., Paduan, J.B., Portner, R.A.,
726 Spelz-Madero, R., Bowles, J.A., Castillo, P.R., Guardado-France, R., 2018. Geology of
727 the Alarcon Rise, Southern Gulf of California. Geochemistry, Geophysics, Geosystems
728 19, 807-837.
729 Clemens, J.D., Wall, V.J., 1981. Origin and crystallization of some peraluminous (S-
730 type) granitic magmas. The Canadian Mineralogist 19, 111-131.
731 Collier, M.L., Kelemen, P.B., 2010. The Case for Reactive Crystallization at Mid-Ocean
732 Ridges. Journal of Petrology 51, 1913-1940.
733 Collins, W.J., Teyssier, C., 1989. Crustal scale ductile fault systems in the Arunta Inlier,
734 central Australia. Tectonophysics 158, 49-66.
735 Daczko, N.R., Piazolo, S., Meek, U., Stuart, C.A., Elliott, V., 2016. Hornblendite
736 delineates zones of mass transfer through the lower crust. Scientific Reports 6, 31369.
737 Deans, J.R.L., Yoshinobu, A.S., 2019. Geographically re-oriented magmatic and
738 metamorphic foliations from ODP Hole 735B Atlantis Bank, Southwest Indian Ridge:

739 Magmatic intrusion and crystal-plastic overprint in the footwall of an oceanic core
740 complex. Journal of Structural Geology 126, 1-10.
741 Dick, H.J.B., Kvassnes, A.J.S., Robinson, P.T., MacLeod, C.J., Kinoshita, H., 2019. The
742 Atlantis Bank Gabbro Massif, Southwest Indian Ridge. Progress in Earth and Planetary
743 Science 6, 64.
744 Dick, H.J.B., Meyer, P.S., Bloomer, S.H., Kirby, S.H., Stakes, D., Mawer, C., 1991. 26.
745 Lithostratigraphic evolution of an in-situ section of oceanic layer 3, in: Von Herzon, R.P.,
746 Fox, J., Palmer-Julson, A., Robinson, P.T. (Eds.), Proceeding of the Ocean Drilling
747 Program, Scientific Results Volume 118. Ocean Drilling Program, Texas, pp. 439-538.
748 Dick, H.J.B., Natland, J.H., Alt, J.C., Bach, W., Bideau, D., Gee, J.S., Haggas, S.,
749 Hertogen, J.G.H., Hirth, G., Holm, P.M., Ildefonse, B., Iturrino, G.J., John, B.E., Kelley,
750 D.S., Kikawa, E., Kingdon, A., LeRoux, P.J., Maeda, J., Meyer, P.S., Miller, D.J.,
751 Naslund, H.R., Niu, Y.-L., Robinson, P.T., Snow, J., Stephen, R.A., Trimby, P.W.,
752 Worm, H.-U., Yoshinobu, A., 2000. A long in situ section of the lower ocean crust:
753 results of ODP Leg 176 drilling at the Southwest Indian Ridge. Earth and Planetary
754 Science Letters 179, 31-51.
755 Dick, H.J.B., Natland, J.H., Miller, D.J., Alt, J.C., Bach, W., Bideau, D., Gee, J.S.,
756 Haggas, S., Hertogen, J.G.H., Hirth, G., Holm, P.M., Ildefonse, B., Iturrino, G.J., John,
757 B., Kelley, D.S., Kikawa, E., Kingdon, A., Le Roux, P., Maeda, J., Meyer, P.S., Naslund,
758 H.R., Niu, Y., Robinson, P.T., Snow, J.E., Stephen, R.A., Trimby, P., Worm, H.-U.,
759 Yoshinobu, A., 1999a. 1. Leg 176 Summary, in: Marin, J.A., Scroggs, J.M. (Eds.),
760 Proceedings of the International Ocean Drilling Program, initial reports volume 176.
761 Ocean Drilling Program, Texas, p. 70.

762 Dick, H.J.B., Natland, J.H., Miller, D.J., Alt, J.C., Bach, W., Bideau, D., Gee, J.S.,
763 Haggas, S., Hertogen, J.G.H., Hirth, G., Holm, P.M., Ildefonse, B., Iturrino, G.J., John,
764 B., Kelley, D.S., Kikawa, E., Kingdon, A., Le Roux, P., Maeda, J., Meyer, P.S., Naslund,
765 H.R., Niu, Y., Robinson, P.T., Snow, J.E., Stephen, R.A., Trimby, P., Worm, H.-U.,
766 Yoshinobu, A., 1999b. 3. Site 735, in: Marin, J.A., Scroggs, J.M. (Eds.), Proceedings of
767 the Ocean Drilling Program, initial reports volume 176. Ocean Drilling Program, Texas,
768 pp. 1-313.
769 Dick, H.J.B., Ozawa, K., Meyer, P.S., Niu, Y., Robinson, P.T., Constantin, M., Hebert,
770 R., Maeda, J., Natland, J.H., Hirth, J.G., Mackie, S.M., 2002. 10. Primary silicate
771 mineral chemistry of a 1.5-km section of very slow spreading lower ocean crust: ODP
772 hole 735B, Southwest Indian Ridge, in: Natland, J.H., Dick, H.J.B., Miller, D.J., Von
773 Herzon, R.P. (Eds.), Proceedings of the Ocean Drilling Program, scientific results
774 volume 176. Ocean Drilling Program, Texas, pp. 1-61.
775 Dixon, S., Rutherford, M.J., 1979. Plagiogranites as late-stage immiscible liquids in
776 ophiolite and mid-ocean ridge suites: An experimental study. Earth and Planetary
777 Science Letters 45, 45-60.
778 Duchesne, J., Charlier, B., 2005. Geochemistry of cumulates from the Bjerkreim
779 Sokndal layered intrusion (S. Norway). Part I: Constraints from major elements on the
780 mechanism of cumulate formation and on the jotunite liquid line of descent. Lithos 83,
781 229-254.
782 Edmond, J.M., Paterson, M.S., 1972. Volume changes during the deformation of rocks
783 at high pressures. International Journal of Rock Mechanics and Mining Sciences &
784 Geomechanics Abstracts 9, 161-182.

785 Emslie, R.F., Hamilton, M.A., Thériault, R.J., 1994. Petrogenesis of a Mid-Proterozoic
786 Anorthosite-Mangerite-Charnockite-Granite (AMCG) Complex: Isotopic and Chemical
787 Evidence from the Nain Plutonic Suite. The Journal of Geology 102, 539-558.
788 Etheridge, M.A., Daczko, N.R., Chapman, T., Stuart, C.A., 2021. Mechanisms of melt
789 extraction during lower crustal partial melting. Journal of Metamorphic Geology 39, 57-
790 75.
791 Fedorov, A., Beichel, R., Kalpathy-Cramer, J., Finet, J., Fillion-Robin, J.-C., Pujol, S.,
792 Bauer, C., Jennings, D., Fennessy, F.M., Sonka, M., Buatti, J., Aylward, S.R., Miller,
793 J.V., Pieper, S., Kikinis, R., 2012. 3D Slicer as an Image Computing Platform for the
794 Quantitative Imaging Network. Magnetic Resonance Imaging 30, 1323-1341.
795 Fischer, G.J., Paterson, M.S., 1989. Dilatancy during rock deformation at high
796 temperatures and pressures. Journal of Geophysical Research: Solid Earth 94, 17607-
797 17617.
798 Fusseis, F., Regenauer-Lieb, K., Liu, J., Hough, R.M., De Carlo, F., 2009. Creep
799 cavitation can establish a dynamic granular fluid pump in ductile shear zones. Nature
800 459, 974-977.
801 Gale, A., Dalton, C.A., Langmuir, C.H., Su, Y., Schilling, J.-G., 2013. The mean
802 composition of ocean ridge basalts. Geochemistry, Geophysics, Geosystems 14, 489-
803 518.
804 Gardner, R.L., Piazolo, S., Daczko, N.R., Trimby, P., 2020. Microstructures reveal
805 multistage melt present strain localisation in mid-ocean gabbros. Lithos 366-367,
806 105572.

807 Gross, G.A., Eckstrand, O.R., Sinclair, W.D., Thorpe, R.I., 1995. Mafic Intrusion-Hosted
808 Titanium-Iron, Geology of Canadian Mineral Deposit Types. Geological Society of
809 America, p. 0.
810 Hand, M., Sandiford, M., 1999. Intraplate deformation in central Australia, the link
811 between subsidence and fault reactivation. Tectonophysics 305, 121-140.
812 Hertogen, J.G.H., R., E., Robinson, P.T., Erzinger, J., 2002. 6. Lithology, mineralogy
813 and geochemistry of the lower ocean crust, ODP hole 735B, Southwest Indian Ridge,
814 in: Natland, J.H., Dick, H.J.B., Miller, D.J., Von Herzon, R.P. (Eds.), Proceedings of the
815 International Ocean Drilling Program, Scientific Results, Volume 176. Ocean Drilling
816 Program, Texas, pp. 1-82.
817 Holness, M.B., Cesare, B., Sawyer, E.W., 2011. Melted rocks under the microscope:
818 microstructures and their interpretation. Elements 7, 247-252.
819 Hopkinson, L., Roberts, S., 1995. Ridge axis deformation and coeval melt migration
820 within layer 3 gabbros: evidence from the Lizard Complex, U.K. Contributions to
821 Mineralogy and Petrology 121, 126.
822 Howarth, G.H., Prevec, S.A., Zhou, M.-F., 2013. Timing of Ti-magnetite crystallisation
823 and silicate disequilibrium in the Panzhihua mafic layered intrusion: Implications for ore-
824 forming processes. Lithos 170-171, 73-89.
825 John, B.E., Foster, D.A., Murphy, J.M., Cheadle, M.J., Baines, A.G., Fanning, C.M.,
826 Copeland, P., 2004. Determining the cooling history of in situ lower oceanic crust—
827 Atlantis Bank, SW Indian Ridge. Earth and Planetary Science Letters 222, 145-160.
828 Koepke, J., Feig, S.T., Snow, J., 2005. Hydrous partial melting within the lower oceanic
829 crust. Terra Nova 17, 286-291.

Lee, A.L., Torvela, T., Lloyd, G.E., Walker, A.M., 2018. Melt organisation and strain partitioning in the lower crust. Journal of Structural Geology 113, 188-199.

Lissenberg, C.J., MacLeod, C.J., 2016. A reactive porous flow control on mid-ocean ridge magmatic evolution. Journal of Petrology 57, 2195-2220.

Lissenberg, C.J., MacLeod, C.J., Howard, K.A., Godard, M., 2013. Pervasive reactive melt migration through fast-spreading lower oceanic crust (Hess Deep, equatorial Pacific Ocean). Earth and Planetary Science Letters 361, 436-447.

March, A., 1932. Mathematische Theorie der Regelung nach der Korngestalt bei affiner Deformation. Z. Kristallogr 81, 285-297.

Meek, U., Piazolo, S., Daczko, N.R., 2019. The field and microstructural signatures of deformation-assisted melt transfer: Insights from magmatic arc lower crust, New Zealand. Journal of Metamorphic Geology 37, 795-821.

Nachit, H., Ibhi, A., Ohoud, M.B., 2005. Discrimination between primary magmatic biotites, reequilibrated biotites and neoformed biotites. Comptes Rendus Geoscience 337, 1415-1420.

Norman, A.R., 1991. The structural and metamorphic evolution of the central Arunta Block: evidence from the Strangways Metamorphic Complex and the Harts Range Group, central Australia, School of Earth Sciences. Macquarie University, Sydney, Australia, p. 13.

Ozawa, K., Meyer, P.S., Bloomer, S.H., 1991. 3. Mineralogy and textures of iron-titanium oxide gabbros and associated olivine gabbros from hole 735B, in: Von Herzon, R.P., Fox, J., Palmer-Julson, A., Robinson, P.T. (Eds.), Proceedings of the International Ocean Drilling Program volume 118. International Drilling Program, Texas, pp. 41-73.

853 Philpotts, A.R., Ague, J.J., 2009. Principles of igneous and metamorphic petrology.
854 CAmbridge University Press, Cambridge, UK.
855 Piazolo, S., Bestmann, M., Prior, D.J., Spiers, C.J., 2006. Temperature dependent grain
856 boundary migration in deformed-then-annealed material: Observations from
857 experimentally deformed synthetic rocksalt. Tectonophysics 427, 55-71.
858 Piazolo, S., Daczko, N.R., Silva, D., Raimondo, T., 2020. Melt-present shear zones
859 enable intracontinental orogenesis. Geology 48, 643-648.
860 Prakash, A., Piazolo, S., Saha, L., Bhattacharya, A., Pal, D.K., Sarkar, S., 2018.
861 Deformation behavior of migmatites: insights from microstructural analysis of a garnet–
862 sillimanite–mullite–quartz–feldspar-bearing anatectic migmatite at Rampura–Agucha,
863 Aravalli–Delhi Fold Belt, NW India. International Journal of Earth Sciences.
864 Putnis, A., 2009. Mineral replacement reactions. Reviews in mineralogy and
865 geochemistry 70, 87-124.
866 Raimondo, T., Clark, C., Hand, M., Faure, K., 2011. Assessing the geochemical and
867 tectonic impacts of fluid–rock interaction in mid-crustal shear zones: a case study from
868 the intracontinental Alice Springs Orogen, central Australia. Journal of Metamorphic
869 Geology 29, 821-850.
870 Raimondo, T., Hand, M., Collins, W.J., 2014. Compressional intracontinental orogens:
871 Ancient and modern perspectives. Earth-Science Reviews 130, 128-153.
872 Rampone, E., Borghini, G., Basch, V., 2020. Melt migration and melt-rock reaction in
873 the Alpine-Apennine peridotites: Insights on mantle dynamics in extending lithosphere.
874 Geoscience Frontiers 11, 151-166.

875 Robinson, P.T., Dick, H., Natland, J.H., Yoshinobu, A.S., Party, L.S., 2000. Lower
876 oceanic crust formed at an ultra-slow-spreading ridge: Ocean Drilling Program Hole
877 735B, Southwest Indian Ridge. Geological Society of America Special Paper 349.
878 Roy, P., Whitehouse, J., Cowell, P., Oakes, G., 2000. Mineral Sands Occurrences in the
879 Murray Basin, Southeastern Australia. Economic Geology 95, 1107-1128.
880 Rutter, E.H., Neumann, D.H.K., 1995. Experimental deformation of partially molten
881 Westerly granite under fluid-absent conditions, with implications for the extraction of
882 granitic magmas. Journal of Geophysical Research: Solid Earth 100, 15697-15715.
883 Ryan, W.B.F., Carbotte, S.M., Coplan, S., O'Hara, A., Melkonian, A., Arko, R., Weissel,
884 R.A., Ferrini, V., Goodwillie, A., Nitche, F., Bonczkowski, J., Zemsky, R., 2009. Global
885 Multi-Resolution Topography (GMRT) synthesis data set. Geochemistry, Geophysics,
886 Geosystems 10.
887 Scoates, J.S., Chamberlain, K.R., 1997. Orogenic to Post‐Orogenic Origin For
888 the 1.76 Ga Horse Creek Anorthosite Complex, Wyoming, Usa. The Journal of Geology
889 105, 331-344.
890 Silva, D., Daczko, N.R., Piazolo, S., Raimondo, T., 2021. Glimmerite: a product of melt-
891 rock interaction within a crustal-scale high-strain zone. Gondwana Research.
892 Silva, D., Piazolo, S., Daczko, N.R., Houseman, G., Raimondo, T., Evans, L., 2018.
893 Intracontinental Orogeny Enhanced by Far-Field Extension and Local Weak Crust.
894 Tectonics 37, 4421-4443.
895 Solano, J., Jackson, M., Sparks, R., Blundy, J., 2014. Evolution of major and trace
896 element composition during melt migration through crystalline mush: implications for
897 chemical differentiation in the crust. American Journal of Science 314, 895-939.

898 Streck, M.J., 2008. Mineral Textures and Zoning as Evidence for Open System
899 Processes. Reviews in mineralogy and geochemistry 69, 595-622.
900 Stuart, C.A., Meek, U., Daczko, N.R., Piazolo, S., Huang, J.X., 2018a. Chemical
901 Signatures of Melt–Rock Interaction in the Root of a Magmatic Arc. Journal of Petrology
902 59, 321-340.
903 Stuart, C.A., Piazolo, S., Daczko, N.R., 2018b. The recognition of former melt flux
904 through high-strain zones. Journal of Metamorphic Geology 36, 1049-1069.
905 Teyssier, C., 1985. A crustal thrust system in an intracratonic tectonic environment.
906 Journal of Structural Geology 7, 689-700.
907 Toplis, M.J., Carroll, M.R., 1995. An Experimental Study of the Influence of Oxygen
908 Fugacity on Fe-Ti Oxide Stability, Phase Relations, and Mineral—Melt Equilibria in
909 Ferro-Basaltic Systems. Journal of Petrology 36, 1137-1170.
910 Toplis, M.J., Libourel, G., Carroll, M.R., 1994. The role of phosphorus in crystallisation
911 processes of basalt: An experimental study. Geochimica et Cosmochimica Acta 58,
912 797-810.
913 van der Molen, I., Paterson, M.S., 1979. Experimental deformation of partially-melted
914 granite. Contributions to Mineralogy and Petrology 70, 299-318.
915 Vernon, R.H., 2000. Review of Microstructural Evidence of Magmatic and Solid-State
916 Flow. Visual Geosciences 5, 1-23.
917 Wenk, H.-R., Kanitpanyacharoen, W., Ren, Y., 2019. Slate–A new record for crystal
918 preferred orientation. Journal of Structural Geology 125, 319-324.
919 Whitney, D.L., Evans, B.W., 2010. Abbreviations for names of rock-forming minerals.
920 American mineralogist 95, 185.

Woodruff, L.G., Bedinger, G.M., Piatak, N.M., 2017. Titanium, in: Schulz, K.J., DeYoung, J.H.J., Seal, R.R.I., Bradley, D.C. (Eds.), Critical mineral resources of the United States—Economic and environmental geology and prospects for future supply. U.S. Geological Survey pp. T1-T23.

Žák, J., Verner, K., Týcová, P., 2008. Grain-scale processes in actively deforming magma mushes: New insights from electron backscatter diffraction (EBSD) analysis of biotite schlieren in the Jizera granite, Bohemian Massif. Lithos 106, 309-322.

Zhang, W.-Q., Dick, H.J.B., Liu, C.-Z., Lin, Y.-Z., Angeloni, L.M., 2021. MORB Melt Transport through Atlantis Bank Oceanic Batholith (SW Indian Ridge). Journal of Petrology 62.

Zhang, W.-Q., Liu, C.-Z., Dick, H.J.B., 2020. Evidence for Multi-stage Melt Transport in the Lower Ocean Crust: the Atlantis Bank Gabbroic Massif (IODP Hole U1473A, SW Indian Ridge). Journal of Petrology 61.

Figure Labels

Figure 1. Geological context of oceanic samples. (a) location of core 735B at Atlantis Bank (made with GeoMapApp (www.geomapapp.org; Deans and Yoshinobu, 2019; Ryan et al., 2009)); (b) graph of Fe_2O_3 vs TiO_2 for whole rock oceanic gabbro data from the database of (Gale et al., 2013) showing core 735B and overall trend in compositions (grey arrow); (c) 735B core section showing properties of oxide-rich (red) vs oxide-poor (blue) oceanic gabbros, (i) rock type and (ii) crystal-plastic deformation in the core after (Dick et al., 2019; Dick et al., 1999b); 0 – no foliation, 1 – some deformation, lacks foliation; 2 – clear foliation; 3 – strongly foliated, protomylonite; 4 – strongly laminated, mylonite; 5 - ultramylonite; blue star indicates location of representative samples 47R2-1 and 47R2-3; (iii) whole rock TiO_2 weight

944 percentage and (iv) plagioclase X_{An} values from shipboard data (Dick et al., 2002); (d) core photo around
945 the location of the samples (blue stars) with matching diagram of oxides, dashed lines indicate foliation
946 trend of oxides.

947

948 Figure 2. Geological context of continental sample. (a) location of the Strangways Metamorphic Complex
949 (SMC) in central Australia after (Silva et al., 2018); (b) location of investigated continental garnet-biotite
950 schist sample CP1604C (marked by red star) in the Cattle Water Pass shear zone (modified from
951 Norman, 1991).

952

953 Figure 3. Overview images (PPL, XPL, BSE and Ti maps) of oxide-rich and oxide-poor samples in oceanic
954 samples: 47R2-3 and 47R2-1 from Atlantis Bank, SWIR) and continental sample CP1604C (central
955 Australia). Note the increased mode of ilmenite in the high oxide oceanic sample (47R2-1; h) and
956 domain in continental sample (CP1604C; above the white dashed line in panel l). The yellow arrow in 'a'
957 shows an ilmenite finger replacing plagioclase; white box in (e) and red box in (k) show the areas of
958 EBSD mapping in Figure 5 and Figure 6, respectively.

959

960 Figure 4. Microstructures showing melt-rock interaction. BSE images of oceanic samples from Atlantis
961 Bank (a-g) and continental sample from central Australia (h-k). 3D microCT scan of oceanic sample 47R2-
962 1(l-n). Arrows point to microstructures: yellow: protrusions of oxides into silicate minerals, red: oxide
963 films along grain boundaries, green: oxides terminating with low dihedral angles, blue: garnet
964 pseudomorphed by oxides, orange: En with same interference colour indicating same orientation,
965 intergrown with Di, white: inclusions. Yellow lines highlight straight versus irregular boundaries,

966 magenta lines (e) highlight parallel protrusions of oxides into diopside, green dashed lines mark the
967 boundaries between ilmenite and magnetite and red lines (g(i)) mark the orientations of exsolutions of
968 ilmenite and spinel in magnetite. Mineral abbreviations are after Whitney and Evans (2010).

969

970 Figure 5. 3D interconnectivity and mineral relationships of oceanic high oxide sample 47R2-1 based on
971 EBSD analysis highlighting connectivity of apparently isolated grains in three dimensions and internal
972 deformation. (a) Phase map of a small section of the sample (see Fig. 3e), areas in b, c and d marked by
973 dashed boxes; (b) Ilmenite grains (I1 to I3) (c) Diopside grains (D1 to D3) and (d) Enstatite grains (E1 and
974 E2) each have an Euler map with c-axis pole figure, and an image and graph of change in orientation
975 within a grain from a reference orientation marked with a white cross. Ilmenite {10-10} pole figure is
976 included in (c) to show that the crystal boundary on diopside grains 1 and 2 are parallel to the relict
977 ilmenite grain 1 crystal face.

978

979 Figure 6. 3D interconnectivity, internal deformation and epitaxy of continental sample CP1604C. (a)
980 Phase map of a small section of the sample (see Fig. 3k), areas in b and c marked in white boxes; (b, c)
981 Ilmenite and garnet Euler maps with c-axis pole figures, and in b_1, c_1 an image showing change in
982 orientation within a grain from a reference orientation marked with a white cross and misorientation
983 profile marked by the yellow line starting at the dot in (a). Crystallographic orientation pole figures for
984 ilmenite (d), garnet (e); and biotite (f). Note: All the grains have been plotted as no single grain has a
985 dominating effect.

986

Figure 7. Comparison of electron microprobe mineral chemistry for both oceanic and continental settings. (a) Ternary diagram of pyroxenes (Wo – wollastonite; En – enstatite; Fs – ferrosilite), plagioclase (An – anorthite; Ab – albite; Or – orthoclase), garnet (Py – pyrope; Al+Sp – almandine-spessartine; Gr – grossular) and biotite (orange apex labels); (b–d) Ilmenite composition showing opposite trends for MgO and MnO for oceanic samples (red arrows in c and d).

Figure 8. Cartoon illustrating the evolution melt composition and impact of melt-rock interaction on the rock composition and microstructure. Melts 1, 2 and 3 refer to dynamic compositional changes in response to melt-rock interaction of the fluxing melt. (a) Oceanic setting (after Fig. 4b, and 5): Step1 – a fractionated gabbroic melt1 (white solid) moves through a precursor olivine gabbro to initiate formation of diopside and ilmenite along enstatite and plagioclase boundaries by melt-rock interaction (step 1). This causes the formation of a modified melt2 (white dashed). Step 2 – interactions between melt2 and the rock causes further growth of diopside and ilmenite and the formation of a new modified melt3 (white dots). Step 3 – interactions between melt3 and the rock causes growth of new diopside and magnetite; *changing conditions, e.g. pressure, temperature, oxygen fugacity, P or Ti content changes in incoming melt (b) Continental setting (after Fig. 3k, 4h-k and 6): Step 1 – a primary or fractionated S-type granitic melt1 (yellow) infiltrates a granulite facies felsic gneiss along a shear zone; melt-rock interaction leads to growth of aligned biotite and minor garnet and the formation of melt2 (orange). Step 2 – interactions between melt2 and the rock increases the mode of biotite and garnet and the formation of melt3 (red). Step 3 – interactions between melt3 and the rock forms interstitial ilmenite and again increases the modes of biotite, garnet and ilmenite. Minerals with their boundaries in the colour of a particular melt (e.g. Melt1) are interpreted to have re-equilibrated with that respective melt.

Oxide enrichment by syntectonic melt-rock interaction

Hindol Ghatak[1], Robyn L. Gardner[1], Nathan R. Daczko[1], Sandra Piazolo[2], Luke Milan[3]

[1]Australian Research Council Centre of Excellence for Core to Crust Fluid Systems/GEMOC, Department of Earth and Environmental Sciences, Macquarie University, NSW 2109, Australia

[2] School of Earth and Environment, University of Leeds, Leeds LS2 9JT, United Kingdom

[3] Earth Sciences, School of Environmental and Rural Science, The University of New England, Armidale, NSW, 2351, Australia

*corresponding author: robyn.gardner@mq.edu.au Phone: 61-2-9850 8371

Abstract

Processes ~~to~~that enrich rocks in oxides, such as ilmenite, are controversial. Current models include magmatic accumulation, crystallisation of veins from immiscible liquids and syntectonic differentiation. In this contribution, we investigate examples of oxide enrichment in both the oceanic and continental crust. The oceanic samples are of oxide gabbros (with up to 45 vol.% oxides) from the Atlantis Bank oceanic core complex, Southwest Indian Ridge. The continental sample is from the Cattle Water Pass shear zone (with up to 20 vol.% oxides) associated with the intracontinental Alice Springs Orogeny, central Australia. We argue for the occurrence of an open chemical system, with melt rock reactions as a key process involved in oxide enrichment in melt-fluxed shear zones. Our detailed microstructural

characterisation reveals that oxides replace silicates and form interstitial grains, grain boundary films and low dihedral angles between silicates often making up an interconnected skeletal texture. Quantitative orientation data reveals that the oxides: 1) have limited internal deformation, 2) form clusters of grains that are connected in 3D, 3) have crystal faces matching the orientation of the grain boundary of nearby newly crystallised diopside (oceanic sample) and 4) form part of the foliation defining assemblage with biotite (continental sample). This evidence suggests the oxides crystallised in the presence of melt and formed during melt-rock interaction. Syntectonic melt migration is known to ~~form very~~result in low strain microstructures in shear zones, as the strain is accommodated by the melt that existed in the deforming rock. This produces a high strain rock with silicate and oxide minerals ~~with~~that show limited internal deformation. Microchemical data shows major element variability in silicates and ilmenite at the thin section scale, supporting an open chemical system with local variability in both oceanic and continental settings. It further argues that syntectonic melt migration is important in oxide enrichment. Mineral chemistry data implies that the oceanic tectonic setting involved melt-rock interaction with fractionated gabbroic melt while the continental setting involved peraluminous granite melt driving ~~the~~mineral replacement~~-~~ and enrichment of oxides. We propose that deformation assisted reactive porous flow of near liquidus melt through rocks in any tectonic setting may result in ~~disequilibrium~~ melt-rock ~~reactions that progressively modify melt compositions and enrich oxide minerals~~interaction induced crystallisation of oxides in preference to silicates~~.~~ and that with high time-integrated melt flux, the accumulation of oxides can be significant.

Highlights:

- Microstructures indicate ~~the~~ former presence of melt within crustal shear zones
- Fractionated gabbroic melt interacts with oceanic crust to enrich oxides
- Peraluminous granite melt interacts with continental crust to enrich oxides

- High volumes of fluxing and reacting melt ~~needed to significantly~~ enrich host rock in oxides
- ~~Evidence of multiple~~Multiple fluxes of external melt are associated with strain localisation

Keywords:

Scientific ocean drilling; oceanic core complex; intracontinental orogeny; melt microstructures; melt-present deformation; oxide enrichment.

1. Introduction

Titanium, a critical industrial metal, is predominantly sourced from rutile and ilmenite in mineral sands (Roy et al., 2000), which ~~are~~have weathered from igneous or metamorphic rocks. Besides mineral sands, hard rock Fe-Ti oxide-rich deposits of magmatic origin like Allard Lake, Canada and Tellnes, Norway have been mined for years ~~(Charlier et al., 2010; Charlier et al., 2007). For an element or mineral to become an economic resource, it needs to be enriched. Thus, in the context of titanium~~(Charlier et al., 2010). For titanium to become an economic resource, it needs to be enriched as the average crustal abundance is < 1% TiO_2 but concentrations > 2 % are needed for viable mining (Woodruff et al., 2017). Thus, it is crucial to understand the primary mechanism of Fe-Ti oxide deposit formation. However, the processes responsible for Fe-Ti oxide enrichment remain controversial. Proposed processes include: (i) formation of oxide cumulate layers ~~(Charlier et al., 2007; Duchesne and Charlier, 2005)~~(Duchesne and Charlier, 2005) through density-driven mineral settling, (ii) crystallisation from immiscible liquids forming ore-rich veins ~~(e.g. Charlier and Grove, 2012; Dixon and Rutherford, 1979; Holness et al., 2011)~~(e.g. Dixon and Rutherford, 1979; Holness et al., 2011), and (iii) crystallisation during syntectonic differentiation ~~(Agar and Lloyd, 1997; Dick et al., 1991; Hopkinson and Roberts, 1995)~~(Agar and Lloyd, 1997; Dick et al., 1991; Hopkinson and Roberts, 1995), where fractionated intercumulus melt is mobilised into shear zones by deformation and compaction (Bloomer et al., 1991).

In this study, we focus on the syntectonic differentiation model which is based on observations from shear zones in oceanic gabbros that are enriched in oxides (Robinson et al., 2000). However, such oxide enrichment associated with shear zones is not restricted to the oceanic crust alone. Geologists have documented several locations within the continental crust ofwhere similar oxide enrichment is associated with high strain zones (Emslie et al., 1994; Gross et al., 1995; Scoates and Chamberlain, 1997)(Emslie et al., 1994; Gross et al., 1995; Scoates and Chamberlain, 1997). The latter may be an important source offor the Fe-Ti sands mined worldwide.

Despite the potential importance of Fe-Ti oxide enrichment in shear zones, there is relatively little work on the processes associated with this mineralisation. For the gabbroic rocks in oceanic settings, two key petrogenetic models relative to the timing of oxide crystallisation, deformation and strain localisation have been proposed: (1) oxides were concentrated by igneous processes of magmatic accumulation or immiscibility processes prior to strain localisation and the formation of shear zones (Cannat et al., 1991), or (2) strain localisation formed a shear zone in oxide-poor gabbro and was followed by metamorphic processes including melt-rock reactions and oxide crystallisation during deformation-assisted diffuse porous melt flow through the shear zone, called syntectonic differentiation (Bloomer et al., 1991; Dick et al., 1991; Hopkinson and Roberts, 1995)(Bloomer et al., 1991; Dick et al., 1991; Hopkinson and Roberts, 1995).

These two petrogenetic models result in the formation of rocks with distinct igneous versus metamorphic microstructures. Igneous processes crystallise minerals directly from a melt whereas metamorphic processes modify these igneous minerals by reactions with a fluid, and/or in response to temperature or pressure changes. In the first model indicative microstructures would be predominantly of igneous origin and include euhedral to subhedral crystals with interlocking and interstitial microstructures with possibly a magmatic foliation. In this scenario, we would expect a typical igneous crystallisation sequence, where both ilmenite and magnetite crystallise from the fractionating melt.

~~The~~In the second model, indicative microstructures would be predominantly metamorphic in origin and include, interstitial microstructures, fewer crystal faces, melt-rock reaction textures and possibly the absence of typical mylonitic shear zone characteristics (Lee et al., 2018; Meek et al., 2019; Prakash et al., 2018; Stuart et al., 2018b).

Consequently, the microstructural characteristics of the minerals in oxide-rich rocks are key to distinguish between these two scenarios. ~~For example~~In addition, in model (1), deformation microstructures will be evident in both the silicate and oxide minerals. In contrast, melt accommodates stress during melt-present deformation in model (2); consequently, the solid framework will remain ~~largely undeformed. In addition, in the second scenario, the microstructural characteristics typical of mylonitic shear zones may be absent and melt-rock reaction textures are predicted (Lee et al., 2018; Meek et al., 2019; Prakash et al., 2018; Stuart et al., 2018b).~~generally undeformed.

To elucidate the processes associated with oxide enrichment in high strain zones, we investigate oxide enrichment in two contrasting environments: oxide-rich gabbros associated with shear zones within an oceanic core complex, and oxide-biotite-rich schist belts from central Australia. Our research is at the interface between igneous and metamorphic systems and involves reactive flow of melt through crustal rocks driving metamorphic reactions.

~~Our study examines two adjacent oceanic oxide gabbro rocks (taken 10 cm apart) in unit IV of the ODP Leg 118 (228 mbsf, hole 735B), from the Atlantis Bank, Southwest Indian Ridge (Fig. 1). They exhibit 15 vol.% and 44 vol.% oxide modes (47R2-3 and 47R2-1, respectively). The continental sample comes from the oxide-rich (15–18 vol.%) Cattle Water Pass (CWP) Shear Zone (Fig. 2) formed during the Alice Springs Orogeny in central Australia. The shear zone is up to 800 m wide, steeply west-dipping and defined by 100300 m wide high strain zones of garnet-biotite schist (Ghatak, 2021).~~

We use detailed microstructural and microchemical analyses to recognise microstructures indicative of the former presence of melt. We determine that flux of externally derived melts caused melt-rock interactions to form new minerals, including oxides, in reaction textures ~~and oxide enrichment~~ in both oceanic and continental crust. Melt present shear zone activity is supported by the fact that minerals identified as solid during syntectonic melt migration remain largely undeformed, as the viscous melt accommodates much of the strain (Stuart et al., 2018b). Consequently, our data supports the syntectonic differentiation model facilitated by reactive porous melt flow as outlined above, in both the oceanic and continental settings. ~~Chemical analysis suggests that high temperature peraluminous granitic melts are important to drive oxide enrichment in the continental setting, while fractionated gabbroic melts are important in the oceanic environment.~~

2. General geological background

2.1. Oceanic environment: Atlantis Bank

The Atlantis Bank oceanic core complex is a ridge ~~720m~~720 m below the sea surface approximately 9 km long and 4 km wide situated south-east of Madagascar (Fig. 1a and inset) on the ultra-slow spreading Southwest Indian Ridge (SWIR). It is adjacent to the Atlantis II transform valley and ~19 km south of the SWIR axis. Pillow basalts and sheeted dykes typically found at the top of oceanic crust are missing suggesting an estimated 1.5–2.0 km of the crust has been unroofed during core complex uplift on the detachment fault ~~(Dick et al., 2000; Dick et al., 1999; John et al., 2004)~~(Dick et al., 2000; Dick et al., 1999a; John et al., 2004), thereby exposing massive gabbro at the seafloor. The 735B (32°43.392'S, 57°15.960'E) core was initially drilled to 500 mbsf on IODP expedition 118, then subsequently drilled to 1508 mbsf on IODP expedition 176 (Dick et al., ~~1999~~1999a).

The following core summary is based on information in ~~Dick et al. (1999)~~ Dick et al. (1999a), unless otherwise specified. The core is divided into 12 rock units (I – XII) based on mineral assemblage and rock type. The major rock types in the core are olivine gabbro (69.9%) and gabbro (14.9%), with lower proportions of oxide-rich gabbro (7%) and gabbronorite/oxide-rich gabbronorite (8%). Rock units can be further simplified ~~(Dick et al., 2002; Hertogen et al., 2002)~~(Dick et al., 2002; Hertogen et al., 2002) into (1) oxide-poor gabbro cut by hundreds of bodies of (2) oxide-rich gabbro (including both disseminated oxide gabbro and oxide gabbro) (Fig. ~~1c(i)).~~1ci). The oxides in the oxide-rich rocks have oxide modes to 45% and are predominantly magnetite and ilmenite with minor presence of sulphides. High titanium concentrations (Fig. 1c(iii)), generally in the form of ilmenite are typical of the oxide-rich gabbros. The core is variably deformed with the extent of crystal-plastic deformation being classed based on observed foliation, recrystallisation and preservation of relict igneous texture (Fig.1c(ii), Dick et al., 2019). Overall, three-quarters of the core lacks a foliation, 18% has a very weak foliation, 6% is strongly foliated and only 1% has mylonitic or ultra-mylonitic characteristics. The upper half of the core has many minor faults with major brittle faults of unknown displacement occurring at 560 and 690–700 mbsf (Fig. 1c(i), yellow dashed lines). A ~~20m~~20 m wide shear zone occurs lower in the core at 944–964 mbsf (Fig. 1c(i), white dashed lines). High strain zones, particularly those in the top half of the core, are often associated with high oxide abundance (Fig. 1c (i) and (ii)), though this is not always the case. Plagioclase compositions are bimodal with oxide-rich gabbros having generally lower X_{An} values (Fig. 1c(~~iii~~iv)). Evidence of melt-rock interaction within shear zones at Atlantis Bank has been previously reported by Gardner et al. (2020) and Zhang et al. (2020). Higher temperature deformation and melt-rock interaction are variably overprinted in the top half of the core by seawater infiltration, brittle deformation and hydrothermal alteration as the rocks were exhumed and cooled. The whole-rock TiO_2 vs Fe_2O_3 plot (Fig. 1b) of oceanic gabbros shows extensive variation of iron and titanium, though a general positive correlation is formed (Fig. 1b, grey arrow). Core 735B samples follow the same general trend.

For this study, we examined two adjacent oxide gabbro samples from unit IV at ~228 mbsf of the 735B core (Fig. 1d). This unit is within the upper half of the core (units I to IX) which is distinguished from the lower half (units X to XII) by higher proportions of oxide-rich gabbros (Fig. 1c(i)) and a weak foliation. However, the boundary between units III and IV (at 224 mbsf) is a <~~1m~~1 m thick mylonitic shear zone. The two oxide-rich gabbro samples are taken within 4 m of this mylonitic shear zone.

2.2. Continental environment: The Alice Springs Orogeny – Cattle Water Pass Shear Zone

The study area lies in the central Australian Arunta region (Fig. 2a, top) where the last ~~major~~regional tectono-metamorphic event was the Upper Palaeozoic (450–300 Ma) Alice Springs Orogeny (ASO) ~~(Hand and Sandiford, 1999; Raimondo et al., 2014).~~(Hand and Sandiford, 1999; Raimondo et al., 2014). The intraplate nature of the ASO involved N-S contraction ~~(Piazolo et al., 2020; Silva et al., 2018; Teyssier, 1985)~~(Piazolo et al., 2020; Silva et al., 2018; Teyssier, 1985) which resulted in the exhumation of mid to deep crustal rocks and the formation of anastomosing shear zones ~~(Cartwright et al., 1999; Raimondo et al., 2011)~~(Cartwright et al., 1999; Raimondo et al., 2011). The orogen (Fig. 2a, bottom) comprises, from W to E, amphibolite facies mid-crustal rocks, the mid to deep crustal Strangways Metamorphic Complex (SMC) and the deep crustal inverted rift-fill Harts Range Group.

The SMC is a broad belt, up to ~ 125 km wide, metamorphosed during the Strangways Event (c. 1735-1690 Ma) cut by schist belts with general S-directed thrusting (Bendall, 2000; Collins and Teyssier, 1989) in the southern side of the orogen (Fig. 2a). The shear zone examined here is the Cattle Water Pass shear zone (Fig. ~~2b) which was melt-present at the time of deformation (Ghatak, 2021; Silva et al., 2021)~~2b) which was melt-present at the time of deformation (Silva et al., 2021). The high strain zones within the Cattle Water Pass shear zone are 100–300 m wide, steeply west-dipping, with reverse shear sense and characterised by sillimanite-garnet-muscovite-biotite schist. The schists cut Proterozoic mafic,

felsic, and pelitic granulites resulting in lenses of variably deformed and modified granulite within high strain zones dominated by schist. Deformed and hydrated granulite contains anastomosing layers rich in biotite ± muscovite where sub-layers rich in ilmenite are also common.

3. Method of analysis

3.1. Petrography and quantitative orientation analysis

Sample mineral observations were made on polished thin sections cut in the structural XZ plane using a petrographic microscope. Microstructural/crystallographic characterisation of thin sections was performed both in the Leeds Electron Microscopy and Spectroscopy Centre, University of Leeds and at Macquarie GeoAnalytical, Macquarie University. The data was acquired using an FEI Quanta 650 FEG-Environmental Scanning Electron Microscope and a Zeiss IVO Scanning Electron Microscope, respectively. Both instruments were equipped with an HKL NordlysNano Electron backscatter diffraction (EBSD) detector and supported by Aztec analysis software (Oxford Instruments). EBSD mapping was performed covering a large area of the thin section in addition to small individual maps in specific regions, recording Energy Dispersive Spectroscopy (EDS) spectra along with the EBSD data. Working conditions were: 20 kV accelerating voltage, 20–26 mm working distance, 70° specimen tilt and step size between 4 and 10 µm depending on the area covered and grain size. ~~Data were processed using HKL Channel5 v5.11 and AztecCrystal with noise reduction performed on the raw data following the procedure of Bestmann and Prior (2003) and~~Data were processed using HKL Channel5 v5.11 and AztecCrystal with noise reduction performed on the raw data following the procedure of Piazolo et al. (2006). Wherever necessary, pole figure representations use one point per grain to eliminate the issue of large grains distorting the interpretation by causing single-crystal maxima. Where there is no dominance of individual grains, all data points have been plotted. We also show maps depicting the

relative change in crystal orientation within grains as a graded colour scale overlay on the phase maps and pole figures. Misorientation angles between adjacent analysed points of 2–10° and ≥ 10° define subgrain and grain boundaries, respectively. We use mineral abbreviations following Whitney and Evans (2010).

A high resolution image of the thin sections and other associated data can be examined at https://imagematrix.science.mq.edu.au/viewer/?mode=view&id=487 for 47R2-1 ~~and~~, id=488 for 47R2-3 and id=443 for CP1604C.

3.2. Imaging and geochemical analysis

3.2.1. Micro X-ray fluorescence (µ-XRF)

Analyses of the polished thin sections were used for mineral identification, to show the spatial distribution of oxide minerals and to calculate modal percentages of oxide minerals. µ-XRF analyses were performed using a Bruker M4 Tornado spectrometer at Macquarie GeoAnalytical, Macquarie University. The µ-XRF analyses were run with tube voltage of 50 kV, beam current of 200 µA, chamber pressure of 20 mbar, acquisition time of 15 ms/pixel and step size of 25 µm. Bruker AMICS (Advanced Mineral Identification and Characterisation System) was used to convert the X-ray fluorescence spectra to produce detailed mineral maps.

3.2.2. Backscatter electron imaging (BSE)

Scanned BSE images were used to identify and show the association of different minerals across the samples. Polished thin sections were carbon coated and imaged in an FEI Teneo Field Emission Scanning Electron Microscope (SEM) with Nanomin software at Macquarie GeoAnalytical, Macquarie University. The operating conditions of the SEM were ~~low~~high vacuum~~, 15 kV accelerating voltage and~~ at 10kV with a dwell time of ~~5µs~~2 µs.

3.2.3. Electron microprobe (EMP)

Additional compositional data of both the silicates and oxides was obtained for the sample from central Australia (CP1604C) using a JEOL JXA 8530F Plus field emission electron microprobe at the Central Science Laboratory, University of Tasmania. The instrument has a field emission source, running at an accelerating voltage of 15 kV, a beam current of 15 nA and a spot size of 10 µm. The ODP samples (47R2-1 and 47R2-3) were analysed using a Cameca SX-100 electron microprobe at Macquarie GeoAnalytical, Macquarie University. The operating conditions were a voltage of 15 kV, a beam current of 20 nA and a spot size of 1 µm. Standards used for calibration are included in Supplementary Table 4. Electron microprobe maps of the minerals were acquired using the Cameca SX-100 electron microprobe at Macquarie GeoAnalytical, Macquarie University. The element maps show the chemical variation within specific grains of interest and were collected with a focused beam of 15 kV, beam current of 100 nA, spot size of 1 µm, step size of 4 µm and dwell time of 100 ms.

3.3. Micro-computed tomography (micro-CT)

Micro-CT analysis of the high-oxide gabbro was undertaken in a GE Phoenix V|tome|xs CT scanner at The University of New England, Australia. The block was rotated about its vertical axis and scans were taken in 3 perpendicular directions. Scanning was performed at voltage of ~~220kV~~220 kV and current of 70 µA for ~~200ms~~200 ms for each scan. Individual ~~tomographs~~sections were extracted and processed in '3D slicer' software (https://www.slicer.org/, Fedorov et al., 2012). Oxide 3D models were made using the density data and Meshlab (Cignoni et al., 2008) was used to highlight the microstructures and oxide 3D connectivity.

4. Results

4.1. General sample description and petrography

4.1.1. Oceanic environment

The investigated samples exhibit moderate (15 vol.%; 47R2-3) to very high (44 vol.%; 47R2-1) modes of ilmenite and magnetite. Both samples are coarse-grained and comprise plagioclase (~18–21 vol.%), diopside (~27–52 vol.%), enstatite (~5–8 vol.%), ilmenite (~13–38 vol.%) and magnetite (~1–6 vol.%) with minor amphibole, sulphides, apatite, and spinel (Fig. 3a–h). Silicates generally lack evidence of crystal-plastic deformation such as bimodal grain size distribution (a signature of dynamic recrystallisation), undulose extinction or deformation twins (Fig. 3b, f). The oxide grains form a network of interconnected grains (Fig. 3c, g, 4l-n). Sample 47R2-3 exhibits 15 vol.% oxides dominated by ilmenite, while 47R2-1 has 44 vol.% oxides ~~characterised by~~with a mix of ilmenite and magnetite (Fig. 3d, h).

Oxide grains show highly irregular shapes with elongate finger-like protrusions that cut into grains of plagioclase (Fig. 4a, d; yellow arrow) and diopside (Fig. 4e; blue lines, yellow arrow), as well as along like and unlike mineral boundaries (Fig. 4b, d, e, f, l, m, red arrows). The oxide-rich domains form skeletal-like textures around silicate grains (Fig. 4e), and the domains are connected in three-dimensions by oxide bridges (Fig. 4l-n, red arrows). These domains preserve low dihedral angles against two adjoining diopside grains (Fig. 4e, f, n, green arrow). Some ilmenite grains appear as inclusions in diopside (Fig. 4f; white arrow), while other ilmenite-magnetite domains show straight faces against diopside (Fig. 4b; yellow line). Ilmenite grain boundaries with plagioclase tend to be more irregular (Fig. 4f; yellow lines). Ilmenite is commonly associated with magnetite in the high oxide content sample (47R2-1), where magnetite is mostly observed at the boundary of ilmenite with other minerals (Fig. 4e–g; green dashed line shows ilmenite-magnetite boundaries). The magnetite has a dusty appearance in BSE images (Fig.

4e–g) due to very fine inclusions of spinel and ilmenite and forms some lobate and finger-like shapes within the ilmenite. The inclusions in magnetite show three preferred orientations (Fig. 4g, inset (i), red lines). Ilmenite commonly lacks inclusions except at the boundaries between ilmenite and magnetite, where fine spinel grains are included in the ilmenite (Fig. 4g, inset (ii)). Diopside appears in two textural settings: (i) as large single grains (Fig. 4c, e, f) and (ii) as rims of diopside around two-pyroxene domains where the proportions of enstatite and diopside are variable (labelled En-Di symplectite on Fig. 4b–d). Neighbouring fine and coarse enstatite grains share similar interference colour under crossed polarised light (orange arrows, Fig. 4c), indicating similar orientation. Fingers of diopside project into enstatite with low dihedral angles (green arrow, Fig. 4c). The finger shown in Figure 4c shares extinction positions with a diopside inclusion within the enstatite (inset Fig. 4c, purple arrow). Plagioclase forms large single grains (Fig. 3f, 4a, d) which rarely show deformation microstructures (e.g., undulose extinction, deformation twins, dynamic recrystallisation). Rare grains of plagioclase are cut by veins of very fine grained green hornblende (Fig. 4a).

4.1.2. Continental environment

The high-strain continental CWP shear zone sample is a fine- to medium-grained rock with a well-developed foliation defined by bands of variable ilmenite content and alignment of biotite and ilmenite minerals. It exhibits two distinct bands based on minerals present: (i) quartz-plagioclase-rich, and (ii) garnet-biotite-ilmenite-rich bands (Fig. 3i). The quartz-plagioclase-rich, low-oxide domain comprises quartz (~45–50 vol.%), plagioclase (~25–30 vol.%), biotite (~10–15 vol.%), garnet (~3–5 vol.%), and minor ilmenite (~2 vol.%) (Fig. 3i–l, bottom). The high-oxide (ilmenite) domain comprises garnet (~25–30 vol.%), biotite (~45–50 vol.%), ilmenite (~16-18 vol.%), and minor apatite (<2 vol.%) (Fig. 3i–l, top). The silicates generally lack evidence of crystal-plastic deformation such as recrystallisation, undulose extinction or deformation twins (Fig. 3j).

Oxide grains form interstitial textures with elongate grain shapes along grain boundaries (Fig. 4h, i; red arrows). The oxide grains show both straight (Fig. 4h, j; yellow lines) and irregular (Fig. 4h–k; yellow arrows) boundaries with garnet and biotite. Some ilmenite grains form lobes (Fig. 4i; yellow arrows) or inclusions (Fig. 4k; white arrow) in garnet, while others have shapes and sizes similar to garnet (Fig. 4j; blue arrow).

4.2. Quantitative orientation data (EBSD analysis)

EBSD analysis is used mainly to identify (i) interconnectivity of interstitial phases in three dimensions, (ii) relationships between grain shape and crystal orientation (e.g., identification of faceting) and (iii) presence of internal deformation features ~~such as~~(e.g., sub-grains and crystallographic orientation variations) which are signatures of dynamic ~~recrystallization~~recrystallisation and crystal plasticity. The assessment of interconnectivity of interstitial phases assumes that in the two-dimensional section of a thin section, grains that are spatially close to each other but not connected to each other, are interconnected in three dimensions if they exhibit the same or very similar crystallographic orientation~~.~~ ~~Such unity of crystallographic orientation suggests that the apparent separate grains in two dimensions are in fact one grain when viewed in three dimensions~~ (Meek et al., 2019)~~).~~.

4.2.1. Oceanic environment

A single area of EBSD phase map with orientation overlays is presented as representative for oxide-rich sample 47R2-1 from the oceanic gabbros (Fig. 5). The map shows two two-pyroxene (enstatite-diopside) domains (Fig. 5a, upper right, lower left) with a distinct diopside rim on the upper right domain. Between the two domains there are grains of plagioclase, ilmenite and magnetite. Most ilmenite grains show only minor internal deformation based on few 2–10° subgrain boundaries (Fig. 5a, b, white lines) and minor changes in internal orientations across a grain (grain I3, Fig. 5b, green overlay, 0–10°, and misorientation profile). The diopside rim shares a straight grain boundary with an oxide rich domain (Fig.

5c). The orientation of the diopside boundary (red line, Fig. 5c) corresponds to the crystal face of the adjacent relict ilmenite, I1, (Fig. 5c, red line, ilmenite {10-10} pole figure). Rare grains of ilmenite and most grains of diopside and enstatite show no internal deformation (i.e., have few white lines on Fig. 5a, c, d).

Small diopside grains within enstatite in the two-pyroxene domain (Fig. 5a, top right) share the same crystallographic orientation with the wide diopside rim (Fig. 5c, grain D1, Euler map and pole figure). The coarse grained diopside rim shows very little crystallographic orientation change across the grain (Fig. 5c, grain D1, misorientation profile). A cluster of enstatite grains, E1, is present at the boundary between two diopside grains forming the diopside rim (Fig. 5c, grains D1 and D2). These enstatite grains show similar orientations to each other (green in Fig. 5d;) and a c axis orientation similar to the two diopside rim grains (compare pole figures; Fig. 5c, d, grains E1, D1 and D2). The cluster of diopside grains (Fig. 5c, grain D2) share the same crystallographic orientation with each other, so are likely to be interconnected in 3D~~, even though they appear to be 3 distinct grains in two dimensions.~~. In the area dominated by oxides (upper left of Fig. 5a), a cluster of ilmenite grains included within magnetite show similar orientation (Fig. 5b, grains marked I3), so are also likely connected in 3D, but the adjacent ilmenite and surrounding magnetite do not share a similar orientation.

4.2.2. Continental environment

A single large area EBSD phase map with orientation overlays is presented for the high-oxide domain of sample CP1604C from the Cattle Water Pass shear zone (Fig. 6). The map shows most oxide grains lack significant internal orientation changes ~~and~~, exhibit a limited number of subgrain boundaries (Fig. 6a, b) and ~~rare~~have little variation in the orientation across individual grains (Fig. $6b_1$, misorientation profile). Two clusters of ilmenite grains (Fig. 6b, I1 and I2) show similar orientation based on Euler orientation maps and a c-axis pole figure. Garnet grains also show very little orientation change within individual

grains (Fig. 6c$_1$) while clusters of adjoining grains have very similar orientation (Fig. 6c, Euler map and pole figure). Clustered c-axis orientations with a maximum of 10 for all ilmenite grains (Fig. 6d) indicate a strong crystallographic preferred orientation (CPO) that matches the strong c-axis alignment of biotite grains (Fig. 6f). In contrast, garnet presents no pronounced ~~crystallographic preferred orientation~~CPO (Fig. 6e).

4.3. Mineral chemistry data

All silicate minerals in all samples show limited chemical variation (Fig. 7; Supplementary Table 1). This is also apparent in microprobe chemical maps (Supplementary Figure 1) which show remarkably uniform compositions for each grain. Below we present the detailed mineral chemistry.

4.3.1. Oceanic environment

Plagioclase in ODP high oxide sample 47R2-1 is andesine of restricted composition (X_{An} = Ca/(Ca+Na+K) = 0.37–0.40) (Fig. 7a), typical of plagioclase compositions in most oxide-rich gabbro in the core (Fig. 1c(~~iii~~iv)). Diopside has the most variability from predominantly diopside to minor augite (X_{Mg} = Mg/(Mg+Fe) = 0.61–0.71) (Fig. 7a). Enstatite composition has little variability (X_{Mg} = 0.60–0.61) (Fig. 7a). Ilmenite grains in the two ODP samples show minor variation in TiO_2 content but increasing FeO and MgO (Fig. 7b, c) and decreasing MnO (Fig. 7d) as the proportion of oxides increased between sample 47R2-3 (low-oxide sample) to 47R2-1 (high-oxide sample).

4.3.2. Continental environment

Plagioclase in sample CP1604C is andesine of restricted composition (X_{An} = 0.43–0.47) with two analyses of lower anorthite content (X_{An} = 0.23 and 0.33) (Fig. 7a). Garnet is ~~pyrope-rich~~ almandine (X_{Alm} = Fe/(Fe+Mg+Ca+Mn) = 0.78–0.82~~;~~) with substantial pyrope (X_{Pyr} = Mg/(Fe+Mg+Ca+Mn) = 0.14–0.18~~;~~) and minor grossular (X_{Grs} = Ca/(Fe+Mg+Ca+Mn) = 0.01–0.06~~;~~) and spessartine (X_{Sps} = Mn/(Fe+Mg+Ca+Mn) = 0.03;) components (Fig. 7a). Biotite is Fe-Mn-rich and plots at the boundary between 'primary magmatic'

and 're-equilibrated' biotite on the classification scheme of Nachit et al. (2005) (X_{Mg} = 0.46–0.51). In contrast to the ODP samples, ilmenite grains from Cattle Water Pass vary from 42–47 wt.% TiO_2 but show very limited variation in MgO, FeO and MnO content (Fig. 7b–d).

5. Discussion

We argue for the occurrence of an open chemical system maintained by syntectonic porous melt flow, with melt rock reactions as a key process involved in oxide enrichment in melt-fluxed shear zones. In the following discussion we provide evidence for a metamorphic rather than ~~*magmatic*~~igneous origin of the oxides and show, using microstructures, that the oxide-rich rocks investigated formed in the presence of a reactive melt. Based on mineral chemistry and the regional tectonic setting of the rocks investigated we infer a fractionated gabbroic melt as the main reactant in the oceanic setting and a high temperature peraluminous granitic melt in the continental setting. ~~*Our data suggests melt-rock interaction occurred in a syn-deformational, open chemical system.*~~ We conclude the discussion by assessing the signatures and consequences of syntectonic reactive porous melt flow in crustal environments.

5.1. The origin of oxide-rich rocks in oceanic tectonic settings

~~*5.1.1. Igneous versus metamorphic character*~~

The two key petrogenetic models, described in the introduction, result in the formation of rocks with distinct igneous versus metamorphic microstructures. ~~In the first model, where oxides are concentrated by magmatic accumulation or immiscibility processes (Charlier and Grove, 2012; Charlier et al., 2007; Dixon and Rutherford, 1979; Duchesne and Charlier, 2005), indicative microstructures would include euhedral to subhedral crystals with interlocking and interstitial microstructures, possibly with a magmatic foliation.~~ In the second model described~~In this scenario, we would expect a typical igneous crystallisation sequence, where both ilmenite and magnetite crystallise from the fractionating melt.~~

~~Interlocking grains lacking crystal-plastic deformation would be expected. In the second model~~, oxide enrichment occurs via melt-rock metamorphic reactions during deformation-assisted melt flow through a shear zone ~~(Bloomer et al., 1991; Dick et al., 1991; Hopkinson and Roberts, 1995).~~(Bloomer et al., 1991; Dick et al., 1991; Hopkinson and Roberts, 1995). Indicative microstructures ~~would~~ include some internal deformation within grains, interstitial microstructures, replacement reaction microstructures and fewer crystal faces.

5.1.1. ~~We interpret that the spatially associated~~ Microstructures showing metamorphic replacement reactions

Although ilmenite and magnetite are spatially associated (e.g. Fig. ~~formed via two different melt-rock reactions. The interpretation that magnetite partially replaces~~4e to g) we interpret earlier ilmenite is ~~supported by~~partially replaced by magnetite based on the following observations: (1) the proportion of ilmenite to magnetite increases from the low oxide sample 47R2-3 ~~where ilmenite predominates,~~ (ilmenite to magnetite proportions 9:1), to the high oxide sample 47R2-1~~, which has~~ (ilmenite to magnetite proportions of 7:1) (Fig. 3h); (2) presence of irregular boundaries between ilmenite and magnetite including finger-like protrusions of magnetite into ilmenite (Fig. 4g); (3) presence of magnetite as rims on ilmenite and as elongate grains at boundaries between ilmenite and silicate minerals (Fig. 4e, f, 5a; e.g., plagioclase and diopside); (4) presence of a cluster of irregular ilmenite grains within magnetite that share identical orientation which represent relicts of a partially replaced single coarse crystal of ilmenite (Fig. 5b, I3); (5) presence of reaction front microstructures where spinel grains are included in ilmenite near the boundaries with magnetite (Fig. 4g(ii), Supplementary Fig. 1f; Bowles et al., 2011); and (6) straight boundaries between new diopside (red line, Fig. 5c) and magnetite that mimic crystal facets of relict ilmenite (Fig. ~~4c, ilmenite pole figure, grain I1). Finer~~4c, ilmenite pole figure, grain I1), indicating the original ilmenite crystal face grew into a melt (Vernon, 2000). In addition, fine grained spinel and ilmenite included within magnetite show three different crystallographic

orientations and are interpreted as exsolution microstructures which formed during cooling (Fig. 4g(i)). Adjacent to the magnetite replacement texture shown in Figure 5a, the diopside (Fig. 5c, grain D1) is partially replaced by a new diopside (Fig. 5c, grain D2) with enstatite (Fig. 5d, grain E1) that is epitaxial on the old diopside (Fig. 5c, d). We interpret these to have formed coevally with the partial replacement of ilmenite by magnetite (Fig. 8a).

In addition to the reaction microstructures associated with magnetite as outlined above, we observe other evidence of metamorphic reactions~~.~~ that involve pyroxenes. A cluster of enstatite grains (orange arrows, Fig. 4c) shares very similar interference colours and extinction angles, suggesting that they formed a single relict enstatite grain partially replaced by the diopside. This is further supported by the finger of diopside projecting into and replacing the coarse enstatite (green arrow, Fig. 4c). The proportion of enstatite is higher in the lower left and lower in the upper right of Figure 4c, consistent with the progressive replacement of enstatite by diopside (Fig. 8a). This reaction replacement microstructure is confirmed by diopside in both the rims around two-pyroxene domains and all the diopside within the two-pyroxene domain sharing a single crystallographic orientation (Fig. 4b, 5c, grain D1), and mineral chemistry (Supplementary Fig. 1e). However, the two-pyroxene domains have previously been interpreted as inverted pigeonite that has rims of later diopside ~~(Dick et al., 1991; Ozawa et al., 1991)~~(Dick et al., 1991; Ozawa et al., 1991). We argue against this as the diopside rim is crystallographically continuous with the diopside in the two-pyroxene domain. Additionally, the elongation of the diopside grains within the two-pyroxene domains is not oriented parallel to either enstatite (001) or (100) as would be expected for inverted pigeonite (Philpotts and Ague, 2009).

The diopside rims around two-pyroxene domains are spatially associated with high proportions of oxides (e.g., Fig. 4b, d, Supplementary Fig. 1e). The oxide grains share some straight boundaries with the diopside rims (e.g., yellow line on Fig. 4b corresponds with an ilmenite {10-10} crystal face, Fig. ~~5c). The oxide grains commonly form films along grain boundaries (Fig. 4, red arrows) and protrusions into~~

~~plagioclase grains (Fig. 4, yellow arrows). These observations of disequilibrium microstructures are consistent with progressive reaction.~~ 5c), suggesting the original ilmenite crystal face grew into a free melt and the diopside rim crystallised later. The oxide grains commonly form films along grain boundaries (Fig. 4, red arrows) and protrusions into plagioclase grains (Fig. 4, yellow arrows). These observations of disequilibrium microstructures are consistent with progressive reaction from the original igneous olivine gabbro to melt-reaction-modified oxide-rich gabbros~~The titanium content in individual ilmenite grains is uniform (Supplementary Fig. 1a, b), ruling out solid-state diffusional processes and consistent with fluid-mediated replacement reactions (e.g. Putnis, 2009) . However, the manganese and magnesium content show minor variation between grains within a sample but form a geochemical trend between the two samples (Fig. 7c, d, red arrows). In addition, the bimodal variation of plagioclase composition between the oxide-rich and oxide-poor gabbros (Fig. 1d(iii)) suggests open system processes rather than diffusional processes were operating. The abundant evidence for replacement microstructures and this chemical variation and trend between the low- and high-oxide samples is consistent with an open system environment lacking a close approach to textural and chemical equilibrium~~.

5.1.2. Former presence of melt and inferred melt-rock reactions

Early research on the oceanic crust drilled at hole 735B inferred melt migration as an important process in the development of the microstructures observed in gabbroic samples (Dick et al., 1991). Recent works have further established multiple fluxes of external melt through shear zones ~~(Casini et al., 2021; Gardner et al., 2020; Zhang et al., 2021; Zhang et al., 2020)~~ (Casini et al., 2021; Gardner et al., 2020; Zhang et al., 2021; Zhang et al., 2020). The flux of a high temperature hydrous fluid is not considered likely as the samples examined lack evidence of hydrous minerals such as chlorite, epidote, sericite replacing feldspar, or veins of these minerals and preservation of reaction textures where igneous minerals are partially consumed. However, these microstructures are documented elsewhere in the

core, suggesting that hydrous fluids are important agents of metamorphism in other sections of the core. Further support for the presence of melt instead of a hot hydrous fluid is the lack of amphibole in our samples. This lack of amphibole suggests either the presence of melt with low activity of water during melt-rock interaction or that the temperature of fluid-rock interaction was higher than the stability field of amphibole.

Microstructures indicative of the former presence of melt ~~(Holness et al., 2011; Lee et al., 2018; Stuart et al., 2018b; Vernon, 2000)~~(Holness et al., 2011; Lee et al., 2018; Stuart et al., 2018b; Vernon, 2000) in the oceanic rocks confirm previous research; they include: (1) films along grain boundaries forming skeletal-like microstructures (Fig. 3g, 4e), with or without crystal faces (Fig. 4b, yellow line, Fig. 5a), (2) grains with low dihedral angles (Fig. 4e, f, green arrows), and (3) 3D connectivity of a cluster of grains (Fig. 5b, c, d). A lack of local partial melting textures (e.g., peritectic minerals surrounded by leucosome) suggests the melt was externally derived, resulting in sequential rock transformation from precursor olivine gabbro under the influence of a chemically dynamic and reactive fluxing melt (forming the En-Pl-rich gabbro shown in Fig. 8a):

Precursor olivine gabbro + melt ➔ En-Pl-rich gabbro + melt1 ~~➔ Di + En + Pl + Ilm + melt2~~ (1)

The replacement of olivine by enstatite during melt-rock interaction is consistent with the findings in Gardner et al. (2020). The lack of olivine in the studied samples, which is nearly ubiquitous in the core at hole 735B (Dick et al., 2019), suggests melt-rock reactions have completely replaced the precursor olivine-bearing gabbroic rocks. The compositions of melt on either side of reaction (1) were likely highly variable depending on the (i) composition of the melt source ~~(i.e., gabbroic versus fractionated gabbroic melts; Dick et al., 2019; Zhang et al., 2020)~~(i.e., gabbroic versus fractionated gabbroic melts; Dick et al., 2019; Zhang et al., 2020), (ii) extent of geochemical modification of the melt during reactive flow

~~(Daczko et al., 2016; Stuart et al., 2018a)~~(Daczko et al., 2016; Stuart et al., 2018a), (iii) variation in rock types interacted with along melt migration pathways, and (iv) possible trapping of early crystallised minerals (i.e. phenocrysts in the migrating melts) during the collapse of pathways ~~(Bons et al., 2004; Silva et al., 2021; Žák et al., 2008)~~(Bons et al., 2004; Silva et al., 2021; Žák et al., 2008) as melt supply is reduced. These variable controls on the compositions of melt in reaction (1) are also true for all melt in all reactions discussed below.

Concurrent and subsequent melt migration of highly variable melts caused local reactions~~:~~ (Fig 8a, steps1 and 2):

En-Pl-rich gabbro + melt1 or 2 ➔ rock + Di + Ilm + melt2 ➔ ~~Di + melt3~~ or 3 (2)

The final melt-rock reaction in the sample (Fig 8a, step3) is:

Ilm + Di + melt3 ➔ Mag + Sp + (new) Di + ~~En +~~ melt4 (3)

Reactions (2) and (3) (Fig. 8a, step 1 to 3) have been discussed earlier (section 5.1.1) wherein diopside replaces enstatite and magnetite replaces ilmenite (Fig. 4 and 5).

~~Reactions (2) and (3) (Fig. 8a, step 1 to 3) have been discussed earlier (section 5.1.1) wherein diopside replaces enstatite and magnetite replaces ilmenite (Fig. 4 and 5).~~

5.1.3. ~~Composition~~Mineral compositions: inferences for composition of the fluxing melt(s)

In the gabbros, the TiO_2 whole rock data (Fig. 1c(iii) shows a distinct increase in titanium in the oxide-rich rocks (Fig. 1c(iii)) relative to the oxide-poor gabbros. From the shipboard mineral analysis data (Dick et al., 2002), olivine has very little titanium (TiO_2 was below detection limit in half of the samples, and most values are <0.013%). Clinopyroxene (0.5 to 1.0 TiO_2 wt%) and orthopyroxene (to 0.5% TiO_2 wt%)

both show no variation between the oxide-rich and oxide-poor samples (Supplementary Figure 2). In a closed system, all titanium to form ilmenite must come from local minerals, hence the whole rock chemistry should not change between oxide rich and oxide poor gabbros. This is not the case in the 735B core data, hence an open system with in-fluxing fluids is required for the increase in TiO_2 and formation of ilmenite. In Supplementary Data 2 we provide the average amount of additional TiO_2 required to form the oxide gabbros from olivine gabbro.

The titanium content in individual ilmenite grains is uniform (Supplementary Fig. 1a, b), ruling out solid-state diffusional processes and is consistent with fluid-mediated replacement reactions (e.g. Putnis, 2009). However, even though manganese and magnesium content show minor variation between grains within a sample, a geochemical trend between the two samples is seen (Fig. 7c, d, red arrows). ~~The oxide gabbro samples under investigation lack olivine. However, the downhole logs show olivine is nearly ubiquitous in gabbroic rocks at hole 735B (Dick et al., 1999; Gardner et al., 2020; Zhang et al., 2021; Zhang et al., 2020). Thus, it is possible that olivine was completely consumed during earlier melt-rock reactions.~~ This suggests while the fluxing melt may have been heterogeneous in composition, the grains in contact with the localised melt are chemically re-equilibrating continuously within the deforming rock; thus, their chemistry and microstructures are continuously reset. The chemistry and microstructure of any given mineral records a snapshot of the last interaction with migrating melt.

The X_{An} composition of plagioclase in the studied samples ranges from 0.37–0.40 (Fig. 7a) which is at the lower end of plagioclase in the oxide-rich gabbro throughout the core at hole 735B ~~(Fig. 1c(iii), Dick et al., 2019)~~(Fig. 1c(iv), Dick et al., 2019). This is consistent with the decreasing anorthite content shown in the later melt-rock reaction events in Gardner et al. (2020) and Zhang et al. (2021) which showed X_{An}=0.40–0.45. ~~Melt~~This bimodal variation of plagioclase composition between the oxide-rich and oxide-poor gabbros (Fig. 1d(iv)) reinforces that open rather than closed system processes were operating during the oxide formation. This is further supported by the abundant evidence for replacement

microstructures. In fluid-rock interaction systems, relationships between fluid-induced reactions and mineral equilibration are very complex and ~~form~~therefore a spectrum of rock-buffered to melt-buffered ~~systems~~mineral compositions may be observed (Rampone et al., 2020)~~. Nevertheless, it can be inferred from the anorthite content of plagioclase that the migrating melt is most likely a fractionated melt (Dick et al., 2019; Zhang et al., 2020). Unlike the melt-rock interaction studied by Gardner et al. (2020), the lack of brown amphibole in our samples suggests either a low activity of water in the melt during melt-rock interaction or that the temperature of melt-rock interaction was higher than the stability field of amphibole.~~. Nevertheless, it can be inferred from the anorthite content of plagioclase that the migrating fluid is most likely a fractionated melt (Dick et al., 2019; Zhang et al., 2020) richer in sodium than the melt forming the original igneous oxide-poor gabbros.

5.1.4. Evidence of deformation in melt-fluxed rocks.

Previous research at Atlantis Bank has shown that the oxide-rich gabbroic rocks are associated along or near zones described in the core ~~description~~descriptions as ~~samples with~~having strong foliation and inferred crystal-plastic deformation ~~(Fig. 1b; Dick et al., 2019; Dick et al., 1991; Dick et al., 2000; Dick et al., 2002; Zhang et al., 2020)~~(Fig. 1b; Dick et al., 2019; Dick et al., 1991; Dick et al., 2000; Dick et al., 2002; Zhang et al., 2020). In contrast, the high oxide samples examined here display low degrees of crystal-plastic deformation when analysed in thin section, particularly in diopside and ilmenite (Figs. 5b, c), which lack a well-defined foliation and show low degrees of ~~crystallographic preferred orientation~~CPO (Fig. 3c, g). The core images (Fig. 1d) do show the oxides form a foliation though this is not evident at the thin section scale. Deformation microstructures can be cryptic in scenarios of melt present deformation ~~(Daczko et al., 2016; Lee et al., 2018; Meek et al., 2019; Stuart et al., 2018b).~~(Daczko et al., 2016; Lee et al., 2018; Meek et al., 2019; Stuart et al., 2018b). Rocks deformed in the presence of melt exhibit several features unusual to solid-state high strain zones, such as thin elongate grain boundary films of plagioclase and low degrees of CPO at least for some minerals (Stuart

et al., 2018b) ~~and low degrees of crystallographic preferred orientation (Smith et al., 2015). We infer that as fluid (including melt).~~ We infer that as melt cannot support shear stresses, deformation of the rock system was accommodated by melt movement rather than the deformation of the solid framework ~~(Rutter and Neumann, 1995; van der Molen and Paterson, 1979).~~(Rutter and Neumann, 1995; van der Molen and Paterson, 1979). This interpretation suggests units III and IV in hole 735B may represent a shear zone system that experienced a very high time-integrated melt flux while being rheologically exceptionally weak. This can explain those parts of the core where high oxide mode is decoupled from features of solid-state, crystal-plastic deformation (Fig. 1c(i) and (ii)).

5.1.5. Near liquidus oxide crystallisation: the role of high-T melt-rock interaction in oxide enrichment

~~The~~Previous researchers have suggested Fe-Ti-rich melts (c.f. Zhang et al., 2020) as the source of iron and titanium for ilmenite and magnetite. However, the source of these Fe-Ti-enriched melts remains an issue. Koepke et al. (2005) found in only one of 25 hydrous partial melting experiments using 735B core gabbros, that two immiscible melts formed: a minor melt rich in REE, P, Zr, Ti and Fe and a larger volume of plagiogranitic melt. However, in agreement with our proposed model for an open system melt influx, Koepke et al. (2005) also found that an external source of titanium was required to form the oxides.

Experiments have shown the onset of Fe-Ti oxide crystallisation in mafic magmas ~~(i)~~ is marked on melt differentiation paths by strong depletion ~~in~~of FeO and TiO_2~~; and (ii)~~ in the melt, and early crystallisation of oxides. Crystallisation onset also has variable timing ~~that depends~~depending on the composition and conditions of the magma, including fugacity of oxygen (Toplis and Carroll, 1995) and concentration of volatiles (e.g., Botcharnikov et al., 2008). For example, water content of ~2% lowers the crystallisation temperature of clinopyroxene and olivine and promotes the early crystallisation of Fe-Ti oxides ~~(Botcharnikov et al., 2008; Howarth et al., 2013; Pang et al., 2007).~~(Botcharnikov et al., 2008; Howarth et al., 2013) and 1% phosphorus can increase ilmenite precipitation (Toplis et al., 1994).

Natural examples of Fe-Ti-rich melts are rare. Clague et al. (2018) document an example of extreme fractionation of mid-ocean ridge basalt at Alarcon Rise where TiO_2 and FeO decrease, and titanomagnetite and ilmenite crystallise as the melts fractionate from andesite, through dacite to rhyolite. In addition, Charlier et al. (2010) hypothesise that ~~oxides may be the first mineral to crystallise in some magmatic systems.~~ ilmenite was the only mineral to crystallise at times during the evolution of the Allard Lake anorthositic system. However, from our study, we suggest melt-rock interaction is the key mechanism to locally produce a near-liquidus oxide-saturated melt which drives oxide-forming reactions in the oceanic crust.

~~In our oceanic samples, we~~We combine ~~the~~this concept of early crystallisation of Fe-Ti oxides at high ~~T~~ temperature with a scenario of melt-buffered melt-rock interaction (Fig. 8a) and infer that a melt migrating with enhanced near liquidus oxide crystallisation conditions will destabilise silicates in favour of Fe-Ti oxides~~.~~ (reactions (2) and (3) above). In our model of melt-rock interaction (Fig. 8a), the stability of oxides over silicates drives reactions that consume silicate minerals and precipitate oxide minerals in an open system. The degree of oxide enrichment is proportional to the time integrated melt flux through the rocks (see Section 5.3). ~~Our model does not require Fe-Ti-rich melts (c.f. Zhang et al., 2020). However, our model of deformation-assisted migration of fractionated melts through gabbroic shear zones is~~Our proposed migrating melt could form rare fractionated volcanic rocks as observed at Alarcon Rise (Clague et al., 2018). Our model of deformation-assisted migration of fractionated melts through gabbroic shear zones is also consistent with the interpretation of (Agar and Lloyd, 1997) who linked fractionated melts with oxide enrichment at the Mid-Atlantic Ridge Kane fracture zone area. Currently our understanding of the timing of the crystallisation of oxides relies on equilibrium experiments. In the future we need disequilibrium melt-rock interaction experiments to replicate our inferred melt-mineral reactions (section 5.1.2). Additionally, new melt-rock interaction experiments involving melt flux through the rock are required to best reproduce our samples and to confirm our model.

5.2. The origin of high-oxide rocks in continental tectonic settings~~:~~

5.2.1. ~~Igneous versus~~Microstructures showing metamorphic ~~character~~replacement reactions

Similar reaction microstructures as those observed in the oceanic setting are observed in the continental case study ~~(~~of sample CP1604C from Cattle Water Pass, central Australia~~).~~. The field relationships show that the precursor rock type, a granulite facies felsic gneiss, is replaced in a high strain zone by the garnet-biotite schist of this study. ~~Key metamorphic reaction microstructures observed within the sample include garnet grains that are partially replaced by ilmenite (yellow arrows, Fig. 4h, i, k); this may progress to form complete pseudomorphs of garnet (blue arrow, Fig.~~ The~~4j).~~ ~~This~~ interpretation that ilmenite partially replaces garnet is supported by the following observations: (1) the presence of irregular boundaries between garnet and ilmenite including finger-like protrusions into garnet (Fig. 4h, k); (2) presence of ilmenite as rims on garnet and as elongate grains at boundaries between garnet and biotite (Fig. 4h-k); (3) multiple groups of neighbouring ilmenite grains, ~~including~~ some of which are inclusions within garnet, that ~~are inferred to be single crystals connected in three dimensions based on their crystal~~ share identical orientation ~~affinity~~ which represent relicts of a partially replaced single coarse garnet grain (e.g., Fig. 6b, grain I2) and (4) straight boundaries on ilmenite that mimic the crystal facets of relict garnet (Fig. 4j). In addition, ilmenite and biotite share a strong CPO (Fig. d and f) without strong internal crystal bending suggesting the grains grew syntectonically i.e. grew in a stressed regime.

5.2.2. Former presence of melt and inferred melt-rock reactions

Melt-present deformation was interpreted for biotite-rich shear zones in central Australia by (Piazolo et al., 2020). In the sample investigated here, microstructures indicative of the former presence of melt (Holness et al., 2011; Lee et al., 2018; Stuart et al., 2018b; Vernon, 2000) confirm this previous research as they include: (1) interstitial ilmenite grains between garnet grains that may have low dihedral angles (Fig. 4h, i, red and green arrows), (2) films along grain boundaries (Fig. 4h, i, red arrows), (3) embayment

microstructures (Fig. 4i, yellow arrows), (4) 3D connectivity of apparently isolated grains (Fig. 6b), and (5) limited internal deformation of grains (Fig. 6b). A lack of local partial melting microstructures and significant hydration of precursor rocks at the site suggest the melt was hydrous and externally derived, resulting in three stages (Fig. 8b) of mineral and melt transformation.

Initially, a granitic melt (melt1) infiltrates into a shear zone cutting the granulite (Fig. 8b, step 1). Melt-rock interactions form biotite and small garnet grains and modifies the melt composition to melt2:

Precursor felsic granulite + melt1 ➔ modified granulite + Bt_1 + Grt_1 + melt2 (4)

Concurrent and subsequent melt2 migration caused the following local reaction (Fig. 8b, step 2), completely replacing the precursor granulite minerals, further increasing the mode of biotite and garnet, and continuing to modify the melt (melt3):

Modified granulite + Bt_1 + Grt_1 + melt2 ➔ Pl + Qz + Bt_2 + Grt_2 + melt3 (5)

Melt3 chemically evolves with continued melt-rock interaction during its flux and promotes ilmenite crystallisation and destabilisation of quartz and plagioclase (Fig., 8b, step 3).

~~).~~Pl + Qz + Bt_2 + Grt_2 + melt3 ➔ Bt_3 + Grt_3 + Ilm + melt4 (6)

Reaction (6) is evident from the replacement microstructures of ilmenite against garnet and biotite grains (Fig. 4h, k, yellow arrows) and the reduced mode of plagioclase and quartz in the domains with high ilmenite mode.

5.2.3. Mineral composition: Composition of the fluxing melt(s)

An open system is also inferred for the continental setting investigated here. Supplementary Data 2 has a discussion of the average amounts of additional TiO_2 required to form the garnet-biotite-ilmenite-rich band from the quartz-plagioclase-rich band.

Although MgO and MnO do not vary much within ilmenite grains in the sample, ilmenite shows a strong variation in TiO_2 content (42–48 wt.%), consistent with open system processes (Fig. 7b), as ilmenites from the adjoining high-grade terrain have higher ~~restricted~~ values for TiO_2 with limited range (51-52 wt%, Cassidy et al., 1988). Moreover, the variability of plagioclase chemistry (Fig. 7a, blue crosses) within the sample also supports an open chemical system with the possibility of multiple melt ~~ingress~~flux events (Streck, 2008).

~~5.2.2.1.1.1.~~ *We interpret melts 1, 2 and 3 (Fig. 8b, Eq. 4, 5 and 6) are likely to be very similar in composition and suggest that they are externally derived S-type granitic melts formed when sedimentary rocks equivalent to the Harts Range Group (Fig. 1a) partially melted. We suggest that garnet and biotite chemistry re-equilibrated continuously with the melt and was aided by syn-melt flux deformation. Previous studies have also shown similar granitic melts fluxed through the nearby Gough Dam shear zone (Fig. 1b, Piazolo et al., 2020; Silva et al., 2021).* ~~*Former presence of melt and inferred melt-rock reactions*~~

~~Melt-present deformation was interpreted for biotite-rich shear zones in central Australia by (Ghatak, 2021; Piazolo et al., 2020). In the sample investigated here, microstructures indicative of the former presence of melt (Holness et al., 2011; Lee et al., 2018; Stuart et al., 2018b; Vernon, 2000) confirm this previous research as they include: (1) interstitial ilmenite grains between garnet grains that may have low dihedral angles (Fig. 4i, red and green arrows), (2) films along grain boundaries (Fig. 4h, i, red arrows), (3) embayment microstructures (Fig. 4i, yellow arrows), (4) 3D connectivity of apparently isolated grains (Fig. 6b), and (5) limited internal deformation of grains (Fig. 6b). A lack of local partial melting microstructures and significant hydration of precursor rocks at the site suggest the melt was hydrous and externally derived, resulting in three stages (Fig. 8b) of mineral and melt transformation.~~

~~Initially, a granitic melt (M1) infiltrates into a shear zone cutting the granulite (Fig. 8b, step 1). Melt-rock interactions form biotite and small garnet grains and modifies the melt composition, which we have designated as melt2 (M2):~~

~~Precursor felsic granulite + melt1 → modified granulite + Bt + Grt + melt2 (4)~~

~~Concurrent and subsequent melt2 migration caused the following local reaction (Fig. 8b, step 2), completely replacing the precursor granulite minerals, further increasing the mode of biotite and garnet, and continuing to modify the melt (melt3, M3):~~

~~Modified granulite + Bt + Grt + melt2 → Pl + Qz + Bt + Grt + melt3 (5)~~

~~Melt3 chemically evolves with continued melt-rock interaction during its flux and promotes ilmenite crystallisation and destabilisation of quartz and plagioclase (Fig., 8b, step 3).~~

~~Pl + Qz + Bt + Grt + melt3 → Bt + Grt + Ilm + melt4 (6)~~

~~The above reaction is evident from the replacement microstructures of ilmenite against garnet and biotite grains (Fig. 4h, k, yellow arrows) and the reduced mode of plagioclase and quartz.~~

~~*5.2.3. Composition of the fluxing melt(s)*~~

The relationships outlined in section 5.2.2 are consistent with melt migration at temperatures below (Fig. 8b, melt1 and 2, Eq. 5), then above (Fig. 8b, melt3, Eq. 6) the stability of plagioclase and quartz ~~(~ 870ºC; Clemens and Wall, 1981).~~(~ 870 ºC; Clemens and Wall, 1981). As ilmenite is a liquidus phase in S-type granites (Clemens and Wall, 1981), any scenario of high temperature (near liquidus) melt flux increases the mode of oxides over silicates (Charlier et al., 2010).

~~Our interpretation of S-type granitic melt flux builds on previous studies which suggest an externally derived granitic melt fluxed through the nearby Gough Dam shear zone (Ghatak, 2021; Piazolo et al., 2020; Silva et al., 2021). The phase diagram of Clemens and Wall (1981) is consistent with the shear~~

~~zones in central Australia having been hydrated in the presence of an S-type granitic melt at variable melt flux temperature conditions (Ghatak, 2021).~~

In addition, the phase diagram of Clemens and Wall (1981) is consistent with the shear zones in central Australia having been hydrated in the presence of an S-type granitic melt at variable melt flux temperature conditions .

5.2.4. Evidence of deformation in melt fluxed rocks

~~Field relationships and a well-developed foliation and lineation show the~~The continental sample formed within the Cattle Water Pass shear zone as demonstrated by field relationships and a well-developed foliation and lineation. The microstructural analysis demonstrates the former presence of melt. However, EBSD analysis shows only minor internal deformation of grains and microstructures contradictory to typical mid to deep crustal shear zones. Only rare ilmenite grains preserve a high degree of internal deformation (Fig. 6b$_1$). Similarly, ~~the~~some garnet grains ~~lack any significant internal deformation. Rather, the patches of garnet have a very similar crystallographic orientation~~display subgrain boundaries (Fig. 6c~~ and e~~) though any consistent CPO is lacking (Fig. 6e). Additionally, biotite lacks evidence of internal deformation when examined under crossed polarised light microscopy. These observations do not support an interpretation of solid-state deformation and instead point to melt-present deformation, suggesting melt flow accommodated most of the strain.

We suggest that a high nucleation rate of garnet grains and random orientation of ~~nucleation, as evident from the random orientation in the~~nuclei, (Fig. 6e, pole figure) and the formation of crystal facets (Fig. ~~6e),~~4h, j) was facilitated by the presence of melt. Despite having no significant internal deformation, the ilmenite grains are aligned and show a CPO (Fig. 5d) which matches that of biotite (Fig. 6f). Since the formation of CPO by solid-state deformation in these rocks ~~has been shown to be~~is highly unlikely, it is inferred that rigid body rotation (e.g., March, 1932)~~ as well as alignment in the presence of external~~

~~stress (Hutton, 1988) aligns the platy biotite. Ilmenite is mostly interstitial between garnet and biotite and shares a similar CPO to biotite (Fig. 6d and f).~~ as well as growth in the presence of external stress (Wenk et al., 2019, and references therein) results in the strong alignment of platy and elastically highly anisotropic biotite.

5.2.5. Near liquidus oxide crystallisation: the role of high-T melt-rock interaction in oxide enrichment

Ilmenite is the first mineral to crystallise from the S-type granite studied by Clemens and Wall (1981), followed by, in crystallisation order, garnet, biotite, quartz, plagioclase and K-feldspar. Although the modal proportion of the oxides in such experiments (1-3%) is not significantly high compared to that seen in our CWP shear zone samples (18%, Fig. 3l), it is important to note the oxides are stable prior to the silicates. Thus, given a melt-rock interaction scenario where the temperature of ~~the~~a fluxing S-type granitic melt is near its liquidus, oxide minerals may be stable while silicate minerals are destabilised ~~in~~during melt-rock interaction with the hot melt. At slightly lower temperatures of melt-rock interaction, garnet and ilmenite are stable and then as the temperature decreases further biotite is added to the stable assemblage. The mineral assemblage and mineral proportions observed in the garnet-biotite schist sample examined here are consistent with having formed by the interaction between the precursor felsic granulite and a migrating S-type granitic melt broadly similar to that studied by Clemens and Wall (1981). Iterative melt-rock reaction and migration of reacted melt out of the local system is needed to significantly enrich the rock in biotite, garnet, and ilmenite and deplete the rock of quartz and feldspar. This suggests a high time-integrated melt flux is required ~~(see Section 5.3; Silva et al., 2021; Stuart et al., 2018b)~~(see Section 5.3; Silva et al., 2021; Stuart et al., 2018b).

5.3. *The signatures and consequences of deformation assisted reactive porous melt flow in crustal environments*

A near liquidus temperature of the melt during melt-rock interaction can stabilise oxides relative to silicate minerals and is necessary to explain the enrichment of ilmenite in both the oceanic and continental case studies. A fractional crystallisation model alone for either a gabbroic melt or an S-type granitic melt cannot explain the high modal proportions of ilmenite in these rocks. Typical silicate melts precipitate only 1-3 vol.% oxides. Therefore, significant enrichment of oxides requires precipitation from multiple batches of fluxing melt, progressively increasing the mode of oxides. ~~Oxide~~Using the upper value of 3% oxides for the precipitation from a typical silicate melt, oxide modes of ~20 vol.% in the continental setting and ~45 vol.% in the oceanic setting require precipitation of oxides from a minimum volume of melt that is in the order of 6 to 15 times the volume of the rock~~.~~, for continental and oceanic crusts, respectively. In other words, a large volume of melt must migrate through our samples to progressively enrich the oxides to the observed degree.

One concept of reactive melt flow involves a crystal mush where a framework of solid crystals reacts as the residual melt is expelled and migrates during compaction. This forms core to rim elemental profiles of reactant minerals (Solano et al., 2014)~~).~~. A similar process occurs during syn-deformational melt migration of an externally derived melt through shear zones cutting formerly solid rocks. Enhanced porosity and permeability in zones of ductile deformation ~~(e.g. Edmond and Paterson, 1972; Fischer and Paterson, 1989)~~(e.g. Edmond and Paterson, 1972; Fischer and Paterson, 1989) result in lower fluid pressure sinks that draw melt towards zones of maximum deformation rate (Etheridge et al., 2021). Fusseis et al. (2009) describe a granular fluid pump model involving the dynamic opening and closing of pores in deforming rocks that facilitates melt migration through shear zones. These concepts of

deformation assisted fluid flow through shear zones provide a mechanism to transport large volumes of melt through small volumes of rock.

One of the outcomes of this study is to ~~show~~highlight the complexity of melt-rock reaction systems, beyond the magma chamber setting, where fractional crystallisation and melt–crystal mush reactions occur. Within magma chambers, the stability of minerals can be determined using experimental petrology and thermodynamic modelling to produce phase diagrams. However, the complexity of modelling increases in an open system melt migration scenario where the composition of both the reactant melts and the rocks they pass through are possibly highly variable and dynamically ~~evolvoing~~evolving.

Studies have shown that reactive melt migration can significantly change the composition of melt by fractionation and/or enrichment of specific elements. This in turn produces an evolved melt which is hard to distinguish from the fractionation of parent melt (Lissenberg et al., 2013). Thus, the derivative melt produced during melt-rock interaction and reactive crystallisation will form different liquid lines of descent (Collier and Kelemen, 2010). Studies have further shown that reactive melt flow is not limited to the grain scale, rather at a macro scale it can lead to complete transformation of one rock type to another (Lissenberg and MacLeod, 2016). These studies reported the preferential growth of a specific mineral over any other (e.g., clinopyroxene over olivine), in turn leading to a modal enrichment in that mineral (Lissenberg and MacLeod, 2016). Similarly, we propose that oxide minerals in our oceanic case study grew by replacing mostly plagioclase and diopside~~.~~ in the oceanic samples. These relationships require an evolved melt infiltrating the precursor gabbro, forming derivative reactant melt, and leading to further reactions and the development of the oxide gabbros. Similarly, in our case study of a continental setting, variably fractionated S-type melt can readily react and enrich rocks in ilmenite.

In the oceanic case study (Fig. 8a), the parent melt forming ilmenite was likely gabbroic in composition and may have fractionated in a magma chamber setting or during melt-rock interaction resulting in the formation of the modified gabbroic melt (~~M1~~melt1) envisaged in our model. Step 1 shows enstatite and plagioclase reacting with ~~a melt, which has migrated along the grain boundaries~~melt1 (Equation 2), causing crystallisation of ~~a precursor rock.~~ilmenite and diopside and the formation of melt2. The derivative ~~melt (M2)~~melt2 has a composition where oxides are also early crystallising minerals, ahead of silicates~~. This reacting melt replaces enstatite and plagioclase silicate minerals with ilmenite and diopside in step 2. The diopside~~ (Equation 2). Diopside replaces enstatite grains to form the two pyroxene domains and diopside rims. In subsequent melt-rock reactions, a later ~~melt (M3)~~melt3 stabilises magnetite over ilmenite and locally recrystallises diopside.

Similarly, in the case of the continental case study (Fig. 8b), a primary or fractionated S-type ~~melt (M1)~~melt1 drives hydration of a granulite facies felsic gneiss in step 1 due to deformation assisted melt migration through the shear zone. This leads to an increased mode of biotite and garnet in a band in step 2 (Fig. 3k), and progressive reaction leads to the formation of derivative melts (~~M2~~melt2 and ~~M3~~melt3). The latter ~~melt (M3)~~melt3 is evolved and has a composition enhancing near liquidus ilmenite growth. In step 3, the reactant ~~melt (M3)~~melt3 forms interstitial ilmenite grains, thus increasing the mode of ilmenite along with consumption of some garnet grains (Fig. 4h, i, k; yellow arrow).

6. Conclusion

The microstructural characterisation of oxide-rich rocks from both oceanic and continental tectonic settings shows that oxide grains are common in metamorphic replacement microstructures, where the oxide grains replace silicate minerals during melt-rock interaction. The former presence of melt is implied by interstitial microstructures involving grain boundary films and grains that subtend to low

dihedral angles. Grains show straight crystal faces and form an interconnected skeletal texture, including clusters of apparently isolated grains that are connected in three dimensions. Limited internal deformation of grains is consistent with ~~stress dissipation~~strain accommodation in shear zones by melt movement between grains in a solid framework, rather than deformation of the solid minerals by, for example, dislocation creep. Microchemical variation in silicates and ilmenite argues for open system behaviour in both oceanic and continental settings. We propose that deformation assisted reactive porous flow of melt through rocks in any tectonic setting, given ~~the right~~near liquidus conditions, may significantly modify melts to enhance their ability to enrich oxide minerals in preference to silicates.

Acknowledgements

Logistical and analytical funding was provided by the Australian IODP Office (ANZIC Legacy Analytical funding~~)~~), ARC Discovery grant DP160103449 and the Department of Earth and Environmental Sciences, Macquarie University. The authors would like to thank Karsten Gorman of University of Tasmania for his assistance collecting the EMP data and Malcolm Lambert from University of New England for his assistance collecting the micro-CT data. We would also like to thank ~~XXX~~Thomas Müller and ~~XXX~~an anonymous reviewer for their careful and constructive reviews, and ~~XXX~~Greg Shellnutt for editorial handling. This is contribution xxx from the ARC Centre of Excellence for Core to Crust Fluid Systems (http://www.ccfs.mq.edu.au) and xxx in the GEMOC Key Centre (http://www.gemoc.mq.edu.au).

References

Agar, S.M., Lloyd, G.E., 1997. Deformation of Fe-Ti oxides in gabbroic shear zones from the MARK area, Proceedings-Ocean Drilling Program Scientific Results. National Science Foundation, pp. 123-142.

809 Bendall, B., 2000. Mid-Palaeozoic shear zones in the Strangways Range : a record of
810 intracratonic tectonism in the Arunta Inlier, Central Australia, Dept. of Geology.
811 University of Adelaide, Adelaide, Australia, p. 210.
812 ~~Bestmann, M., Prior, D.J., 2003. Intragranular dynamic recrystallization in naturally~~
813 ~~deformed calcite marble: diffusion accommodated grain boundary sliding as a result of~~
814 ~~subgrain rotation recrystallization. Journal of Structural Geology 25, 1597-1613.~~
815 Bloomer, S.H., Meyer, P.S., Dick, H.J.B., Ozawa, K., Natland, J.H., 1991. 2. Textural
816 and mineralogic variations in gabbroic rocks from hole 735B, in: Von Herzon, R.P., Fox,
817 J., Palmer-Julson, A., Robinson, P.T. (Eds.), Proceedings of the International Ocean
818 Drilling Program volume 118. International Drilling Program, Texas, pp. 21-39.
819 Bons, P.D., Druguet, E., Hamann, I., Carreras, J., Passchier, C.W., 2004. Apparent
820 boudinage in dykes. Journal of Structural Geology 26, 625-636.
821 Botcharnikov, R., Almeev, R., Koepke, J., Holtz, F., 2008. Phase relations and liquid
822 lines of descent in hydrous ferrobasalt—implications for the Skaergaard intrusion and
823 Columbia River flood basalts. Journal of Petrology 49, 1687-1727.
824 Bowles, J., Howie, R., Vaughan, D., Zussman, J., 2011. Rock-forming minerals, 2nd ed.
825 The Geological Society, London, UK.
826 Cannat, M., Mével, C., Stakes, D., 1991. 24. Normal ductile shear zones at an oceanic
827 spreading ridge: tectonic evolution of site 735 gabbros (Southwest Indian Ocean), in:
828 Von Herzon, R.P., Fox, J., Palmer-Julson, A., Robinson, P.T. (Eds.), Proceedings fo the
829 Ocean Drilling Program, scientific results volume 118. Ocean Drilling Program, Texas,
830 pp. 415-429.

Cartwright, I., Buick, I.S., Foster, D.A., Lambert, D.D., 1999. Alice Springs age shear zones from the southeastern Reynolds Range, central Australia. Australian Journal of Earth Sciences 46, 355-363.

Casini, L., Maino, M., Sanfilippo, A., Ildefonse, B., Dick, H.J.B., 2021. High-Temperature Strain Localization and the Nucleation of Oceanic Core Complexes (16.5°N, Mid-Atlantic Ridge). Journal of Geophysical Research: Solid Earth 126, e2021JB022215.

Cassidy, K.F., Groves, D.I., Binns, R.A., 1988. Manganoan ilmenite formed during regional metamorphism of Archean mafic and ultramafic rocks from Western Australia. The Canadian Mineralogist 26, 999-1012.

Charlier, B., ~~Grove, T.L., 2012. Experiments on liquid immiscibility along tholeiitic liquid lines of descent. Contrib Mineral Petrol 164, 27-44.~~

~~Charlier, B.,~~ Namur, O., Malpas, S., de Marneffe, C., Duchesne, J.-C., Auwera, J.V., Bolle, O., 2010. Origin of the giant Allard Lake ilmenite ore deposit (Canada) by fractional crystallization, multiple magma pulses and mixing. Lithos 117, 119-134.

~~Charlier, B., Skår, Ø., Korneliussen, A., Duchesne, J.-C., Vander Auwera, J., 2007. Ilmenite composition in the Tellnes Fe–Ti deposit, SW Norway: fractional crystallization, postcumulus evolution and ilmenite–zircon relation. Contrib Mineral Petrol 154, 119-134.~~

Cignoni, P., Callieri, M., Corsini, M., Dellepiane, M., Ganovelli, F., Ranzuglia, G., 2008. MeshLab: an Open-Source Mesh Processing Tool, Sixth Eurographics Italian Chapter Conference. The Eurographics Association, pp. 129-136.

Clague, D.A., Caress, D.W., Dreyer, B.M., Lundsten, L., Paduan, J.B., Portner, R.A., Spelz-Madero, R., Bowles, J.A., Castillo, P.R., Guardado-France, R., 2018. Geology of

the Alarcon Rise, Southern Gulf of California. Geochemistry, Geophysics, Geosystems 19, 807-837.

Clemens, J.D., Wall, V.J., 1981. Origin and crystallization of some peraluminous (S-type) granitic magmas. The Canadian Mineralogist 19, 111-131.

Collier, M.L., Kelemen, P.B., 2010. The Case for Reactive Crystallization at Mid-Ocean Ridges. Journal of Petrology 51, 1913-1940.

Collins, W.J., Teyssier, C., 1989. Crustal scale ductile fault systems in the Arunta Inlier, central Australia. Tectonophysics 158, 49-66.

Daczko, N.R., Piazolo, S., Meek, U., Stuart, C.A., Elliott, V., 2016. Hornblendite delineates zones of mass transfer through the lower crust. Scientific Reports 6, 31369.

Deans, J.R.L., Yoshinobu, A.S., 2019. Geographically re-oriented magmatic and metamorphic foliations from ODP Hole 735B Atlantis Bank, Southwest Indian Ridge: Magmatic intrusion and crystal-plastic overprint in the footwall of an oceanic core complex. Journal of Structural Geology 126, 1-10.

Dick, H.J.B., Kvassnes, A.J.S., Robinson, P.T., MacLeod, C.J., Kinoshita, H., 2019. The Atlantis Bank Gabbro Massif, Southwest Indian Ridge. Progress in Earth and Planetary Science 6, 64.

Dick, H.J.B., Meyer, P.S., Bloomer, S.H., Kirby, S.H., Stakes, D., Mawer, C., 1991. 26. Lithostratigraphic evolution of an in-situ section of oceanic layer 3, in: Von Herzon, R.P., Fox, J., Palmer-Julson, A., Robinson, P.T. (Eds.), Proceeding of the Ocean Drilling Program, Scientific Results Volume 118. Ocean Drilling Program, Texas, pp. 439-538.

Dick, H.J.B., Natland, J.H., Alt, J.C., Bach, W., Bideau, D., Gee, J.S., Haggas, S., Hertogen, J.G.H., Hirth, G., Holm, P.M., Ildefonse, B., Iturrino, G.J., John, B.E., Kelley,

D.S., Kikawa, E., Kingdon, A., LeRoux, P.J., Maeda, J., Meyer, P.S., Miller, D.J., Naslund, H.R., Niu, Y.-L., Robinson, P.T., Snow, J., Stephen, R.A., Trimby, P.W., Worm, H.-U., Yoshinobu, A., 2000. A long in situ section of the lower ocean crust: results of ODP Leg 176 drilling at the Southwest Indian Ridge. Earth and Planetary Science Letters 179, 31-51.

Dick, H.J.B., Natland, J.H., Miller, D.J., Alt, J.C., Bach, W., Bideau, D., Gee, J.S., Haggas, S., Hertogen, J.G.H., Hirth, G., Holm, P.M., Ildefonse, B., Iturrino, G.J., John, B., Kelley, D.S., Kikawa, E., Kingdon, A., Le Roux, P., Maeda, J., Meyer, P.S., Naslund, H.R., Niu, Y., Robinson, P.T., Snow, J.E., Stephen, R.A., Trimby, P., Worm, H.-U., Yoshinobu, A., ~~1999~~1999a. 1. Leg 176 Summary, in: Marin, J.A., Scroggs, J.M. (Eds.), Proceedings of the International Ocean Drilling Program, initial reports volume 176. Ocean Drilling Program, Texas, p. 70.

Dick, H.J.B., Natland, J.H., Miller, D.J., Alt, J.C., Bach, W., Bideau, D., Gee, J.S., Haggas, S., Hertogen, J.G.H., Hirth, G., Holm, P.M., Ildefonse, B., Iturrino, G.J., John, B., Kelley, D.S., Kikawa, E., Kingdon, A., Le Roux, P., Maeda, J., Meyer, P.S., Naslund, H.R., Niu, Y., Robinson, P.T., Snow, J.E., Stephen, R.A., Trimby, P., Worm, H.-U., Yoshinobu, A., 1999b. 3. Site 735, in: Marin, J.A., Scroggs, J.M. (Eds.), Proceedings of the Ocean Drilling Program, initial reports volume 176. Ocean Drilling Program, Texas, pp. 1-313.

Dick, H.J.B., Ozawa, K., Meyer, P.S., Niu, Y., Robinson, P.T., Constantin, M., Hebert, R., Maeda, J., Natland, J.H., Hirth, J.G., Mackie, S.M., 2002. 10. Primary silicate mineral chemistry of a 1.5-km section of very slow spreading lower ocean crust: ODP hole 735B, Southwest Indian Ridge, in: Natland, J.H., Dick, H.J.B., Miller, D.J., Von

Herzon, R.P. (Eds.), Proceedings of the Ocean Drilling Program, scientific results volume 176. Ocean Drilling Program, Texas, pp. 1-61.

Dixon, S., Rutherford, M.J., 1979. Plagiogranites as late-stage immiscible liquids in ophiolite and mid-ocean ridge suites: An experimental study. Earth and Planetary Science Letters 45, 45-60.

Duchesne, J., Charlier, B., 2005. Geochemistry of cumulates from the Bjerkreim Sokndal layered intrusion (S. Norway). Part I: Constraints from major elements on the mechanism of cumulate formation and on the jotunite liquid line of descent. Lithos 83, 229-254.

Edmond, J.M., Paterson, M.S., 1972. Volume changes during the deformation of rocks at high pressures. International Journal of Rock Mechanics and Mining Sciences & Geomechanics Abstracts 9, 161-182.

Emslie, R.F., Hamilton, M.A., Thériault, R.J., 1994. Petrogenesis of a Mid-Proterozoic Anorthosite-Mangerite-Charnockite-Granite (AMCG) Complex: Isotopic and Chemical Evidence from the Nain Plutonic Suite. The Journal of Geology 102, 539-558.

Etheridge, M.A., Daczko, N.R., Chapman, T., Stuart, C.A., 2021. Mechanisms of melt extraction during lower crustal partial melting. Journal of Metamorphic Geology 39, 57-75.

Fedorov, A., Beichel, R., Kalpathy-Cramer, J., Finet, J., Fillion-Robin, J.-C., Pujol, S., Bauer, C., Jennings, D., Fennessy, F.M., Sonka, M., Buatti, J., Aylward, S.R., Miller, J.V., Pieper, S., Kikinis, R., 2012. 3D Slicer as an Image Computing Platform for the Quantitative Imaging Network. Magnetic Resonance Imaging 30, 1323-1341.

Fischer, G.J., Paterson, M.S., 1989. Dilatancy during rock deformation at high temperatures and pressures. Journal of Geophysical Research: Solid Earth 94, 17607-17617.

Fusseis, F., Regenauer-Lieb, K., Liu, J., Hough, R.M., De Carlo, F., 2009. Creep cavitation can establish a dynamic granular fluid pump in ductile shear zones. Nature 459, 974-977.

Gale, A., Dalton, C.A., Langmuir, C.H., Su, Y., Schilling, J.-G., 2013. The mean composition of ocean ridge basalts. Geochemistry, Geophysics, Geosystems 14, 489-518.

Gardner, R.L., Piazolo, S., Daczko, N.R., Trimby, P., 2020. Microstructures reveal multistage melt present strain localisation in mid-ocean gabbros. Lithos 366-367, 105572.

~~Ghatak, H., 2021. Deformation-assisted melt migration and melt-rock interaction during the intraconinental Alice Springs orogeny, central Australia, Faculty of Science and Engineering, Department of Earth and Environmental Sciences. Macquarie University,, Sydney, Australia, p. 218.~~

Gross, G.A., Eckstrand, O.R., Sinclair, W.D., Thorpe, R.I., 1995. Mafic Intrusion-Hosted Titanium-Iron, Geology of Canadian Mineral Deposit Types. Geological Society of America, p. 0.

Hand, M., Sandiford, M., 1999. Intraplate deformation in central Australia, the link between subsidence and fault reactivation. Tectonophysics 305, 121-140.

Hertogen, J.G.H., R., E., Robinson, P.T., Erzinger, J., 2002. 6. Lithology, mineralogy and geochemistry of the lower ocean crust, ODP hole 735B, Southwest Indian Ridge,

in: Natland, J.H., Dick, H.J.B., Miller, D.J., Von Herzon, R.P. (Eds.), Proceedings of the International Ocean Drilling Program, Scientific Results, Volume 176. Ocean Drilling Program, Texas, pp. 1-82.

Holness, M.B., Cesare, B., Sawyer, E.W., 2011. Melted rocks under the microscope: microstructures and their interpretation. Elements 7, 247-252.

Hopkinson, L., Roberts, S., 1995. Ridge axis deformation and coeval melt migration within layer 3 gabbros: evidence from the Lizard Complex, U.K. ~~Contrib Mineral Petrol~~Contributions to Mineralogy and Petrology 121, 126.

Howarth, G.H., Prevec, S.A., Zhou, M.-F., 2013. Timing of Ti-magnetite crystallisation and silicate disequilibrium in the Panzhihua mafic layered intrusion: Implications for ore-forming processes. Lithos 170-171, 73-89.

~~Hutton, D.H.W., 1988. Granite emplacement mechanisms and tectonic controls: inferences from deformation studies. Earth and Environmental Science Transactions of the Royal Society of Edinburgh 79, 245-255.~~

John, B.E., Foster, D.A., Murphy, J.M., Cheadle, M.J., Baines, A.G., Fanning, C.M., Copeland, P., 2004. Determining the cooling history of in situ lower oceanic crust—Atlantis Bank, SW Indian Ridge. Earth and Planetary Science Letters 222, 145-160.

Koepke, J., Feig, S.T., Snow, J., 2005. Hydrous partial melting within the lower oceanic crust. Terra Nova 17, 286-291.

Lee, A.L., Torvela, T., Lloyd, G.E., Walker, A.M., 2018. Melt organisation and strain partitioning in the lower crust. Journal of Structural Geology 113, 188-199.

Lissenberg, C.J., MacLeod, C.J., 2016. A reactive porous flow control on mid-ocean ridge magmatic evolution. Journal of Petrology 57, 2195-2220.

Lissenberg, C.J., MacLeod, C.J., Howard, K.A., Godard, M., 2013. Pervasive reactive melt migration through fast-spreading lower oceanic crust (Hess Deep, equatorial Pacific Ocean). Earth and Planetary Science Letters 361, 436-447.

March, A., 1932. Mathematische Theorie der Regelung nach der Korngestalt bei affiner Deformation. Z. Kristallogr 81, 285-297.

Meek, U., Piazolo, S., Daczko, N.R., 2019. The field and microstructural signatures of deformation-assisted melt transfer: Insights from magmatic arc lower crust, New Zealand. Journal of Metamorphic Geology 37, 795-821.

Nachit, H., Ibhi, A., Ohoud, M.B., 2005. Discrimination between primary magmatic biotites, reequilibrated biotites and neoformed biotites. Comptes Rendus Geoscience 337, 1415-1420.

Norman, A.R., 1991. The structural and metamorphic evolution of the central Arunta Block: evidence from the Strangways Metamorphic Complex and the Harts Range Group, central Australia, School of Earth Sciences. Macquarie University, Sydney, Australia, p. 13.

Ozawa, K., Meyer, P.S., Bloomer, S.H., 1991. 3. Mineralogy and textures of iron-titanium oxide gabbros and associated olivine gabbros from hole 735B, in: Von Herzon, R.P., Fox, J., Palmer-Julson, A., Robinson, P.T. (Eds.), Proceedings of the International Ocean Drilling Program volume 118. International Drilling Program, Texas, pp. 41-73.

~~Pang, K.-N., Zhou, M.-F., Lindsley, D., Zhao, D., Malpas, J., 2007. Origin of Fe–Ti Oxide Ores in Mafic Intrusions: Evidence from the Panzhihua Intrusion, SW China. Journal of Petrology 49, 295-313.~~

Philpotts, A.R., Ague, J.J., 2009. Principles of igneous and metamorphic petrology. CAmbridge University Press, Cambridge, UK.

Piazolo, S., Bestmann, M., Prior, D.J., Spiers, C.J., 2006. Temperature dependent grain boundary migration in deformed-then-annealed material: Observations from experimentally deformed synthetic rocksalt. Tectonophysics 427, 55-71.

Piazolo, S., Daczko, N.R., Silva, D., Raimondo, T., 2020. Melt-present shear zones enable intracontinental orogenesis. Geology 48, 643-648.

Prakash, A., Piazolo, S., Saha, L., Bhattacharya, A., Pal, D.K., Sarkar, S., 2018. Deformation behavior of migmatites: insights from microstructural analysis of a garnet–sillimanite–mullite–quartz–feldspar-bearing anatectic migmatite at Rampura–Agucha, Aravalli–Delhi Fold Belt, NW India. ~~Int J~~International Journal of Earth ~~Sci (Geol Rundsch).~~Sciences.

Putnis, A., 2009. Mineral replacement reactions. Reviews in mineralogy and geochemistry 70, 87-124.

Raimondo, T., Clark, C., Hand, M., Faure, K., 2011. Assessing the geochemical and tectonic impacts of fluid–rock interaction in mid-crustal shear zones: a case study from the intracontinental Alice Springs Orogen, central Australia. Journal of Metamorphic Geology 29, 821-850.

Raimondo, T., Hand, M., Collins, W.J., 2014. Compressional intracontinental orogens: Ancient and modern perspectives. Earth-Science Reviews 130, 128-153.

Rampone, E., Borghini, G., Basch, V., 2020. Melt migration and melt-rock reaction in the Alpine-Apennine peridotites: Insights on mantle dynamics in extending lithosphere. Geoscience Frontiers 11, 151-166.

Robinson, P.T., Dick, H., Natland, J.H., Yoshinobu, A.S., Party, L.S., 2000. Lower oceanic crust formed at an ultra-slow-spreading ridge: Ocean Drilling Program Hole 735B, Southwest Indian Ridge. Geological Society of America Special Paper 349.

Roy, P., Whitehouse, J., Cowell, P., Oakes, G., 2000. Mineral Sands Occurrences in the Murray Basin, Southeastern Australia. Economic Geology 95, 1107-1128.

Rutter, E.H., Neumann, D.H.K., 1995. Experimental deformation of partially molten Westerly granite under fluid-absent conditions, with implications for the extraction of granitic magmas. Journal of Geophysical Research: Solid Earth 100, 15697-15715.

Ryan, W.B.F., Carbotte, S.M., Coplan, S., O'Hara, A., Melkonian, A., Arko, R., Weissel, R.A., Ferrini, V., Goodwillie, A., Nitche, F., Bonczkowski, J., Zemsky, R., 2009. Global Multi-Resolution Topography (GMRT) synthesis data set. Geochemistry, Geophysics, Geosystems 10.

Scoates, J.S., Chamberlain, K.R., 1997. Orogenic to Post‐Orogenic Origin For the 1.76 Ga Horse Creek Anorthosite Complex, Wyoming, Usa. The Journal of Geology 105, 331-344.

Silva, D., Daczko, N.R., Piazolo, S., Raimondo, T., 2021. Glimmerite: a product of melt-rock interaction within a crustal-scale high-strain zone. Gondwana Research.

Silva, D., Piazolo, S., Daczko, N.R., Houseman, G., Raimondo, T., Evans, L., 2018. Intracontinental Orogeny Enhanced by Far-Field Extension and Local Weak Crust. Tectonics 37, 4421-4443.

~~Smith, J., Piazolo, S., Daczko, N., Evans, L., 2015. The effect of pre-tectonic reaction and annealing extent on behaviour during subsequent deformation: Insights from paired~~

~~shear zones in the lower crust of Fiordland, New Zealand. Journal of Metamorphic Geology 33, 557-670.~~

Solano, J., Jackson, M., Sparks, R., Blundy, J., 2014. Evolution of major and trace element composition during melt migration through crystalline mush: implications for chemical differentiation in the crust. American Journal of Science 314, 895-939.

Streck, M.J., 2008. Mineral Textures and Zoning as Evidence for Open System Processes. Reviews in ~~Mineralogy~~mineralogy and ~~Geochemistry~~geochemistry 69, 595-622.

Stuart, C.A., Meek, U., Daczko, N.R., Piazolo, S., Huang, J.X., 2018a. Chemical Signatures of Melt–Rock Interaction in the Root of a Magmatic Arc. Journal of Petrology 59, 321-340.

Stuart, C.A., Piazolo, S., Daczko, N.R., 2018b. The recognition of former melt flux through high-strain zones. Journal of Metamorphic Geology 36, 1049-1069.

Teyssier, C., 1985. A crustal thrust system in an intracratonic tectonic environment. Journal of Structural Geology 7, 689-700.

Toplis, M.J., Carroll, M.R., 1995. An Experimental Study of the Influence of Oxygen Fugacity on Fe-Ti Oxide Stability, Phase Relations, and Mineral—Melt Equilibria in Ferro-Basaltic Systems. Journal of Petrology 36, 1137-1170.

Toplis, M.J., Libourel, G., Carroll, M.R., 1994. The role of phosphorus in crystallisation processes of basalt: An experimental study. Geochimica et Cosmochimica Acta 58, 797-810.

van der Molen, I., Paterson, M.S., 1979. Experimental deformation of partially-melted granite. ~~Contrib Mineral Petrol~~Contributions to Mineralogy and Petrology 70, 299-318.

Vernon, R.H., 2000. Review of Microstructural Evidence of Magmatic and Solid-State Flow. ~~Vis Geosci~~Visual Geosciences 5, 1-23.

Wenk, H.-R., Kanitpanyacharoen, W., Ren, Y., 2019. Slate–A new record for crystal preferred orientation. Journal of Structural Geology 125, 319-324.

Whitney, D.L., Evans, B.W., 2010. Abbreviations for names of rock-forming minerals. American mineralogist 95, 185.

Woodruff, L.G., Bedinger, G.M., Piatak, N.M., 2017. Titanium, in: Schulz, K.J., DeYoung, J.H.J., Seal, R.R.I., Bradley, D.C. (Eds.), Critical mineral resources of the United States—Economic and environmental geology and prospects for future supply. U.S. Geological Survey pp. T1-T23.

Žák, J., Verner, K., Týcová, P., 2008. Grain-scale processes in actively deforming magma mushes: New insights from electron backscatter diffraction (EBSD) analysis of biotite schlieren in the Jizera granite, Bohemian Massif. Lithos 106, 309-322.

Zhang, W.-Q., Dick, H.J.B., Liu, C.-Z., Lin, Y.-Z., Angeloni, L.M., 2021. MORB Melt Transport through Atlantis Bank Oceanic Batholith (SW Indian Ridge). Journal of Petrology 62.

Zhang, W.-Q., Liu, C.-Z., Dick, H.J.B., 2020. Evidence for Multi-stage Melt Transport in the Lower Ocean Crust: the Atlantis Bank Gabbroic Massif (IODP Hole U1473A, SW Indian Ridge). Journal of Petrology 61.

Figure Labels

Figure 1. Geological context of oceanic samples. (a) location of core 735B at Atlantis Bank (made with GeoMapApp ~~(www.geomapapp.org; Ryan et al., 2009));~~(www.geomapapp.org; Deans and Yoshinobu,

2019; Ryan et al., 2009)); (b) graph of Fe_2O_3 vs TiO_2 for whole rock oceanic gabbro data from the database of (Gale et al., 2013) showing core 735B and overall trend in compositions (grey arrow); (c) 735B core section showing properties of oxide-rich (red) vs oxide-poor (blue) oceanic gabbros, (i) rock type~~, (iii) X_{An} values and (ii) crystal-plastic deformation in the core after (Dick et al., 2019)~~ and (ii) crystal-plastic deformation in the core after (Dick et al., 2019; Dick et al., 1999b); 0 – no foliation, 1 – some deformation, lacks foliation; 2 – clear foliation; 3 – strongly foliated, protomylonite; 4 – strongly laminated, mylonite; 5 - ultramylonite; blue star indicates location of representative samples 47R2-1 and 47R2-3; (~~d) core photos~~iii) whole rock TiO_2 weight percentage and (iv) plagioclase X_{An} values from shipboard data (Dick et al., 2002); (d) core photo around the location of the samples (blue stars) with matching diagram of oxides, dashed lines indicate foliation trend of oxides.

Figure 2. Geological context of continental sample. (a) location of the Strangways Metamorphic Complex (SMC) in central Australia after (Silva et al., 2018); (b) location of investigated continental garnet-biotite schist sample CP1604C (marked by red star) in the Cattle Water Pass shear zone (modified from Norman, 1991).

Figure 3. Overview images (PPL, XPL, BSE and Ti maps) of oxide-rich and oxide-poor samples in oceanic samples: 47R2-3 and 47R2-1 from Atlantis Bank, SWIR) and continental sample CP1604C (central Australia). Note the increased mode of ilmenite in the high oxide oceanic sample (47R2-1; h) and domain in continental sample (CP1604C; above the white dashed line in panel l). The yellow arrow in 'a' shows an ilmenite finger replacing plagioclase; white box in (e) and red box in (k) show the areas of EBSD mapping in Figure 5 and Figure 6, respectively.

Figure 4. Microstructures showing melt-rock interaction. BSE images of oceanic samples from Atlantis Bank (a-g) and continental sample from central Australia (h-k). 3D microCT scan of oceanic sample 47R2-1(l-n). Arrows point to microstructures: yellow: protrusions of oxides into silicate minerals, red: oxide films along grain boundaries, green: oxides terminating with low dihedral angles, blue: garnet pseudomorphed by oxides, orange: En with same interference colour indicating same orientation, intergrown with Di, white: inclusions. Yellow lines highlight straight versus irregular boundaries, ~~blue~~magenta lines (e) highlight parallel protrusions of oxides into diopside, green dashed lines mark the boundaries between ilmenite and magnetite and red lines (g(i)) mark the orientations of exsolutions of ilmenite and spinel in magnetite. Mineral abbreviations are after Whitney and Evans (2010).

Figure 5. 3D interconnectivity and mineral relationships of oceanic high oxide sample 47R2-1 based on EBSD analysis highlighting connectivity of apparently isolated grains in three dimensions and internal deformation. (a) Phase map of a small section of the sample (see Fig. 3e), areas in b, c and d marked by dashed boxes; (b) Ilmenite grains (I1 to I3) (c) Diopside grains (D1 to D3) and (d) Enstatite grains (E1 and E2) each have an Euler map with c-axis pole figure, and an image and graph of change in orientation within a grain from a reference orientation marked with a white cross. Ilmenite {10-10} pole figure is included in (c) to show that the crystal boundary on diopside grains 1 and 2 are parallel to the relict ilmenite grain 1 crystal face.

Figure 6. 3D interconnectivity, internal deformation and epitaxy of continental sample CP1604C. (a) Phase map of a small section of the sample (see Fig. 3k), areas in b and c marked in white boxes; (b, c) Ilmenite and garnet Euler maps with c-axis pole figures, and in b_1, c_1 an image showing change in orientation within a grain from a reference orientation marked with a white cross and misorientation

profile marked by the yellow line starting at the dot in (a). Crystallographic orientation pole figures for ilmenite (d), garnet (e); and biotite (f). Note: All the grains have been plotted as no single grain has a dominating effect.

Figure 7. Comparison of electron microprobe mineral chemistry for both oceanic and continental settings. (a) Ternary diagram of pyroxenes (Wo – wollastonite; En – enstatite; Fs – ferrosilite), plagioclase (An – anorthite; Ab – albite; Or – orthoclase), garnet (Py – pyrope; Al+Sp – almandine-spessartine; Gr – grossular) and biotite (orange apex labels); (b–d) Ilmenite composition showing opposite trends for MgO and MnO for oceanic samples (red arrows in c and d).

Figure 8. Cartoon illustrating the evolution melt composition and impact of melt-rock interaction on the rock composition and microstructure. Melts 1, 2 and 3 refer to dynamic compositional changes in response to melt-rock interaction of the fluxing melt. (a) Oceanic setting (after Fig. 4b, and 5): Step1 – a fractionated gabbroic melt1 (white solid) moves through a precursor olivine gabbro to initiate formation of diopside and ilmenite along enstatite and plagioclase boundaries by melt-rock interaction (step 1). This causes the formation of a modified melt2 (~~orange~~white dashed). Step 2 – interactions between melt2 and the rock causes further growth of diopside and ilmenite and the formation of a new modified melt3 (~~black~~white dots). Step 3 – interactions between melt3 and the rock causes growth of new diopside and magnetite~~.~~; *changing conditions, e.g. pressure, temperature, oxygen fugacity, P or Ti content changes in incoming melt (b) Continental setting (after Fig. 3k, 4h-k and 6): Step 1 – a primary or fractionated S-type granitic melt1 (~~blue~~yellow) infiltrates a granulite facies felsic gneiss along a shear zone; melt-rock interaction leads to growth of aligned biotite and minor garnet and the formation of melt2 (~~yellow~~orange). Step 2 – interactions between ~~melt 2~~melt2 and the rock ~~increased~~increases the

mode of biotite and garnet and the formation of melt3 (red). Step 3 – interactions between melt3 and the rock forms interstitial ilmenite and again increases the modes of biotite, garnet and ilmenite. Minerals with their boundaries in the colour of a particular melt (e.g. Melt1) are interpreted to have re-equilibrated with that respective melt.

Figure

Click here to access/download;Figure;Fig1.pdf

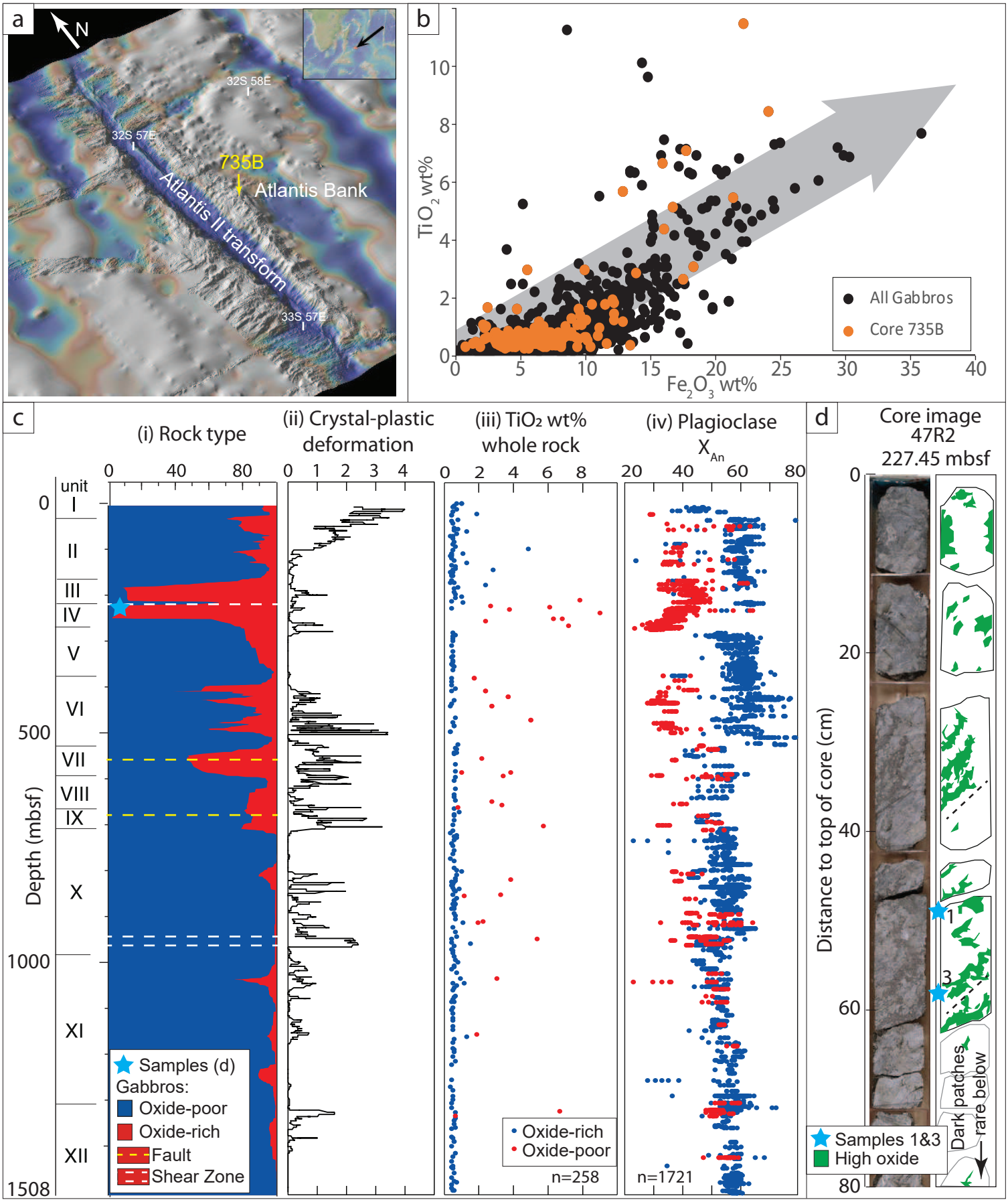

Figure

Click here to access/download;Figure;Fig2.pdf

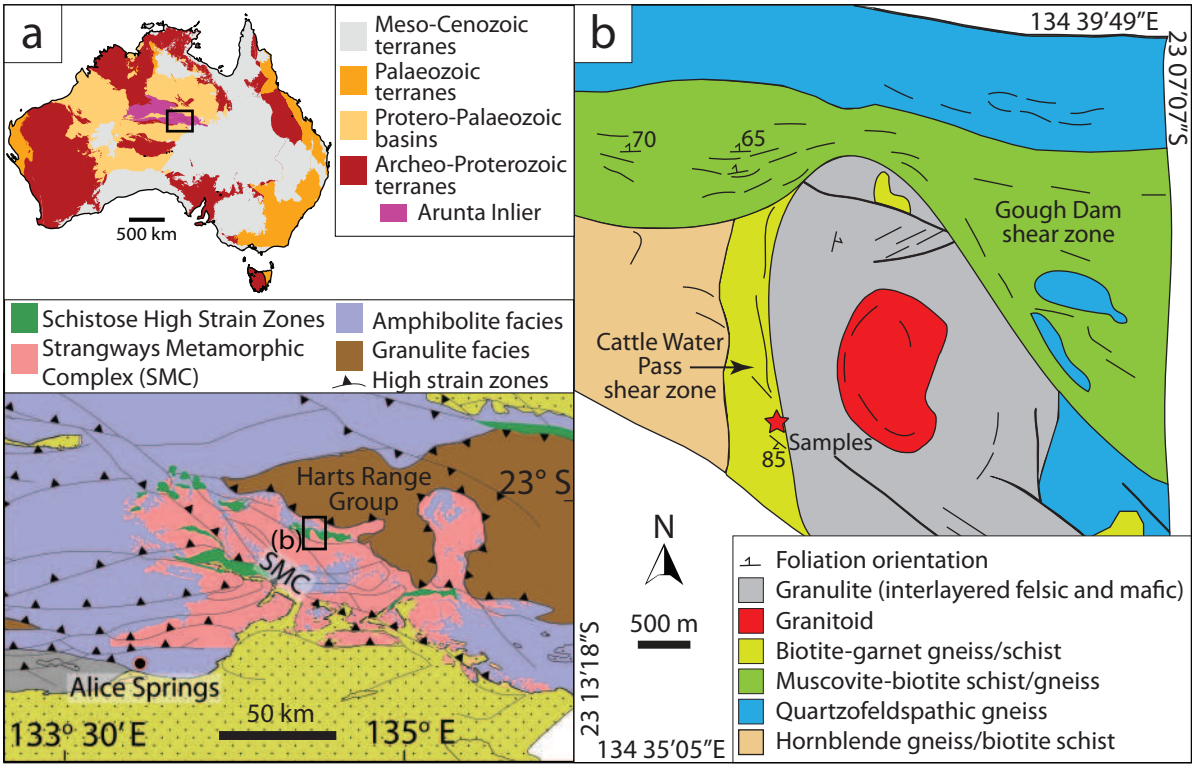

Figure

Click here to access/download;Figure;Fig3.pdf

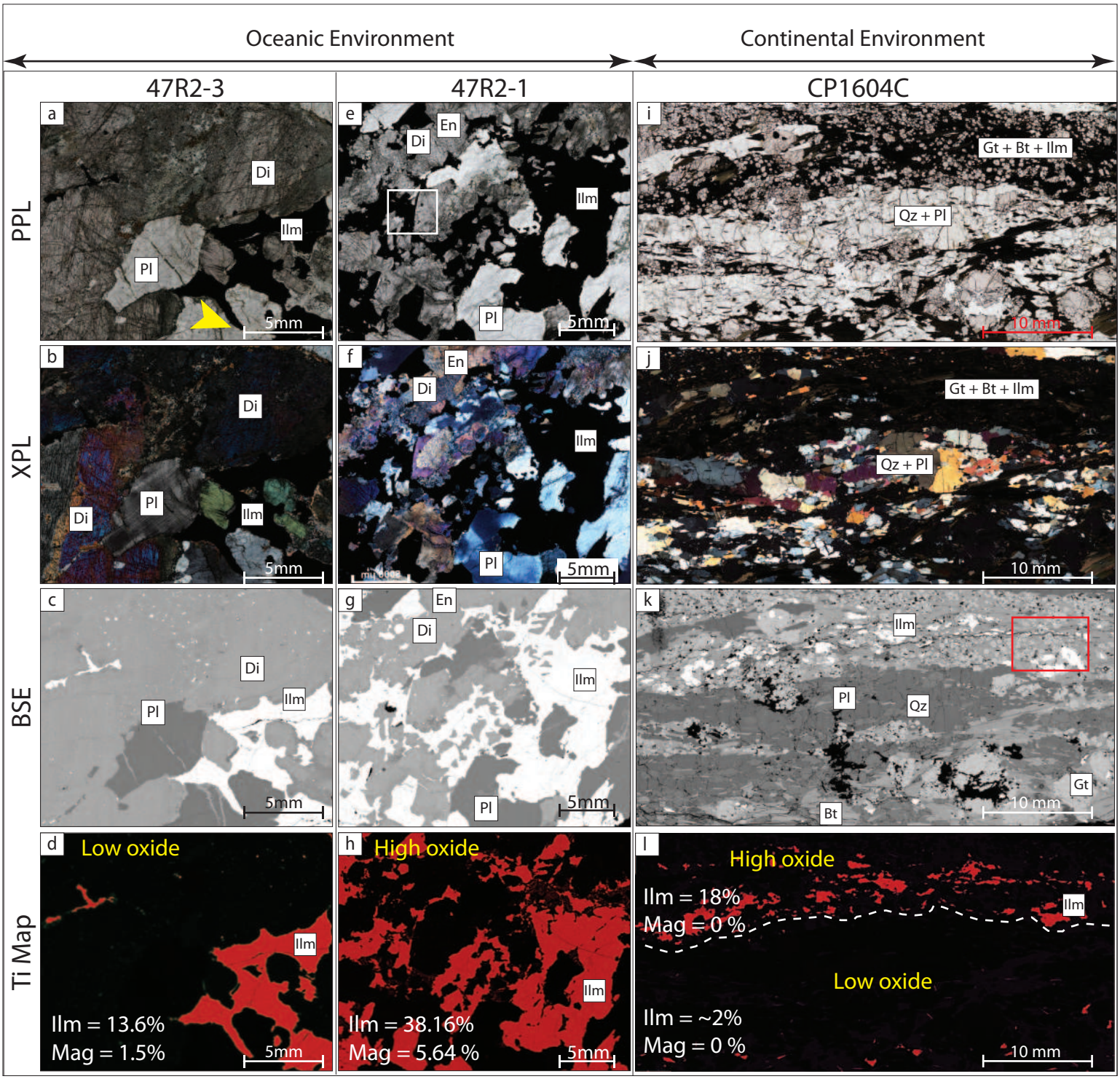

Figure

Click here to access/download;Figure;Fig4.pdf

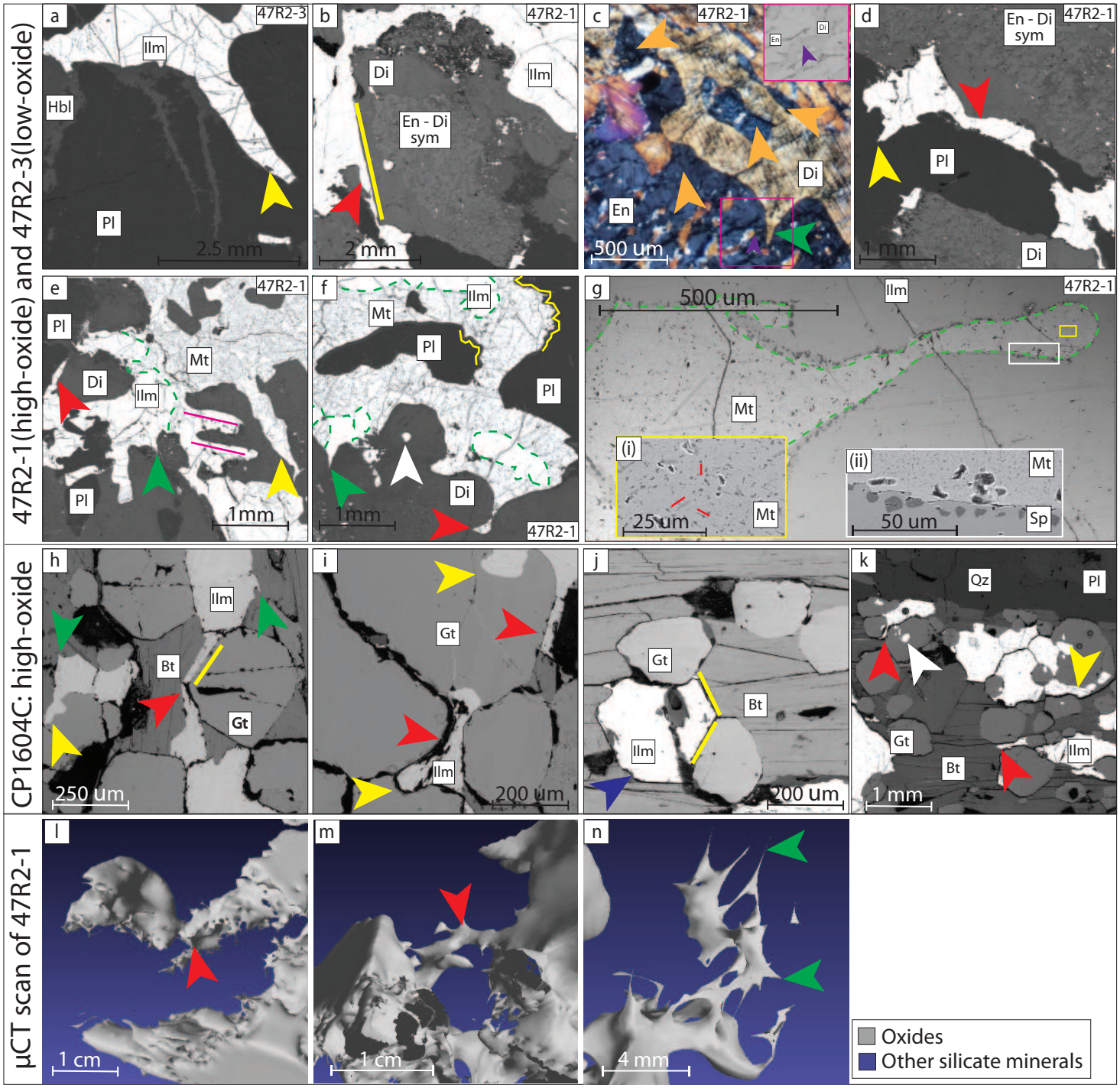

Figure

Click here to access/download;Figure;Fig5.pdf

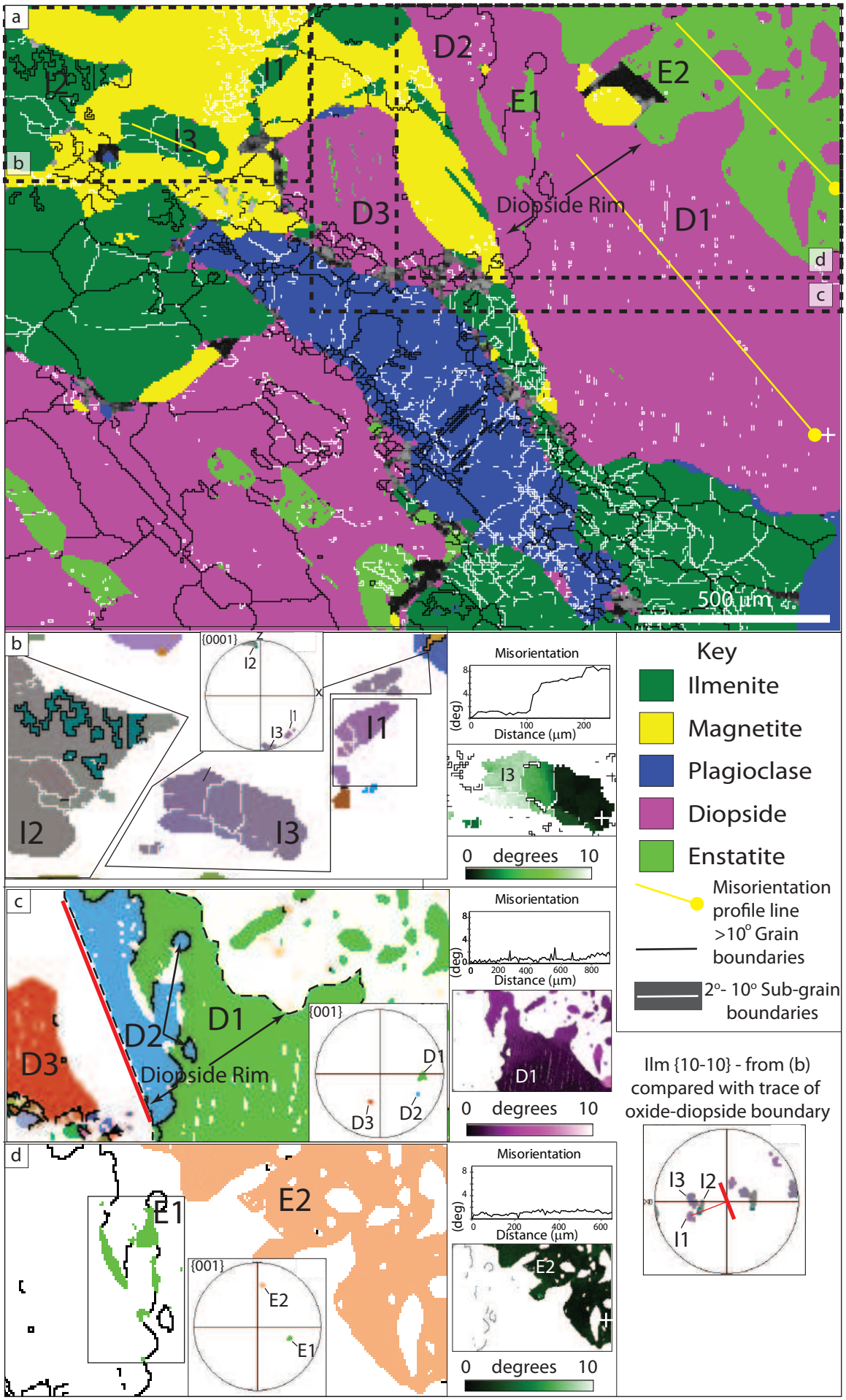

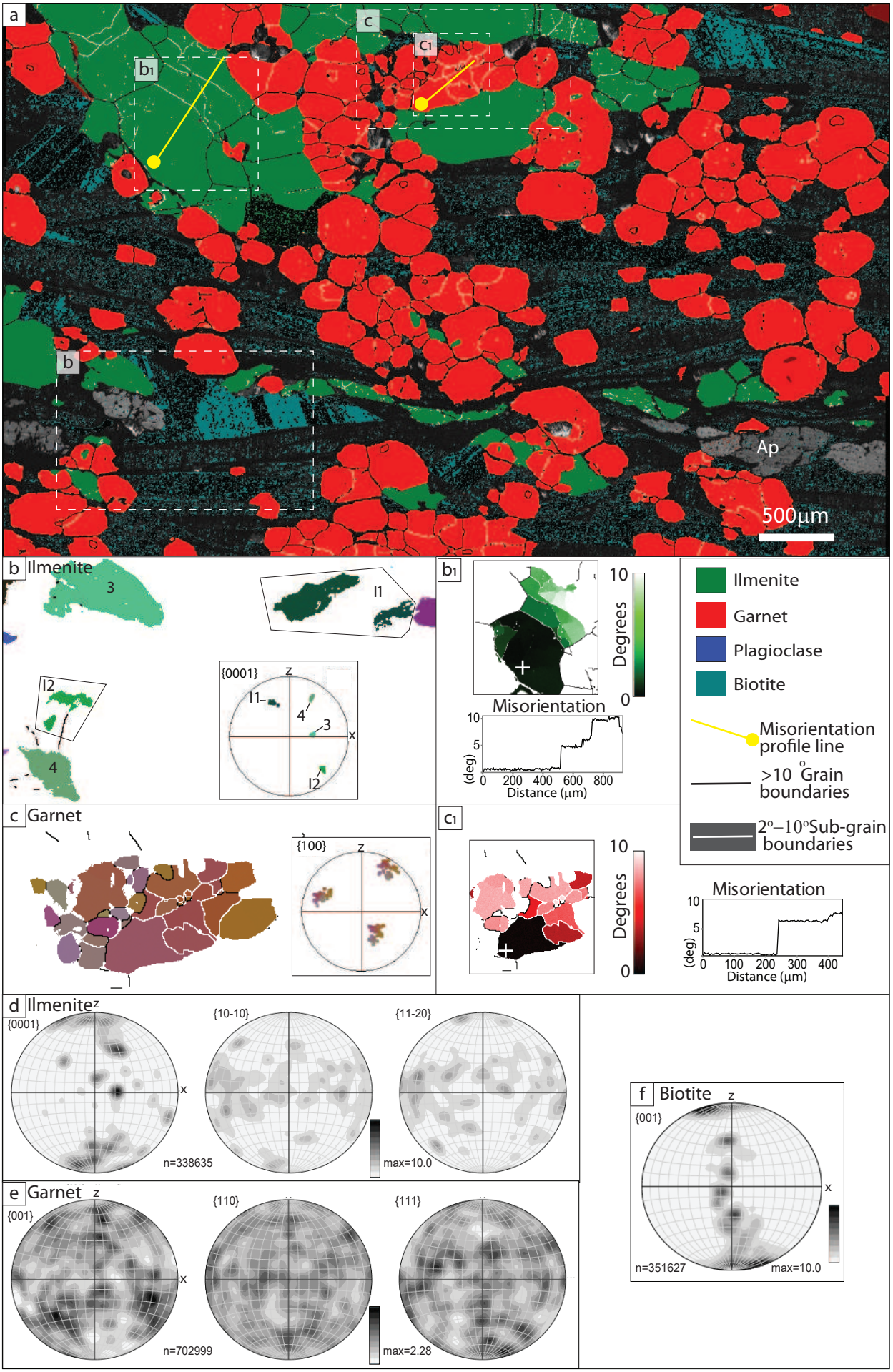

Figure

Click here to access/download;Figure;Fig7.pdf

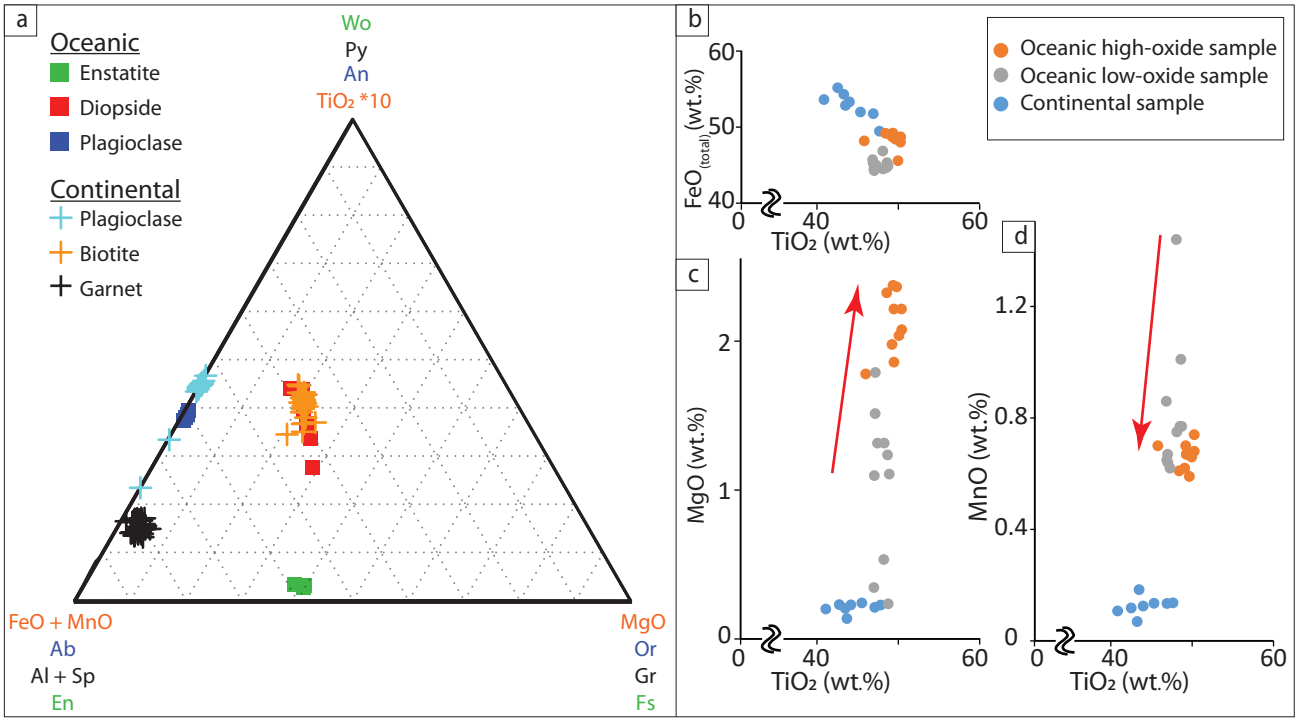

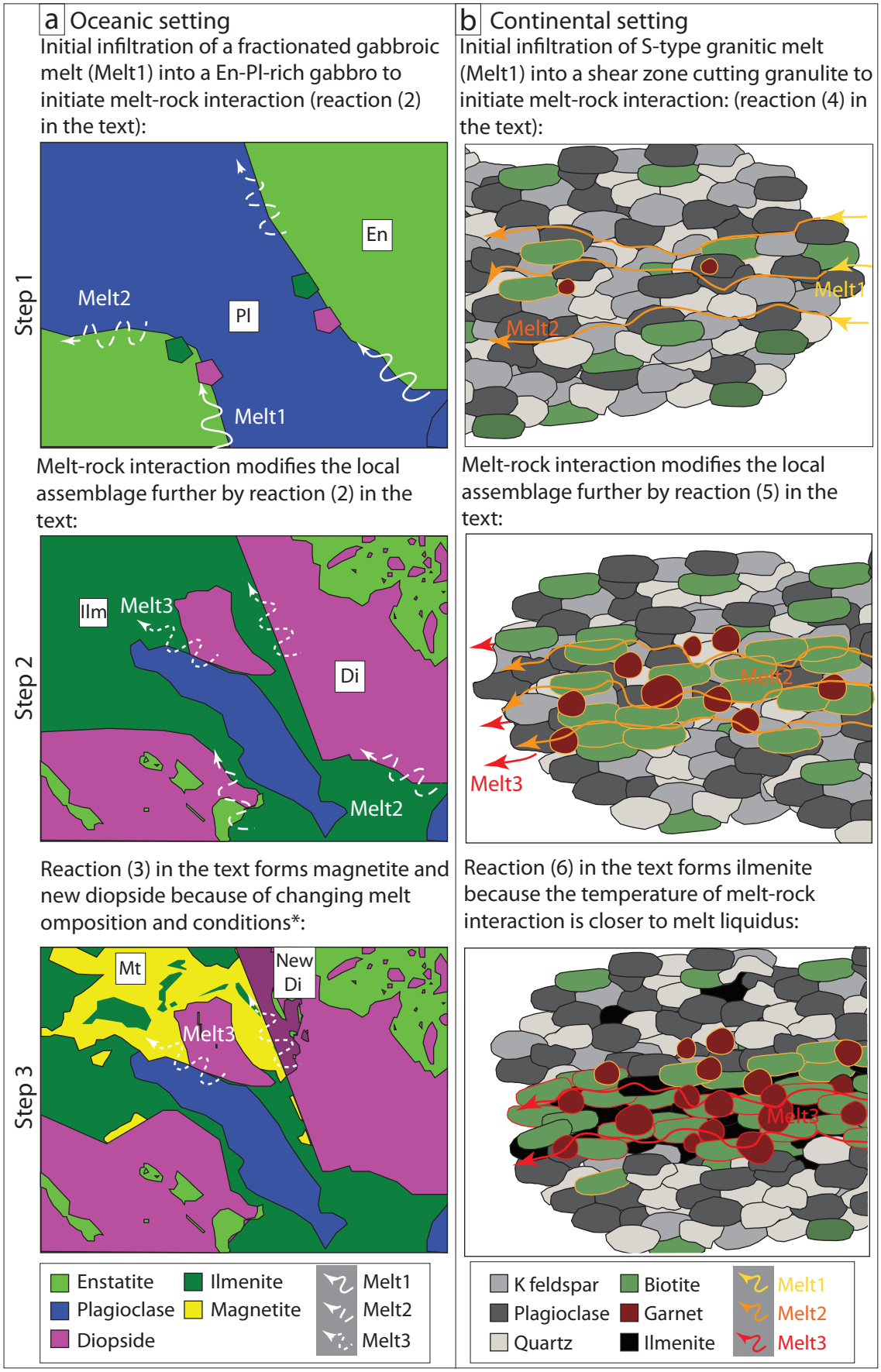

Declaration of interests

☒ The authors declare that they have no known competing financial interests or personal relationships that could have appeared to influence the work reported in this paper.

☐The authors declare the following financial interests/personal relationships which may be considered as potential competing interests: